The
PHILOSOPHICAL MAGAZINE

FIRST PUBLISHED IN 1798

UNIVERSITY OF HAWAII
LIBRARY
AUG 17 '54

. 45 SEVENTH SERIES No. 366 July 1954

A Journal of Theoretical Experimental and Applied Physics

EDITOR
PROFESSOR N. F. MOTT, M.A., D.Sc., F.R.S.

EDITORIAL BOARD
SIR LAWRENCE BRAGG, O.B.E., M.C., M.A., D.Sc., F.R.S.
SIR GEORGE THOMSON, M.A., D.Sc.. F.R.S.
PROFESSOR A. M. TYNDALL, C.B.E., D.Sc., F.R.S.

PRICE 15s. 0d.
Annual Subscription £8 0s. 0d. payable in advance

AND PUBLISHED BY TAYLOR & FRANCIS LTD., RED LION COURT, FLEET ST., LONDON, E.C.4.

Commemoration Number

To mark the 150th Anniversary of the

PHILOSOPHICAL MAGAZINE

Natural Philosophy through the

Eighteenth Century & Allied Topics

CONTENTS

The Philosophical Magazine. By ALLAN FERGUSON, M.A., D.Sc., and JOHN FERGUSON, M.A., B.D.

Astronomy through the Eighteenth Century. By Sir H. SPENCER-JONES, F.R.S.

Physics in the Eighteenth Century. By Prof. HERBERT DINGLE, D.Sc.

Chemistry through the Eighteenth Century. By Prof. J. R. PARTINGTON, D.Sc.

Mathematics through the Eighteenth Century. By J. F. SCOTT, Ph.D.

Engineering and Invention in the Eighteenth Century. By Engineer-Captain EDGAR C. SMITH, O.B.E., R.N.

Scientific Instruments in the Eighteenth Century. By ROBERT S. WHIPPLE, M.I.E.E., F.Inst.P.

The Scientific Periodical from 1665 to 1798. By DOUGLAS McKIE, D.Sc., Ph.D.

Scientific Societies to the end of the Eighteenth Century. By DOUGLAS McKIE, D.Sc., Ph.D.

The Teaching of the Physical Sciences at the end of the Eighteenth Century. By F. SHERWOOD TAYLOR, Ph.D.

viii + 164 pages

15/6

POST FREE

TAYLOR & FRANCIS, LTD.

RED LION COURT, FLEET ST., LONDON, E.C.4

PRINTERS & PUBLISHERS FOR OVER 150 YEARS

LXXIV. *A New Type of Interferometer for Use in Radio Astronomy*

By R. Hanbury Brown
Jodrell Bank Experimental Station, Cheshire
and
R. Q. Twiss
Services Electronics Research Laboratory, Baldock, Herts.*

[Received March 20, 1954]

Summary

A new type of interferometer for measuring the diameter of discrete radio sources is described and its mathematical theory is given. The principle of the instrument is based upon the correlation between the rectified outputs of two independent receivers at each end of a baseline, and it is shown that the cross-correlation coefficient between these outputs is proportional to the square of the amplitude of the Fourier transform of the intensity distribution across the source. The analysis shows that it should be possible to operate the new instrument with extremely long baselines and that it should be almost unaffected by ionospheric irregularities.

§1. Introduction

At the present time more than one hundred discrete sources of extra-terrestrial radio-frequency radiation have been observed, and it is to be expected that this number will increase rapidly as the sensitivity and resolving power of current equipment is improved. A knowledge of the angular sizes of the discrete sources is fundamental to their general study and is of particular importance to their identification with objects observed photographically.

The first attempts to measure the angular size of the two most intense sources were unsuccessful since they proved to be below the resolving power of the instruments then available. Thus Bolton and Stanley (1948), using a 'Lloyds Mirror' interferometer mounted on a cliff, showed that the apparent diameter of the intense source in Cygnus is less than 8 minutes of arc; while Ryle and Smith (1948), using a 'Michelson' interferometer with a baseline of 500 m, showed that the intense sources in Cygnus and in Cassiopeia both have angular diameters less than 6 minutes of arc. Stanley and Slee (1950), using a similar equipment to that used by Bolton and Stanley, gave a limit of 1·5 minutes of arc for the angular diameter of the source in Cygnus.

The problem of improving upon the resolving power used in these previous measurements was reviewed in 1949, and an examination of the existing instruments suggested that a considerable improvement could readily be made by extending the baseline of the ' Michelson ' type of interferometer. It was estimated, as discussed in § 2, that the baseline might be extended to about 50 km without great difficulty, but that an extension to distances of 100 km or more would involve elaborate equipment. Since at that time it was assumed that the angular sizes of the discrete sources might be comparable with those of the visible stars, the maximum resolving power was sought and a new type of interferometer for use with extremely long baselines was proposed by one of the authors (R.H.B.).

---

* Communicated by Professor A. C. B. Lovell.

The present paper discusses only the principle and mathematical theory of the new interferometer; a preliminary account of the experimental results has already been published (Hanbury Brown, Jennison and Das Gupta 1952), and a more detailed discussion of these results and of the apparatus will be given elsewhere (Jennison and Das Gupta, in preparation).

§ 2. THE ' MICHELSON ' INTERFEROMETER

The application of the ' Michelson ' interferometer to radio astronomy has been discussed by McCready, Pawsey and Payne-Scott (1947) and also by Ryle (1950). A brief description of its theory will be given here for comparison with that of the new instrument described in § 3.

2.1. *The Theory of the ' Michelson ' Interferometer*

A simplified diagram of a ' Michelson ' interferometer is shown in fig. 1. Two aerials A and B, separated by a horizontal baseline of length L, are joined by a cable; the centre of the cable is connected to a receiver, the output of which is recorded. When a discrete source transits the plane normal to the baseline the receiver output exhibits oscillations, as shown in fig. 2, which correspond to the fringes observed in a stellar interferometer. The amplitude and phase of these oscillations will be calculated

Fig. 1

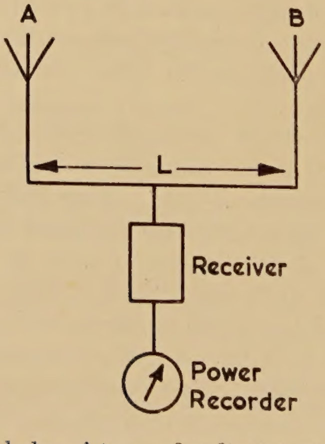

The ' Michelson ' type of radio interferometer.

for the simple case shown in fig. 3, where the source is a narrow strip FG coplanar with the baseline of the interferometer AB. Since the distance of the source is much greater than the length of the baseline, the relative phase of the voltages received by the two aerials from a radiating element E at an angle θ from the line CD, is

$$(\omega_0 L/c) \sin (\theta+\theta_0),$$

where ω_0 is the angular frequency to which the receiver is tuned, and θ_0 is the angle between CD and a plane normal to the baseline. If the receiver output is linearly proportional to the input power, the interaction of these two voltages produces a term in the receiver output proportional to

$$P(\theta) \cos [(\omega_0 L/c) \sin \overline{\theta_0+\theta}]\, d\theta,$$

Fig. 2

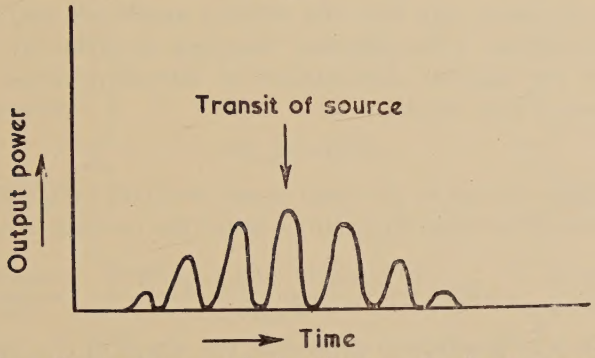

The variation of output power during the transit of a source, as observed with a ‘ Michelson ’ type interferometer.

Fig. 3

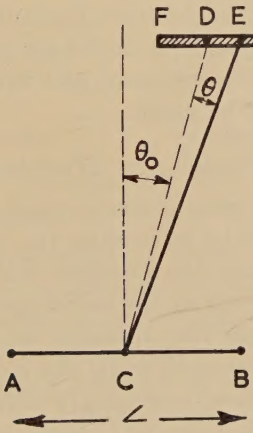

The geometry of the ‘ Michelson ’ type interferometer.

where $P(\theta)\,d\theta$ is the power received from the element E at angular frequency ω_0. The receiver output due to the signal from the whole source is given by

$$K \sim \int_{-\alpha/2}^{\alpha/2} P(\theta) \cos [(\omega_0 L/c) \sin \overline{\theta_0+\theta}]\, d\theta, \quad . \quad . \quad . \quad (1)$$

where α is the maximum angular extension of the source. If $\alpha \ll 1$, so that $\sin\theta \simeq \theta$ and $\cos\theta \simeq 1$ for $|\theta| < \alpha$, eqn. (1) may be expanded to give

$$K(l)=F_{\cos}\left(\frac{\omega_0 l}{c}\right).\cos\left(\frac{\omega_0 l \tan\theta_0}{c}\right)-F_{\sin}\left(\frac{\omega_0 l}{c}\right).\sin\left(\frac{\omega_0 l \tan\theta_0}{c}\right), \quad . \quad . \quad . \quad (2)$$

where l is the length of the baseline projected on to the plane perpendicular to CD and where

$$l=L\cos\theta_0, \quad . \quad . \quad . \quad . \quad . \quad . \quad . \quad . \quad . \quad . \quad . \quad . \quad (3)$$

$$\left.\begin{aligned} F_{\cos}\left(\frac{\omega_0 l}{c}\right) &= \int_{-\alpha/2}^{\alpha/2} P(\theta)\cos\left(\frac{\omega_0 l\theta}{c}\right)d\theta, \\ F_{\sin}\left(\frac{\omega_0 l}{c}\right) &= \int_{-\alpha/2}^{\alpha/2} P(\theta)\sin\left(\frac{\omega_0 l\theta}{c}\right)d\theta. \end{aligned}\right\} \quad . \quad . \quad . \quad . \quad . \quad (4)$$

Equation (2) shows that the output of the receiver oscillates sinusoidally as the angle θ_0 varies, and that the relative amplitude and phase of the oscillations observed with different baselines is given by the Fourier transform of the angular distribution of intensity across the source. For a baseline of zero length,

$$K(0)=F_{\cos}(0), \quad . \quad . \quad . \quad . \quad . \quad . \quad . \quad . \quad . \quad . \quad (5)$$

and $K(0)$ is proportional to the total power received from the source.

The modulus of the ratio $K(l)/K(0)$ is called the *correlation coefficient* $\rho(l)$, where*

$$\rho(l)=\frac{[F^2_{\cos}(\omega_0 l/c)+F^2_{\sin}(\omega_0 l/c)]^{1/2}}{F_{\cos}(0)}. \quad . \quad . \quad . \quad . \quad . \quad . \quad (6)$$

In principle it is possible to determine the shape of the distribution of intensity across the source by measuring the relative amplitude and phase of the oscillations with different baselines ; however, the measurement of the relative phase presents considerable experimental difficulty and so far has not been attempted. If the relative amplitude only and not the phase of the oscillations is measured, it is no longer possible to determine the distribution across the source uniquely and some *a priori* assumptions about its general shape must be made.

2.2. *The Resolving Power of a ' Michelson ' Interferometer*

The resolving power of an interferometer is of the order of (λ/l) and can therefore be improved either by extending the baseline or by decreasing the wavelength. At the time the problem was reviewed a substantial improvement in resolving power by the use of shorter wavelengths was not regarded as practicable, since the intensity of the discrete sources was known to decrease with wavelength while the construction of large aerials and sensitive receivers becomes increasingly difficult as the wavelength is decreased ; furthermore it is desirable to know the effective diameter of a source as a function of frequency. The alternative possibility of extending the baseline was therefore considered; initially in relation to the 'Michelson' interferometer.

---

* This result has been derived for a single frequency and only applies to a practical interferometer if the fractional radio-frequency bandwidth is sufficiently small.

The baseline of the simple instrument shown in fig. 1 is limited to a few hundred metres by attenuation in the cable between the aerials. This can be overcome by a variety of techniques of which the simplest is the use of radio-frequency amplifiers at both ends of the cable; however, for baselines exceeding about 1 km a cable is both cumbersome and expensive and may advantageously be replaced by a radio link. It is difficult to estimate the maximum length of baseline over which such a link may be used since it depends on the location of the equipment and on details of the installation; nevertheless, it seems likely that in practice the maximum length would be limited by instability of phase in the transmission. If the diameter of a source is to be measured reliably, any variations introduced by the equipment into the relative phase of the signals must be slow compared with the period of oscillation of the receiver output, and the published data on short wave propagation suggest that rapid and significant changes of phase may be expected with baselines exceeding 25–50 km unless the equipment is restricted to special sites and operating times. For this reason it was decided to adopt a new technique, specifically designed to reduce the requirements for phase stability in the link, which promised simple and reliable operation with baselines considerably in excess of 25–50 km.

Fig. 4

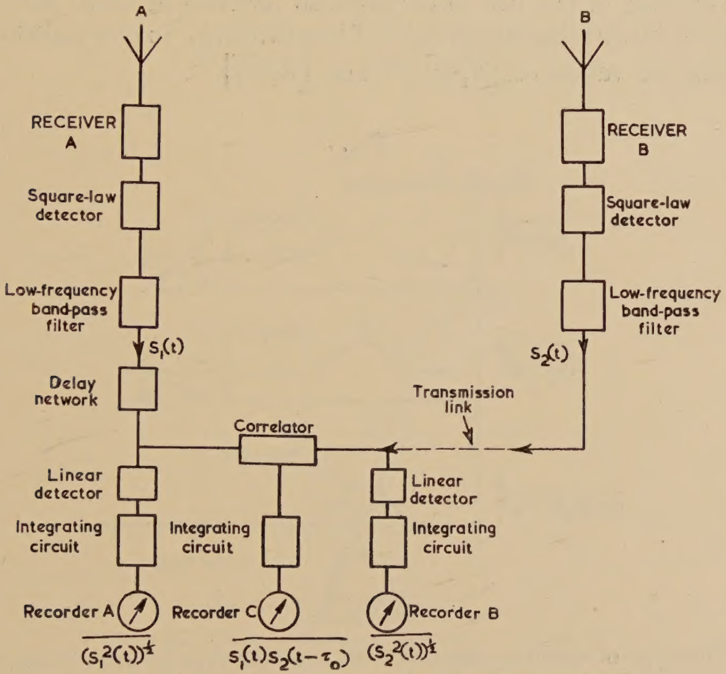

Block diagram of new type of interferometer.

§ 3. DESCRIPTION OF THE NEW TYPE OF INTERFEROMETER

A simplified diagram of the equipment is given in fig. 4. Two aerials, A and B, feed two independent receivers tuned to the same frequency with identical band-pass characteristics. The output of each receiver is rectified in a *square-law* detector and is fed to a low-frequency band-pass filter. The outputs $S_1(t)$, $S_2(t)$ of these filters are combined in a correlator the output of which is passed, via an integrating circuit of bandwidth b_I, to a pen recording the time-dependent signal

$$K(t)=\overline{S_1(t)\,.\,S_2(t-\tau_0)}, \quad . \quad . \quad . \quad . \quad . \quad . \quad . \quad . \qquad (7)$$

where τ_0 is a delay time, discussed later, and the bar denotes the averaging process in the integrating circuit.

The outputs of the two filters are also rectified in *linear detectors* and passed, via integrating circuits also of bandwidth b_I, to two additional pens recording the values of $\left[\overline{S_1^2(t)}\right]^{1/2}$ and $\left[\overline{S_2^2(t)}\right]^{1/2}$.

Fig. 5

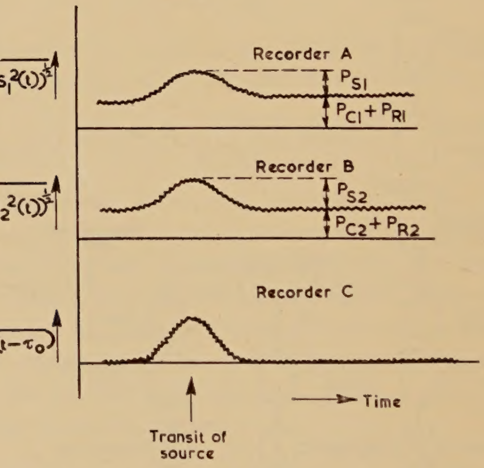

The type of records obtained with the new type of interferometer during the transit of a source.

The appearance of the records obtained from a discrete source is shown in fig. 5. The envelopes of the three curves correspond to the variation of the power received as the source passes through the polar diagram of the aerials, and it can be seen that none of the records exhibit the oscillations observed with a ' Michelson ' interferometer. The output of each receiver is proportional to the sum of the signal power received from the source P_S, the noise power generated by the receiver itself P_R, and the cosmic noise power P_C due to the general radiation from the area of sky covered by the aerial beam. The two latter components have been represented in fig. 5 as a steady displacement of the records of $\left[\overline{S_1^2(t)}\right]^{1/2}$ and $\left[\overline{S_2^2(t)}\right]^{1/2}$

since, for the purpose of the diagram, it has been assumed that both the cosmic and receiver noise remain constant during the observation. The mean deflection of the record of $\overline{S_1(t) \,.\, S_2(t-\tau_0)}$ is due to the radiation from the source alone since the receiver noise in the two channels is independent and the cosmic noise, for most practical values of the baseline, is effectively uncorrelated.

From the three records of the transit of a source the *normalized correlator output*,

$$c(l, t) \equiv \frac{\overline{S_1(t) \,.\, S_2(t-\tau_0)}}{\{[\overline{S_1^2(t)}]^{1/2} - P_{N1}\}\{[\overline{S_2^2(t)}]^{1/2} - P_{N2}\}}, \quad . \quad . \quad (8)$$

is calculated at any time t where P_{N1}, P_{N2} are the average values of the

Fig. 6

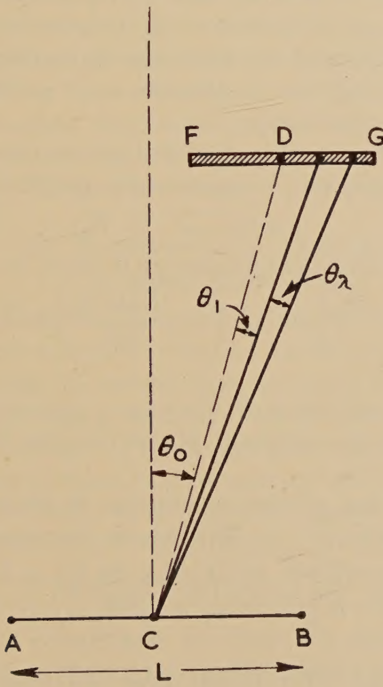

The geometry of the new type of interferometer.

low-frequency filter outputs observed when the source is outside the aerial beam. $C(l)$ the mean value of $c(l, t)$ is found by averaging over an arbitrarily large number of complete transits of the source. The measurements are then repeated with a number of different lengths of the baseline and the resulting values are used to determine the angular distribution of intensity across the source by means of eqn. (32).

The first equipment of this type has two aerials each with an aperture of 500 m^2, the receivers are tuned to 125 Mc/s with a pre-detector bandwidth of 200 kc/s and the band-pass of the low-frequency filters extends from 1–2·5 kc/s. The correlator is sited for convenience at one end of the baseline and the low-frequency signals from the remote station are transmitted along the baseline as amplitude modulation of the carrier of a radio link. To compensate for the time taken for the signals to travel along the baseline and for the difference in the time of arrival of the signals at the two aerials when the direction of the source is not normal to the baseline, an adjustable delay is inserted between one equipment and the correlator.

§ 4. The Principle of the New Interferometer

It was shown in § 2 that the ' Michelson ' interferometer can be analysed by considering the radiation at a *single* frequency from a *single* point in the source. The interaction of radiation from different points in the source or of signals at different frequencies can be neglected, since, as long as they are uncorrelated, they contribute nothing to the average value of the output. In an equivalent analysis of the new type of interferometer it is necessary to consider signals of *different* frequencies ω, ω' emitted by *different* points in directions θ_l, θ_λ respectively.

The contribution to the output of the square-law detector at A due to the interaction of these two components is proportional to

$$\cos(\overline{\omega-\omega'}\,.\,t-\Psi_1),$$

and the phase Ψ_1 of this beat-frequency is given by

$$\Psi_1=\phi_l(\omega)-\phi_\lambda(\omega')+\frac{R_0}{c}\left[\overline{\omega-\omega'}\left(1+\frac{L\sin\theta_0}{2R_0}\right)+\frac{L\cos\theta_0}{2R_0}(\theta_l\omega-\theta_\lambda\omega')\right], \quad . \ . \ . \ (9)$$

where $\phi_l(\omega)$, $\phi_\lambda(\omega')$ are the radio-frequency phases at the source and R_0 is the distance from the midpoint of the baseline to a fixed point in the source.

Similarly the output of the detector at B contains a beat-frequency proportional to $\cos(\overline{\omega-\omega'}\,.\,t-\Psi_2)$, where the phase Ψ_2 is given by

$$\Psi_2=\phi_l(\omega)-\phi_\lambda(\omega')+\frac{R_0}{c}\left[\overline{\omega-\omega'}\left(1-\frac{L\sin\theta_0}{2R_0}\right)-\frac{L\cos\theta_0}{2R_0}(\theta_l\omega-\theta_\lambda\omega')\right]. \quad . \ . \ . \ . \ . \ (10)$$

The difference in phase $\Delta\Psi$ between these two beat-frequencies is given by

$$\Delta\Psi=\overline{\omega-\omega'}\,\frac{L\sin\theta_0}{c}+\frac{L\cos\theta_0}{c}(\omega\theta_l-\omega'\theta_\lambda). \quad . \ . \ . \ (11)$$

The first term in eqn. (11) represents the difference in the time of arrival of the signals at the two aerials. In principle it can be made zero by inserting a compensating delay $\tau_0=L\sin\theta_0/c$ in the appropriate receiver channel. In this case the difference in phase between the two beat-frequencies may be written

$$\Delta\Psi=l/c[\omega\theta_l-\omega'\theta_\lambda], \quad . \ . \ . \ . \ . \ . \ . \ (12)$$

where l, defined in eqn. (3), is the projected length of the baseline normal to the direction of the source.

Equation (12) shows that the difference in phase between the two beat-frequency components at the detectors is equal to the difference between the relative phase of the two radio-frequency components in each aerial. Thus, although the use of two independent receivers destroys all information about the absolute phase in either aerial of any single radio-frequency component, information about the angular size of the source is preserved by the relative phase of corresponding beat-frequencies in the detector outputs.

If their frequency $(\omega-\omega')$ lies within the bandwidth of the low-frequency filters, the two beat-frequencies are transmitted to the correlator where they are multiplied together and form a direct current output proportional to the cosine of their phase difference. It is shown in the next section that the total direct current output from the correlator is the sum of the outputs due to all the beat-frequencies produced by the interaction of all pairs of points in the source. It is further shown that the correlator output, when suitably normalized, is equal to the square of the correlation coefficient measured by the 'Michelson' interferometer. Hence, by measuring the normalized correlator output with different lengths of baseline, it is possible to obtain information about the distribution of intensity across an equivalent line source coplanar with the baseline.

§ 5. MATHEMATICAL THEORY

5.1. *A Model Radio Source*

It is assumed that a discrete radio source can be divided into a system of regions each very small compared with the resolving power of the interferometer, yet large enough to ensure that the total radio-frequency power generated in any one region has the overall characteristics of thermal radiation and is independent of the power generated in any other region.* As long as the baseline of the interferometer is fixed in space and provided that the angular dimensions of the source are not too large, the actual three-dimensional distribution of intensity in the source cannot be distinguished from that of an equivalent line source coplanar with the baseline. For simplicity we shall consider this idealized case and shall use a Cartesian system of coordinates in which the equivalent line source is parallel to the x axis and the z axis lies along the line joining a fixed point in the source to the midpoint of the baseline. The coordinates of the receiving aerials A, B are then $(-l/2, 0, -l\tan\theta_0/2)$ and $(l/2, 0, l\tan\theta_0/2)$ respectively, where l is related to the baseline length L by eqn. (3).

The field radiated by a region at an angle θ from the axis has components which may be represented by the stationary time series,

$$\sum_{r=0}^{\infty} \frac{c_r(\theta)}{R} \cos\left[\frac{2\pi r t}{T} - \phi_r(\theta)\right]_{t-R/c},$$

---

* This assumption does not exclude the possibility that the radio-frequency power is generated by plasma oscillations provided that such oscillations are not coherent over volumes comparable with the resolving power of the interferometer.

where R is the distance from the radiating region to the point at which the field is measured, T is the observation time, $\phi_r(\theta)$ is a random variable distributed with uniform probability between 0 and 2π so that there is zero correlation between the phases of different frequencies and between the radiation from different regions, and $c_r(\theta)$ is a quantity proportional to

$$[2p_r(\theta)\, d\theta/T]^{1/2},$$

where $p_r(\theta)\, d\theta$ is the power radiated from the region of angular width $d\theta$ at the frequency r/T. As has been shown by Rice (1944) representations of this kind are equivalent to the more familiar representations introduced into radiation theory by Einstein (1915) and by von Laue (1915).

5.2. *The Correlator Output in the Absence of Receiver and Aerial Noise*

The voltages $V_1(t)$, $V_2(t)$ developed across the inputs to the square-law detectors in the two receivers by the signals received from the source are given by

$$\left.\begin{aligned} V_1(t) &\sim \int d\theta_l \sum_{r=0}^{\infty} \frac{A_{1r}}{R_1(\theta_l)} c_r(\theta_l) \cos\left[\frac{2\pi r}{T}\left(t-\frac{R_1(\theta_l)}{c}\right)-\phi_r(\theta_l)-\psi_{1r}\right], \\ V_2(t) &\sim \int d\theta_{l'} \sum_{r'=0}^{\infty} \frac{A_{2r'}}{R_2(\theta_{l'})} c_{r'}(\theta_{l'}) \cos\left[\frac{2\pi r'}{T}\left(t-\frac{R_2(\theta_{l'})}{c}\right)-\phi_{r'}(\theta_{l'})-\psi_{2r'}\right], \end{aligned}\right\} \quad . \; . \; . \; . \; . \; . \quad (13)$$

where to the first order in θ_l, $\theta_{l'}$,

$$\left.\begin{aligned} R_1(\theta_l) &= [R_0^2+(L^2/4)+R_0 l \tan\theta_0 - R_0 l \theta_l]^{1/2}, \\ R_2(\theta_{l'}) &= [R_0^2+(L^2/4)-R_0 l \tan\theta_0 + R_0 l \theta_{l'}]^{1/2}, \end{aligned}\right\} \quad . \; . \; . \quad (14)$$

and where A_r, ψ_r are the amplitude and phase characteristics of the pre-detector amplifiers.*

In the present case, where the fractional pre-detector bandwidth is small compared with unity, the output of the low-frequency filters following the square-law detectors is given by

$$\begin{aligned} S_1(t) \sim \int d\theta_l \int d\theta_\lambda \sum_{r,s=0}^{\infty} & \frac{A_{1r}A_{1s}c_r(\theta_l)c_s(\theta_\lambda)}{R_1(\theta_l)\,.\,R_1(\theta_\lambda)} \\ & \times G_1\left(\frac{2\pi\,.\,\overline{r-s}}{T}\right) \cos\left\{\frac{2\pi t}{T}\overline{r-s}-\left[\frac{rR_1(\theta_l)}{c}-\frac{sR_1(\theta_\lambda)}{c}\right]\right. \\ & \left. -\overline{\psi_{1r}-\psi_{1s}}-\overline{\phi_{1r}(\theta_l)-\phi_{1s}(\theta_\lambda)}-\chi_1\left(\frac{2\pi\,.\,\overline{r-s}}{T}\right)\right\}, \quad . \; . \; . \quad (15) \end{aligned}$$

---

* The aerial gains and any time-independent phase and amplitude distortions introduced by the ionosphere should also be included in A_r, ψ_r. It is assumed that the angular dimensions of the source are very small compared with the angular width of the aerial beams: the extension to the general case can easily be made by suitably modifying the definition of $c_r(\theta_l)$.

together with a similar expression for $S_2(t)$ where $G(\omega)\exp[-i\chi(\omega)]$, the steady state response of the low-frequency filter, is zero both for direct current and for radio-frequencies.

The outputs of the two low-frequency filters are multiplied together in the correlator the output of which is proportional to

$$S_1(t)\,.\,S_2(t-\tau_0),$$

where τ_0 is the delay inserted to compensate for the difference in the time of arrival of the signals at the two aerials.

A typical term in the time-independent part of $S_1(t)\,.\,S_2(t-\tau_0)$ is proportional to

$$\begin{aligned}\cos\,[(2\pi/cT)\{r\,.\,\overline{R_1(\theta_l)-R_2(\theta_{l'})}-s\,.\,\overline{R_1(\theta_\lambda)-R_2(\theta_{\lambda'})}\}\\ +\overline{\phi_r(\theta_l)-\phi_r(\theta_{l'})}-\overline{\phi_s(\theta_\lambda)-\phi_s(\theta_{\lambda'})}-(2\pi/T)\,.\,\overline{r-s}\tau_0\\ +\Theta_1(r,s)-\Theta_2(r,s)],\end{aligned} \qquad (16)$$

where $\Theta(r,s)=\psi_r-\psi_s+\chi[\overline{r-s}\,.\,(2\pi/T)]$.

To find the average value of $S_1(t)\,.\,S_2(t-\tau_0)$ as $T\to\infty$ use is made of the fact that the noise radiation is expressible by a *stationary* time series. In this case the distinction between a time and an ensemble average disappears so that the time-averaged value of $S_1(t)\,.\,S_2(t-\tau_0)$ is equal to the mean value of $S_1(t)\,.\,S_2(t-\tau_0)$ averaged over N different measurements, each of duration T, where $N\to\infty$. Accordingly an average is taken over the independent random phase angles $\phi_r(\theta_l)$ etc. and the only terms which contribute to $\langle S_1(t)\,.\,S_2(t-\tau_0)\rangle_{\text{AV}}$ are those for which $\theta_l=\theta_{l'}$ and $\theta_\lambda=\theta_{\lambda'}$. Since the angular dimensions of this source are small $\theta_\lambda\ll 1$ and $R_1(\theta_l)-R_2(\theta_l)$ may be expanded by the binomial theorem to give

$$\frac{R_1(\theta_l)-R_2(\theta_l)}{R_0}=\frac{l\tan\theta_0}{R_0}-\frac{l\theta_l}{R_0}, \qquad (17)$$

where $R_1(\theta_l)$, $R_2(\theta_l)$ are given by eqn. (14).

If the analysis is restricted to the case where the phase characteristics of the two channels are linear, but have different slopes, then

$$\Psi(r,s)=(2\pi/T)\overline{r-s}[\tau_0-(l\tan\theta_0/c)]+\Theta_1(r,s)-\Theta_2(r,s), \qquad (18)$$

which may be written

$$\Psi(r,s)=(2\pi/T)\overline{r-s}\,t_0, \qquad (19)$$

where t_0 is equivalent to a differential time delay.

In the limiting case where $T\to\infty$ one may put

$$2\pi r/T=\omega,\qquad 2\pi s/T=\omega', \qquad (20)$$

and then,

$$\begin{aligned}\langle S_1(t)\,.\,S_2(t-\tau_0)\rangle_{\text{AV}}\sim\int_{-\alpha/2}^{\alpha/2}d\theta_l\int_{-\alpha/2}^{\alpha/2}d\theta_\lambda\int_0^\infty d\omega\int_0^\infty d\omega' P(\omega,\theta_l)P(\omega',\theta_\lambda)\\ \times A_1(\omega)A_2(\omega)A_1(\omega')A_2(\omega')G_1(\omega-\omega')G_2(\omega-\omega')\\ \times\cos\,[-(l/c)\overline{\omega\theta_l-\omega'\theta_\lambda}-\overline{\omega-\omega'}\,.\,t_0],\end{aligned} \qquad (21)$$

where $P(\omega,\theta_l)$ is the power at an angular frequency ω in unit angular frequency bandwidth received from the region of width $d\theta_l$. If it is assumed that $P(\omega, \theta_l)$ does not change with frequency over the receiver bandwidth and if the low-frequency filter amplitude characteristic is expressed by the integral

$$G_1(\omega-\omega')G_2(\omega-\omega')=\int_0^\infty G_1(\sigma)G_2(\sigma)[\delta(\omega-\omega'-\sigma)+\delta(\omega-\omega'+\sigma)]\,d\sigma, \quad (22)$$

where δ is the Dirac delta-function, then

$$\begin{aligned}\langle S_1(t)\,.\,S_2(t-\tau_0)\rangle_{\mathrm{AV}} \sim &\int_{-\alpha/2}^{\alpha/2} P(\omega_0, \theta_l)\,d\theta_l \int_{-\alpha/2}^{\alpha/2} P(\omega_0, \theta_\lambda)\,d\theta_\lambda \\ &\times \int_0^\infty G_1(\sigma)G_2(\sigma)\,d\sigma \int_0^\infty A_1(\omega)A_2(\omega)A_1(\omega-\sigma)A_2(\omega-\sigma)d\omega \\ &\times \{\cos[-(l\omega/c)\overline{\theta_l-\theta_\lambda}-\overline{(l\theta_l/c)+t_0}\,.\,\sigma] \\ &+\cos[-(l\omega/c)\overline{\theta_l-\theta_\lambda}+\overline{(l\theta_\lambda/c)+t_0}\,.\,\sigma]\}. \quad (23)\end{aligned}$$

This expression is valid whatever the form of $A(\omega)$ and $G(\omega)$; but in the only case considered here the pre-detector and low-frequency filter bandwidths both have rectangular amplitude characteristics such that

$$\left.\begin{aligned}&A_1(\omega)\,.\,A_2(\omega)=A^2 \text{ when } \omega_0-\pi B_R<\omega<\omega_0+\pi B_R \\ &A_1(\omega)\,.\,A_2(\omega)=0 \text{ when } \omega<\omega_0-\pi B_R\,;\ \omega_0>\omega_0+\pi B_R\end{aligned}\right\}, \quad (24)$$

$$\left.\begin{aligned}&G_1(\sigma)\,.\,G_2(\sigma)=G^2 \text{ when } \Omega_0-\pi b_V<\sigma<\Omega_0+\pi b_V \\ &G_1(\sigma)\,.\,G_2(\sigma)=0 \text{ when } \sigma<\Omega_0-\pi b_V\,;\ \sigma>\Omega_0+\pi b_V\end{aligned}\right\}. \quad (25)$$

It must be noted that B_R is the width of the pre-detector band common to both receivers, which in general will be less than the pre-detector bandwidth of either receiver separately.

Integrating first over ω and then over σ, and assuming that $b_V \ll B_R$,

$$\begin{aligned}\langle S_1(t)\,.\,S_2(t-\tau_0)\rangle_{\mathrm{AV}} \sim &\int_{-\alpha/2}^{\alpha/2} P(\omega_0, \theta_l)\,d\theta_l \int_{-\alpha/2}^{\alpha/2} P(\omega_0, \theta_\lambda)\,d\theta_\lambda\, B_R b_V A^4 G^2 \\ &\times \cos\left(\frac{\omega_0 l\,.\,\overline{\theta_l-\theta_\lambda}}{c}\right)\frac{\sin[(\pi B_R l\,.\,\overline{\theta_l-\theta_\lambda})/c]}{\pi B_R l\,.\,\overline{\theta_l-\theta_\lambda}/c} \\ &\times \cos\Omega_0\left(t_0+\frac{l\,.\,\overline{\theta_l+\theta_\lambda}}{2c}\right)\frac{\sin \pi b_V[t_0+(l\,.\,\overline{\theta_l+\theta_\lambda}/2c)]}{\pi b_V[(l\,.\,\overline{\theta_l+\theta_\lambda}/2c)+t_0]}. \quad (26)\end{aligned}$$

If the bandwidths B_R and b_V and the time delay t_0 are restricted so that

$$\frac{\pi B_R l\alpha}{c} \ll 1, \quad (27)$$

$$\frac{\pi b_V l\alpha}{2c} \ll 1, \quad (28)$$

$$(\pi b_V+\Omega_0)(t_0+l\alpha/2c) \ll 1, \quad (29)$$

where α is the maximum angular extension of the source, then the correlator output given by eqn. (26) is

$$\begin{aligned}\langle S_1(t)\,.\,S_2(t-\tau_0)\rangle_{\mathrm{AV}} \sim &\int_{-\alpha/2}^{\alpha/2} P(\omega_0, \theta_l)\,d\theta_l \int_{-\alpha/2}^{\alpha/2} P(\omega_0, \theta_\lambda)\,d\theta_\lambda \\ &\times B_R b_V A^4 G^2 \cos\left(\frac{\omega_0 l\,.\,\overline{\theta_l-\theta_\lambda}}{c}\right), \quad (30)\end{aligned}$$

which may be written

$$\langle S_1(t) \,.\, S_2(t-\tau_0) \rangle_{\text{AV}} \sim B_R b_V A^4 G^2 [F^2_{\cos}(\omega_0 l/c) + F^2_{\sin}(\omega_0 l/c)], \quad . \quad (31)$$

where $F_{\cos}(\omega_0 l/c)$ and $F_{\sin}(\omega_0 l/c)$ are defined by eqn. (4).

The output of the correlator may be normalized by dividing by the product of the r.m.s. filter outputs due to the radiation from the source alone. Since each of these outputs is proportional to the total input power to each aerial it follows that their product is proportional to $B_R b_V A^4 G^2 F^2_{\cos}(0)$ and hence $c(l, t)$ the *normalized correlator output* is given by

$$c(l, t) \equiv \frac{[S_1(t) \,.\, S_2(t-\tau_0)]}{\{[\overline{S_1{}^2(t)}]^{1/2} - P_{N1}\}\{[\overline{S_2{}^2(t)}]^{1/2} - P_{N2}\}} = \frac{F^2_{\cos}(\omega_0 l/c) + F^2_{\sin}(\omega_0 l/c)}{F^2_{\cos}(0)} . \quad . \quad . \quad . \quad (32)$$

Comparison of eqns. (32) and (6) shows that, subject to the inequalities (27), (28) and (29), the normalized correlator output is equal to the square of the correlation coefficient $\rho^2(l)$ measured by an ideal ‘ Michelson ’ interferometer of zero bandwidth.

§6. THE EFFECTS OF FINITE BANDWIDTHS AND DIFFERENTIAL TIME DELAYS

6.1. *The Pre-Detector Bandwidth*

The principal effect of the finite pre-detector bandwidth is to introduce a dispersion into the relative phase of the signals from a source of finite size and thereby to reduce the output of the correlator, but this effect is negligible if the inequality (27) is satisfied. It can be shown that this is equivalent to the requirement that the fractional radio-frequency bandwidth shall be small compared with $1/\pi$.

It is also important that the pre-detector characteristics of the two receiving channels should be identical, since any difference in the width of the pass bands will introduce uncorrelated components of the signal and the normalized value of the correlator output will be correspondingly reduced. It also follows that any difference between the frequencies of the local oscillators of the two receivers must be small compared with the pre-detector bandwidths.

6.2. *Differential Time Delays and the Bandwidth of the Low-Frequency Filters*

It is shown in §7 that fluctuations in the measured value of the normalized correlator output are proportional to $(b_V)^{-1/2}$ and thus to obtain the best signal to noise ratio the bandwidth of the low-frequency filters must be kept as wide as possible. A theoretical upper limit to this bandwidth is set by the inequalities (28,) (29), but in practice the bandwidth is restricted to a much lower value by a variety of factors of which the more important are the frequency response of the baseline transmission link and the presence of differential time delays in the two channels.

Since the relative amplitude and phase of the low-frequency components in the two channels must be preserved, any amplitude or phase distortion in the transmission link must be kept to a negligible value.

A difference in the time delays associated with the two channels will introduce a dispersion of the relative phase of corresponding low-frequency components at the correlator, and it follows from eqn. (26) that, in the case of a point source ($\alpha=0$), the presence of a differential time delay t_0 will reduce the correlator output by a factor

$$\cos \Omega_0 t_0 \frac{\sin \pi b_V t_0}{\pi b_V t_0},$$

if it is assumed that the bandwidths are rectangular in shape. The error introduced by a differential time delay t_0 is negligible provided that

$$(\pi b_V+\Omega_0)t_0 \ll 1,$$

as is shown by inequality (29) in the case where $\alpha=0$. The total differential time delay for a point source is given by

$$t_0=\Delta T_D+\Delta T_B+\Delta T_C, \qquad . \; . \; . \; . \; . \; . \; . \quad (33)$$

where $\Delta T_D=[\tau_0-(L \sin \theta_0/c)]$ is the error in compensating for the time delay introduced by the length of the baseline projected in the direction of the source, ΔT_B is the difference in the time delays in the two receiving channels and ΔT_C is the error in compensating for the time delay introduced by the transmission along the baseline. ΔT_D, which depends upon the direction of the source relative to the baseline, is discussed in § 9. ΔT_B, which depends upon the accuracy with which the two receivers are matched, can in practice be made negligibly small. ΔT_C, which depends upon the length of the baseline, is only likely to prove important for very long baselines where there are uncertainties in the time of transmission along the link ; however, even for extremely long baselines, it is unlikely that the low-frequency bandwidth would be restricted by the presence of differential time delays to less than about 1 kc/s.

In the above discussion it has been assumed that the source is a point and the dispersion introduced by its finite angular diameter has been neglected. It follows from eqn. (26) that this dispersion may be represented by an additional differential time delay of the order of $l\alpha/2c$ and this is negligible when inequality (27) is satisfied since $b_V \ll B_R$.

It is also essential that the phase and amplitude characteristics of the low-frequency filters should be identical, since any difference in the width of the two pass-bands will introduce uncorrelated low-frequency components and will reduce the observed value of the normalized correlator output. This requirement is similar to that stated previously for matching the two pre-detector bandwidths.

6.3. *The Bandwidth of the Integrating Circuits*

It is shown in § 7 that the overall signal to noise ratio is independent of the bandwidth of the integrating circuit b_I for a given total time of observation. However, the number of separate readings may be reduced by restricting b_I, and the theoretical limit is set by the requirement that the outputs of the three recorders shall follow the rate of variation of the total power received from the source as it transits the aerial beams. In practice the minimum bandwidth is much greater than this, being determined by the need to recognize such effects as the scintillation of the source or short bursts of interference. These requirements have been found by experience to limit the minimum bandwidth of the integrating circuits to between 1 and 0·1 c.p.s.

§ 7. THE EFFECTS OF RECEIVER AND AERIAL NOISE

The noise generated in the two receivers is completely uncorrelated and hence contributes nothing to the direct current output from the correlator.

It is difficult to calculate the contribution from the 'background radiation' in the general case when the effective temperature in the aerial side-lobes is different from that in the main beam. However when the effective background temperature of the sky is uniform, it can be shown by thermodynamical reasoning that the associated contribution to the correlator direct-current output is proportional to the real part of the mutual aerial impedance and to the effective temperature of the sky. This contribution falls rapidly to zero as the length of the baseline becomes large compared with the aperture of the aerials,* and since the majority of observations are made under these conditions, it will be assumed that the cosmic noise contributes nothing to the direct current output from the correlator.

However, both the receiver and cosmic noise will contribute to the fluctuations in the measured value of the normalized correlator output and also to the r.m.s. outputs of the low-frequency filters.

7.1. *Fluctuations in the Normalized Correlator Output*

If the pre-detector bandwidth B_R is large compared with the bandwidth b_V of the low-frequency filters, the noise outputs from the latter will have a normal distribution with r.m.s. amplitudes proportional to the sum of the noise powers due to the cosmic noise P_C, the receiver noise P_R and the source P_S.

The calculation of the fluctuations in $K(l, t)$, the correlator output, is complicated by the presence in each channel of partially correlated components from the source, but it can be shown by a straightforward extension of the analysis in § 5 that the r.m.s. fluctuations in the correlator output $[K(l, t)]$ are given by

$$\frac{[K^2(l,t)-\langle K(l,t)^2\rangle_{\mathrm{AV}}]^{1/2}}{\langle K(l,t)\rangle_{\mathrm{AV}}} = \left[\frac{b_I}{b_V}\right]^{1/2}\frac{[1+C(l)+(P_{N1}/P_{S1})][1+C(l)+(P_{N2}/P_{S2})]}{C(l)}, \quad . \quad . \quad . \quad (34)$$

---

* The contribution of the cosmic noise to the correlator output is completely negligible as long as the aerial separation exceeds ten times the aerial aperture.

where $P_{N1}=P_{C1}+P_{R1}$, $P_{N2}=P_{C2}+P_{R2}$ and all the band-pass amplitude characteristics are rectangular in shape. However, it is the fluctuations in $c(l, t)$, the *normalized* correlator output, which are of primary interest and these are extremely difficult to evaluate rigorously especially as the three quantities $[S_1(t)S_2(t-\tau_0)]$, $[(\overline{S_1^2(t)})^{1/2}-P_{N1}]$ and $[(\overline{S_2^2(t)})^{1/2}-P_{N2}]$ are not independent. Indeed, when the contribution from the receiver and cosmic noise are small compared with the signal from the source and when the source is unresolved, the correlation between the fluctuations in these quantities is nearly unity, and hence the associated fluctuations in the normalized correlator output are very small. An upper limit to these fluctuations, which is approached asymptotically as $P_N/P_S \rightarrow \infty$, can be found by assuming that the fluctuations in the three records are uncorrelated. In this case the fluctuations in $c(l, t)$ have an approximately normal distribution as long as $b_I \ll b_V$ and their r.m.s. value is given by

$$\frac{\langle c^2(l, t)-C^2(l)\rangle_{\mathrm{AV}}^{1/2}}{C(l)}=\left(\frac{b_I}{b_V}\right)^{1/2}\frac{\{[1+C(l)+(P_N/P_S)]^4+2[1+(P_N/P_S)^4]\}^{1/2}}{C(l)} \quad . \; . \; . \quad (35)$$

in the special case when the receiver gains and noise factors are the same. For $P_N \equiv P_G+P_C \gg P_S$ this expression reduces to

$$\frac{\langle c^2(l, t)-C^2(l)\rangle_{\mathrm{AV}}^{1/2}}{C(l)} \sim \sqrt{\left(\frac{3b_I}{b_V}\right)} \cdot \frac{P_N{}^2}{P_S{}^2C(l)} \cdot \quad . \; . \; . \quad (36)$$

In practice the r.m.s. fluctuations will always be appreciably less than the upper limit given in eqn. (35) since, for all practical values of the signal to noise ratio, there will be a marked correlation between the fluctuations of the three records.

If the normalized correlator output is measured by taking a large number N of independent observations over a period T_0, where $N \simeq 2b_IT_0$, then the r.m.s. error in the result is reduced by the factor $N^{-1/2}=[2b_IT_0]^{-1/2}$. It is therefore independent of the bandwidth of the integrating circuits and depends only upon the length of the observation time.

§ 8. THE EFFECTS OF THE IONOSPHERE

Observations of the scintillation of the discrete sources have shown that there are minor irregularities in the ionosphere which introduce irregular changes in the intensity of the radiation received at the earth's surface. It is to be expected that the use of very long baselines will be further complicated by major differences in the characteristics of the ionized layers above the two receiving sites. An idea of the order of magnitude of these effects can be derived from the following simple analysis.

It is assumed, for simplicity, that the down-coming waves from the source are propagated in a direction *parallel* to the earth's magnetic field through a uniform ionosphere of thickness H. Under these conditions the propagation constant k for a circularly polarized wave may be written

$$k \simeq \frac{\omega}{c}\left[1-\frac{\omega_C^2}{2\omega^2}\left(1\pm\frac{\omega_H}{\omega}\right)\right], \quad . \quad . \quad . \quad . \quad . \quad (37)$$

where ω_C is the critical angular frequency, ω_H is the gyro angular frequency, ω is the angular frequency of the incident wave, and it is assumed that $\omega \gg \omega_H$ and $\omega^2 \gg \omega_C^2$. The choice of sign in (37) depends upon the direction of the rotation of the polarization of the circularly polarized wave. The total change in phase $\Delta\phi$ of a circularly polarized wave crossing the ionosphere, relative to a similar wave in free space is, therefore,

$$\Delta\phi=\frac{H\omega}{c}\left(\frac{\omega_C^2}{2\omega^2}\right)\left(1\pm\frac{\omega_H}{\omega}\right)\text{ radians.} \quad . \quad . \quad . \quad . \quad (38)$$

Substituting very approximate values for the F region ($\omega_C=2\pi\times6\times10^6$, $\omega_H=2\pi\times10^6$, $H=2\times10^5$ m) the total phase shift relative to propagation in free space is about 750 radians at 100 Mc/s, which represents a time delay of 1·2 microseconds. Since in practice the bandwidth of the low-frequency filters is limited to a few kilocycles, it follows from the analysis in §6 that the effects of the maximum differential delay which can be introduced by the ionosphere are negligible at this frequency.

A more serious source of error with long baselines is likely to be the rotation of the polarization of the down-coming waves due to the earth's magnetic field. It follows directly from eqn. (38) that the polarization of a plane wave in the ionosphere is rotated relative to that of a similar wave in free space by

$$\frac{H}{c}\frac{\omega_C^2\omega_H}{\omega^2}\text{ radians,}$$

and, substituting the parameters of the ionosphere assumed previously, the polarization at 100 Mc/s is rotated by about 15 radians. Since the radiation emitted by the discrete sources is unpolarized, a difference of ϕ radians in the polarization of the received signals at each end of the baseline will reduce the normalized correlator output by a factor $\cos^2\phi$. For short baselines this effect should be negligible, but it may prove to be serious for very long baselines. The rotation of the polarization is proportional to $(\omega)^{-2}$ and thus may be reduced by using higher frequencies, but with very long baselines it may be necessary to make use of aerials sensitive to both planes of polarization.

Finally there are the random time-dependent changes in the relative amplitude and phase of the signals at the two receiving sites which are produced by minor irregularities in the ionosphere (Smith 1950, Little and Lovell 1950). At 100 Mc/s these irregularities introduce random changes in phase of the order of one or two radians with corresponding fluctuations of intensity which may be as great as 100%.

It has already been shown that the large phase shift introduced by the whole ionosphere may be neglected if the low-frequency filter bandwidth is suitably restricted, and it follows that the effects of these comparatively small changes of phase will be negligible. The associated amplitude fluctuations will not affect the instantaneous value of the *normalized* correlator output provided that their period is long compared with the response time of the integrating circuits. However, a detailed analysis shows that errors will be introduced if the amplitude fluctuations at the two receiving stations are partially correlated and if their period is comparable with, or shorter than, the response time of the integrating circuits. Since the period of the ionospheric ‘ scintillations ’ is normally of the order of 30 seconds (Maxwell and Little 1952) and since the response time of the integrating circuits is chosen in practice to lie between about 0·1 and 1·0 second, it follows that the new type of interferometer is virtually unaffected by ionospheric ‘ scintillations ’.

§ 9. The Effects of the Rotation of the Earth

Due to the rotation of the earth both the difference in the time of arrival of corresponding signals at the two aerials ($L \sin \theta_0/c$) and the effective length of the baseline ($L \cos \theta_0$) will vary with time.

The rate of change of $L \cos \theta_0$ is a maximum for an east–west baseline and for a source of zero declination, and in that case it is simple to show that the change in the effective length of the baseline may be limited to 1% by restricting the total period of observation to about one hour.

It can also be shown that, for the same direction of the baseline, the effect of the variable time delay is negligible provided that the product of the total period of observation (T_0) in seconds and the low-frequency filter bandwidth (b_V) in c.p.s. is restricted so that

$$b_V T_0 \ll \frac{c}{\pi^2} \frac{T_S}{L \cos \delta}$$

where T_S is the length of a sidereal day in seconds and δ is the declination of the source. For example, for a source of zero declination, a baseline of 100 km and a filter bandwidth of 1 kc/s, the period of observation should not exceed about 1 hour.

§ 10. Discussion

The new type of interferometer described in this paper differs radically from the ‘ Michelson ’ type of instrument. In principle the latter can measure both the phase and amplitude of the Fourier transform of the intensity distribution across the source, whereas the new instrument gives information about the amplitude alone and therefore cannot yield a unique solution to the intensity distribution. It should however be noted that it is not clear how significant this loss of information will prove in practice.

A more important disadvantage of the new instrument is that it is relatively insensitive to weak sources. Thus eqn. (36) shows that, if the power from a source (P_S) is small compared with the sum of the receiver and cosmic noise powers (P_R+P_C), the signal to noise ratio at the correlator output $\propto [P_S/(P_C+P_R)]^2$. Under equivalent conditions the signal to noise ratio of a 'Michelson' interferometer $\propto [P_S/(P_C+P_R)]$ and hence the new instrument is relatively insensitive when $P_S < P_C+P_R$.

The most obvious advantage of the new instrument is that the technical problem of combining the signals from two widely spaced receivers is relatively simple, since there is no need to maintain the high degree of phase stability in the link which is required if the radio-frequency phase of the signals must be preserved. The simplicity of operation and the reliability of the instrument have been shown by an extensive series of measurements of the distribution of intensity across the intense sources in Cygnus and Cassiopeia using baselines of between 300 m and 15 km at 125 Mc/s (Hanbury Brown, Jennison and Das Gupta 1952, Jennison and Das Gupta 1953), and there appears to be no practical reason why the baseline should not be extended further. Indeed it should be possible to eliminate the transmission link altogether and to record the low-frequency outputs of the two receivers on, say, magnetic tape. The records could be compared subsequently in a correlator and it seems that by the use of this technique a baseline of indefinite length could be used.

A second important advantage of the new instrument is that its accuracy should be independent of scintillations caused by the ionosphere so long as the bandwidth of the integrating circuits is not made too small, and this property should prove particularly valuable when operating at the longer wavelengths. Practical experience with the instrument on short baselines has already confirmed that it will operate satisfactorily in the presence of large fluctuations introduced by the ionosphere, even when these fluctuations are partially correlated at the two receiving sites.

The rotation of the polarization of the radiation from the source due to the ionosphere introduces an additional complication into the use of very long baselines. This effect, as has been pointed out in § 8, can be reduced by decreasing the wavelength or by using aerials which accept both planes of polarization.

The use of the 'Michelson' interferometer at radio wavelengths is a logical extension of optical practice and it is interesting to enquire whether the principle of the new type of interferometer can in turn be applied to visual astronomy, since in this way it might be possible to increase the resolving power and mitigate the effects of atmospheric turbulence. A preliminary examination of this question, which will be discussed in a later communication, suggests that the technique cannot be applied to optical wavelengths and that it breaks down due to the limitations imposed by 'photon noise'.

REFERENCES

BOLTON, J. G., and STANLEY, G. J., 1948, *Nature, Lond.*, **161,** 312.
EINSTEIN, A., 1915, *Ann. d. Physik*, **47,** 879.
HANBURY BROWN, R., JENNISON, R. C., and DAS GUPTA, M. K., 1952, *Nature, Lond.*, **170,** 1061.
JENNISON, R. C., and DAS GUPTA, M. K., 1953, *Nature, Lond.*, **172,** 996.
JENNISON, R. C., and DAS GUPTA, M. K., in preparation.
LITTLE, C. G., and LOVELL, A. C. B., 1950, *Nature, Lond.*, **165,** 422.
MAXWELL, A., and LITTLE, C. G., 1952, *Nature, Lond.*, **169,** 746.
MCCREADY, L. L., PAWSEY, J. L., and PAYNE-SCOTT, R., 1947, *Proc. Roy. Soc.* A, **190,** 357.
RICE, S. O., 1944, *Bell Syst. Tech. J.*, **24,** 306.
RYLE, M., and SMITH, F. G., 1948, *Nature, Lond.*, **162,** 462.
RYLE, M., 1950, *Rep. Prog. Phys.*, **13,** 184 (London : Physical Society).
SMITH, F. G., 1950, *Nature, Lond.*, **165,** 422.
STANLEY, G. J., and SLEE, O. B., 1950, *Aust. J. Sci. Res.* A, **3,** 234.
VON LAUE, M., 1915, *Ann. d. Physik*, **47,** 668.

LXXV. *The Natural Radioactivity of Lutetium*

By D. Dixon, A. McNair and S. C. Curran
Department of Natural Philosophy, The University, Glasgow, W.2*

[Received March 15, 1954]

Abstract

The radiations from the decay of naturally occurring ^{176}Lu are studied in detail. The β^--spectrum, which was found to be of allowed shape, was investigated using internally mounted sources of thickness $0{\cdot}49$ mg/cm^2 and $0{\cdot}149$ mg/cm^2 in a well-shielded proportional tube spectrometer. A half-life of $4{\cdot}56 \pm 0{\cdot}3 \times 10^{10}$ years was obtained for the β-transition with a maximum energy of 425 ± 15 kev and the log *ft* value, 18·75, suggests a 3rd or 4th forbidden transition. Strong electron peaks arising from the internal conversion of an 89 kev γ-ray were observed and a K-capture branching ratio of $3 \pm 1\%$ is derived from a study of the intensity and nature of the L x-rays accompanying the disintegrations.

NaI scintillation counters were used for the measurement of γ-rays of energy 310 ± 10 kev and 190 ± 10 kev and the evaluation of their internal conversion coefficients classifies them as E.Q. transitions. The intensities of the γ-quanta and the occurrence of γ–γ coincidences conclusively establish the decay scheme as suggested by Goldhaber and Hill, in which the β^--transition is followed by the γ-rays in cascade. The energies and character of the γ-ray transitions are in close agreement with those predicted from the Bohr–Mottelson rotational model of the nucleus (Bohr and Mottelson 1953).

§1. Introduction

The position of ^{176}Lu in the nuclear table is of particular interest. This isotope, of even A and odd Z, and of $2{\cdot}6\%$ relative abundance (Hayden *et al.* 1950) is the centre of one of three naturally occurring neighbouring isobars and throughout the nuclear table there exist only four such isobaric triplets. ^{176}Lu is further distinguished by its unusually high spin value, $\geqslant 7$ (Schüler and Gollnow 1939). Its occurrence in nature, alongside its neighbouring stable isobars, can be explained by its instability to β-decay and K, L capture with lifetimes $\sim$ age of the earth. The β^--decay of natural lutetium to ^{176}Hf has now been firmly established with a half-life $> 10^{10}$ years and the transition leads to an even–even nucleus far removed from any of the generally accepted closed shell groups. As is to be expected, in view of the very large spin change involved in a ground state to ground state transition an excited state of ^{176}Hf is formed and the succeeding γ-rays, since reported as proceeding

---

* Communicated by the Authors.

to the ground state, have given evidence in support of the Bohr–Mottelson rotational model of the nucleus.

The β^--decay of ^{176}Lu was first reported by Libby (1939), with an end point energy of 220 kev obtained by absorption methods. Later investigations by Flammersfeld (1943, 1947) gave the β-ray end point as 400 kev with a half-life of $2{\cdot}4\times 10^{10}$ years and the process of K-capture involving the emission of a γ-radiation of energy 260 kev, was estimated to account for 67% of the disintegrations. More recent unpublished work by Scharff–Goldhaber agreed with the 400 kev β-ray end point but failed to reveal any K-capture branch in the decay. Two γ-rays of 270 kev and 180 kev energy were reported, together with one strongly internally converted γ-ray of 89 kev energy. Measurement of the K/γ ratio for the 89 kev γ-ray, regarded as identical with that occurring in the isomeric decay (3·75 h) of ^{176}Lu, was made by McGowan (1952) who identified this γ-ray as an E.2 transition. In the decay scheme of ^{176}Lu proposed by Goldhaber and Hill (1952), spin values and parities of 2+, 4+ and 6+ were assigned to excited states of ^{176}Hf and the 270 kev, 200 kev and 89 kev γ-rays were assumed to follow in cascade the 400 kev β-ray transition. Arnold and Sugihara (1953) using NaI scintillation counters and an end window G.M. counter, obtained a count rate for the electromagnetic radiations twice that of the β-ray count rate as observed by Suttle (unpublished). Energy values of the γ-rays were given as 200 ± 20 kev and 300 ± 20 kev and a peak corresponding to the K x-rays of Hf was attributed to the internal conversion of the γ-rays. Coincidence measurements were said to show the occurrence of two γ-rays in cascade of about 250 kev energy and β–γ coincidences were observed.

The interest devoted to the decay of ^{176}Lu has thus been considerable and it was with the intention of providing the β^--and γ-ray spectra that the authors included this investigation of the natural decay of ^{176}Lu in their study of the natural radio-elements. Previous investigations of the β-rays occurring in the decay have been confined to end point measurements, and it seemed necessary to establish conclusively the cascade process proposed for the γ-radiations by careful measurement of the intensities of the β-rays and the γ-quanta. It was hoped to complete the spin assignments to the excited levels of ^{176}Hf from a knowledge of the shape and degree of forbiddeness of the β-ray spectrum, together with the measurement of the internal conversion of the higher energy γ-rays. In view of the agreement between reported γ-ray energies and those predicted from the Bohr–Mottelson rotational model of the nucleus, this is of added importance. An accurate measurement of the intensity and energy of the L x-rays occurring in the disintegrations would confirm or rule out the possibility of K- or L-capture.

§ 2. EXPERIMENTAL ARRANGEMENT

The same proportional counter and G.M. counters arranged in anticoincidence were used as in previous experiments and are to be described elsewhere. Improvements in the equipment and experimental technique have reduced the background count of the proportional counter from 1250 C.P.M. to below 20 C.P.M. and the advantages of such a system in the detection of weak radiation are detailed in an earlier paper (Curran *et al.* 1951). The proportional tube spectrometer was of the end-corrected type (Cockroft and Curran 1951), and had a maximum internal source area of ~ 1100 cm^2. Two rings of G.M. counters, 72 cm in length, surrounded the spectrometer and this was enclosed in a lead castle with approximately 8 in. lead and 1 in. iron on all sides. The apparatus was situated in the most shielded part of the building some 10 ft. below ground level. The proportional counter was filled to 4 atm with a mixture of argon and methane. Lutetium oxide of the highest spectrographic purity was used in the source preparations. The first was deposited on the removable steel lining of the counter as $LuCl_3$ of thickness 0·49 mg/cm^2 over an area ~ 650 cm^2, which was well within the effective counting volume of the tube. The second was spread over the lining in the form of finely divided Lu_2O_3 powder, suspended in amyl acetate, in which was dissolved a minute trace of Durofix to act as an adhesive agent. This source was of thickness 0·149 mg/cm^2.

The counting rates obtained with the above sources were 480 C.P.M. and 200 C.P.M. respectively, thus giving very favourable source/background count ratios.

§ 3. Spectrum Analysis

Photographic recording of the pulses observed on a cathode ray tube was followed by amplitude analysis. The amplifier gain was set to include three different regions of the spectrum and the complete spectrum is shown in fig. 1. With both sources the spectrum shape was essentially the same with the β-ray end point occurring at ~ 500 kev. The presence of an electron peak B, at ~ 78 kev, corresponding to the internal conversion in the L and M shells of an 89 kev γ-ray, is clearly indicated and further small peaks at C, 125 kev, D, 180 kev and E, 300 kev were observed using both sources. The first two of these can be ascribed to the K and L internal conversion of a 190 kev γ-ray and the last to L conversion of a 310 kev γ-ray. Observations in the lower energy region of the spectrum were made with higher amplifier gain and the results fitted to the main graph. This region shows the electron peak A, due to K conversion of the 89 kev γ-ray and a peak due to L x-rays of Hf.

A Fermi plot of the spectrum is shown in fig. 2. This is seen to be an almost straight line above ~ 70 kev, which is surprising in view of the complex nature of the proposed decay scheme. According to this, a proportion of the β-rays should give pulses coincident with those due to electrons (and x-rays), arising in the internal conversion of the γ-rays, particularly that γ-ray of energy 89 kev, which produces electrons of energy ~ 80 kev. The superposition of an allowed spectrum, extending from zero energy to $E_{\max}=425$ kev with one extending from 80 kev to $(80+425)$ kev (due to the 80 kev electron line) would, however, give a

Fig. 1

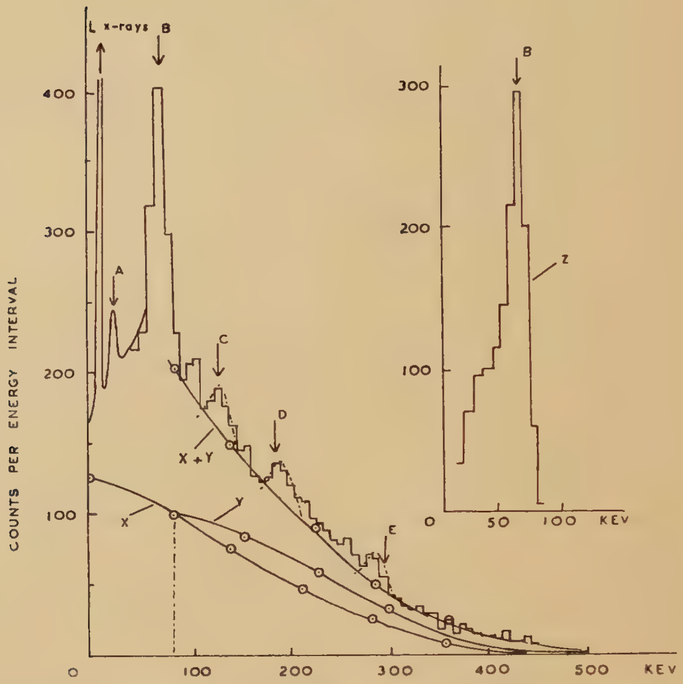

The spectrum of ^{176}Lu using a 0·149 mg/cm^2 source. The continuous spectrum is shown resolved into its three main components. Curve X is the theoretical allowed shape, curve Y the spectrum carried out to higher energies by the electron peak B. This electron peak is resolved in full in curve Z, shown in the inset figure.

Fig. 2

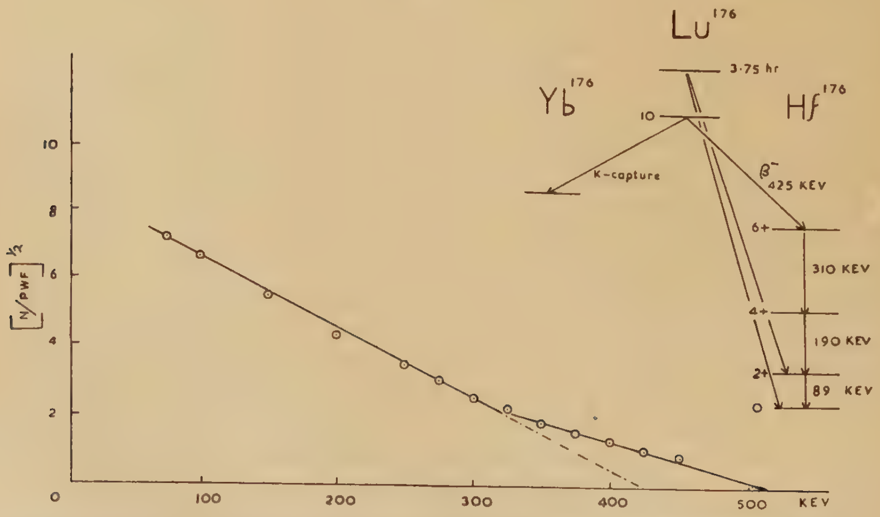

The Fermi plot of the β-spectrum and the proposed decay scheme of ^{176}Lu.

straight line plot over the whole region from 80 kev to 350 kev and a further straight line plot between ~350 kev and the end point corresponding to the β-ray maximum energy + the electron line energy. From the above similarity between the experimental and theoretical curves we are led to the conclusion that the β-ray spectrum is of allowed shape with $E_{\mathrm{max}}=425\pm15$ kev. The intensities of the two component spectra can be shown to be in the ratio 4 : 3. This follows from a knowledge of the internal conversion coefficient for the 89 kev γ-ray and the total observed count rate, corrected for backscattering. The component spectra are thus resolved assuming an allowed shape and the resultant composite graph lies close to the experimental points, thus confirming the shape of the β-ray spectrum.

Accurate measurements of the counting rates at high amplifier gain showed that the rate was practically independent of voltage over a range of several hundred volts and down to pulses of energy 200 ev. The difference count with and without source of total mass 0·2141 g of Lu_2O_3 was 480 per minute, measured to a statistical accuracy of 2%. Corrections due to self absorption in the source were small and the 25% correction due to backscattering of particles in the source and support was derived from the as yet unpublished work of J. G. Balfour, of this department, on the backscattering of electrons in solid supports. Allowing for the 2π geometry, the mode of decay and isotopic abundance, the half-life, τ, was calculated as $4{\cdot}56\pm0{\cdot}3\times10^{10}$ years. This corresponds to a value of log ft of 18·75 for a 425 kev β-ray end point and appears to classify the β-ray transition as at least 3rd forbidden, in the same category as ^{87}Rb.

§ 4. INTERNAL CONVERSION OF γ-RAYS

The electron lines due to the internal conversion of the 89 kev γ-ray are shown in greater detail, using a higher amplifier gain, in fig. 3. The relative intensities of the electrons from the 89 kev γ-ray produced in the 3·75 h decay of the artificially produced ^{176}Lu isomer have been studied by Mihelich and Church (1952). Their results are tabulated below.

γ-ray	ϵ^- kev		Rel. int.	K/L exptl.	K/L emp.
89 kev γ-ray from the isomeric decay of ^{176}Lu (3·75 h)	23·09	K	0·24	E.2 0·14	7·5 M.1 0·14 E.2
	78·12	L_{II}	0·71		
	79·33	L_{III}	1·0		
	86·78	M_{III}	0·84		
	88·4	N_{III}	0·23		

The complete resolution of all those electron lines was not achieved in our experiments with the natural element, due to the necessary source thickness, but the L_{II}, L_{III} and M_{III} electron line energies and their relative intensities are sufficiently accurate to identify this γ-ray with that following the isomeric decay of ^{176}Lu. Using the above data on the relative intensities of the electron lines and taking the value of $e_K/\gamma=1{\cdot}3$ (McGowan 1952), it was then possible to calculate the number of disintegrations occurring per hour corresponding to the observed count rate and to deduce the magnitudes of the electron peaks (both K and L internal conversion), and the L x-ray peak.

Fig. 3

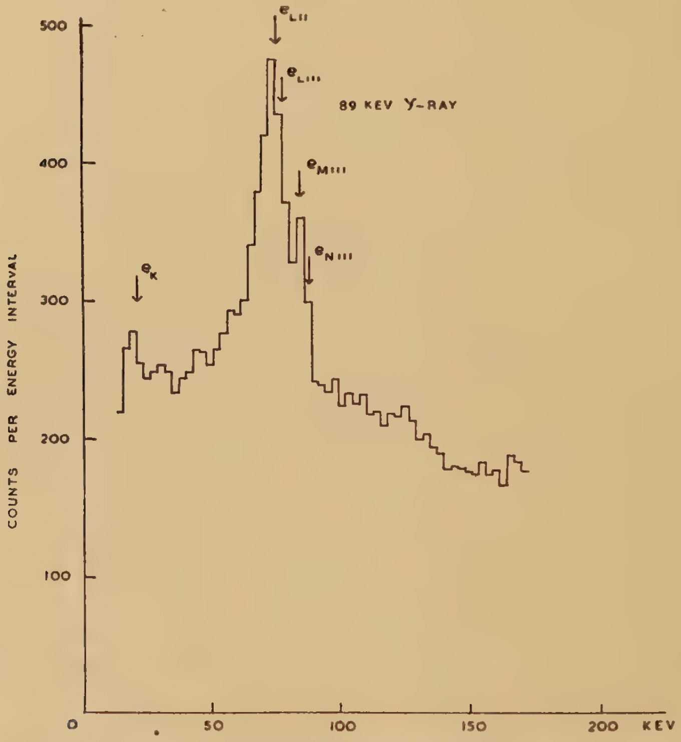

Electron peaks due to the internal conversion of an 89 kev γ-ray in the K, L, M and N shells using a 0·149 mg/cm^2 source.

The search for the 89 kev γ-ray and the K x-rays of Hf was made over a period of 6 hours using a 500 mg/cm^2 steel lining to cut out the β-rays. The results of this experiment are shown in fig 4, which reveals the presence of the 89 kev γ-ray and K x-rays in intensities comparable with those calculated by the above method.

Anticipating our results on the detection of the γ-rays using NaI scintillation counters where γ-rays of energy 190 kev and 310 kev were found to be in coincidence with each other, an estimate was made of the K and L internal conversion of the higher energy γ-rays. The values of the K internal conversion coefficients obtained were compared with those evaluated theoretically by Rose *et al.* (1951) for M.D., E.D. and E.Q. transitions. Despite the obvious uncertainty of an accurate measurement of the magnitudes of these electron peaks the results obtained using the spectra from both sources were markedly in favour of E.Q. transitions. The following table gives the estimated number of counts in the electron peaks.

Fig. 4

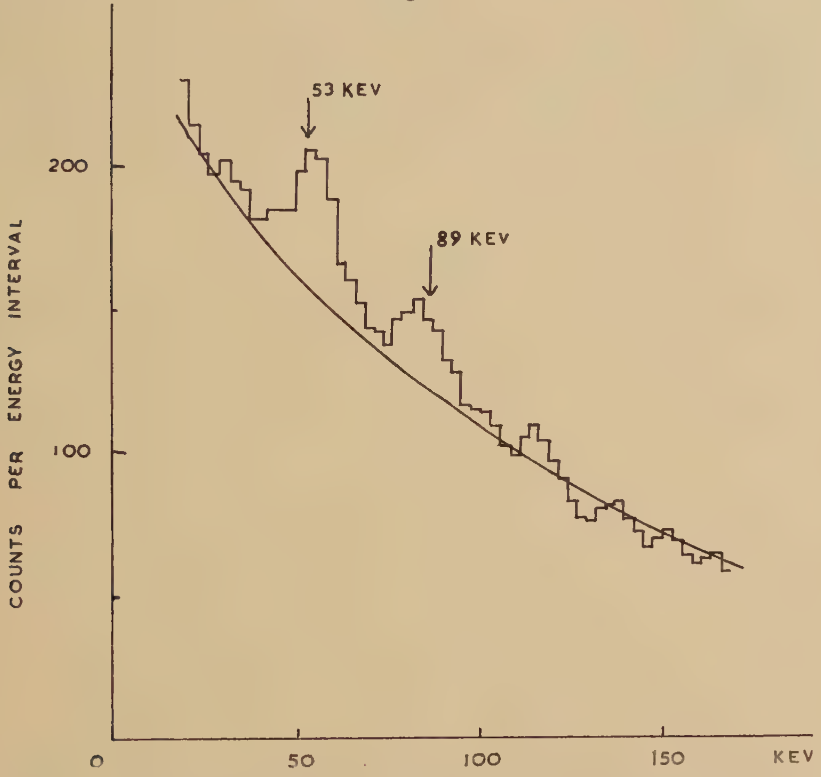

The γ-ray spectrum obtained with the proportional counter using a steel absorber (500 mg/cm^2) over the source (0·49 mg/cm^2).

γ-ray energies	No. of counts observed in e_K peaks	Theoretical estimate of no. of counts in e_K peaks		
		E.Q.	E.D.	M.D.
190 kev	120	145	25	750
310 kev	20	25	16	188

The spins and parities of the excited states of ^{176}Hf corresponding to the above γ-ray transitions are assigned as in the decay scheme shown in fig. 2.

§ 5. L X-RAYS

The proportional counter filled to a pressure of 4 atmospheres of Argon is well suited to the measurement of low energy x-rays ~10 kev, originating from an internally mounted source. Its efficiency of detection is high ~97% and the energy resolution is good, ~12% width at half maximum height. The L x-rays of Hf arising in K and L internal conversion of the 89 kev γ-rays and to a lesser extent in the conversion of the higher energy γ-rays are emitted coincidently with conversion electrons and beta particles, so that only one-eighth of such x-rays are unaccompanied by other particles. On the other hand, should K-capture occur in the decay of ^{176}Lu, half of the L_{II} L_{III} x-rays following these events can be recorded as isolated x-ray peaks. This situation, which depends upon the integral behaviour of the proportional counter, is very favourable to the measurement of a possibly weak K-capture branch in the decay scheme, even when its presence tends to be masked by L x-rays of Hf arising otherwise.

Fig. 5

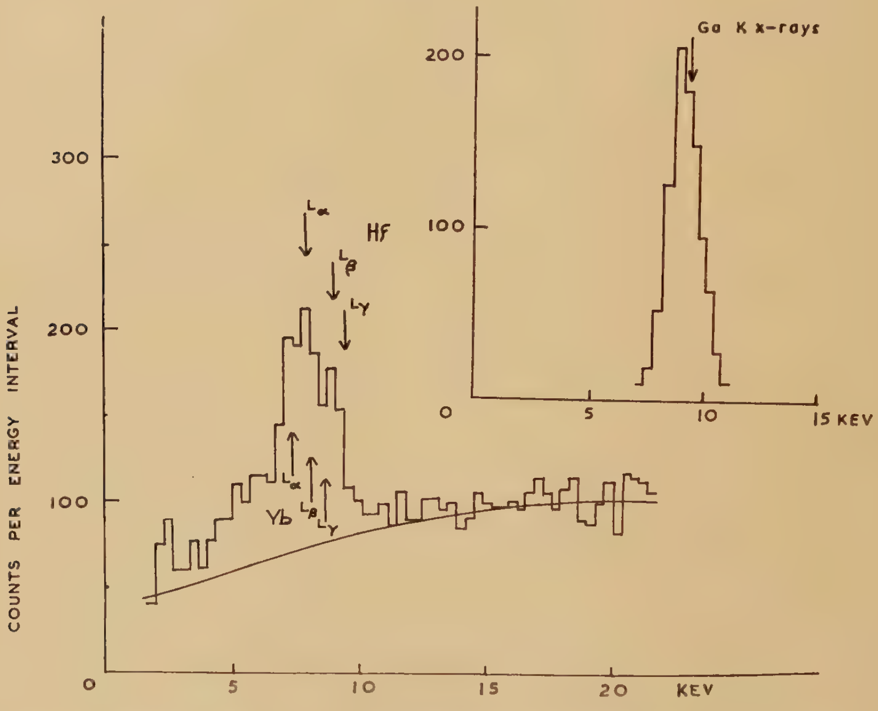

L x-rays observed with ^{176}Lu. The inset figure shows a Ga K x-ray peak for comparison.

Evidence for the existence of a K-capture branch rests partly on the width of the observed L x-ray peak, fig. 5, compared with the Ga K x-ray calibration and would be compatible with the presence of L_{II} L_{III} x-rays of Hf and L_{III} L_{II} x-rays of Yb in the ratio 5 : 1. The contribution to the x-ray peak of Lu L x-rays from external γ-ray conversion and from β-ray excitation we know to be negligible. Assuming the fluorescence yield to be 0·20 for Hf L x-rays (Kinsey 1948), further agreement is obtained between the number of L x-rays due to K and L internal conversion of the γ-rays and the number of L x-rays observed in the peak, allowing ~15% of the peak intensity due to x-rays following K-capture. This gives the K-capture/β^- ratio as $3 \pm 1\%$.

§ 6. γ-RAY DETECTION WITH SCINTILLATION COUNTERS

Insufficient evidence regarding the decay scheme of ^{176}Lu was available from investigations using the proportional counter to enable us to confirm with certainty the decay scheme suggested by Goldhaber and Hill. The lack of accurate quantitative data concerning the γ-ray spectrum and the nature of the γ–γ coincidences seemed to warrant a reasonably detailed study of the electromagnetic radiations accompanying the decay of ^{176}Lu.

Fig. 6

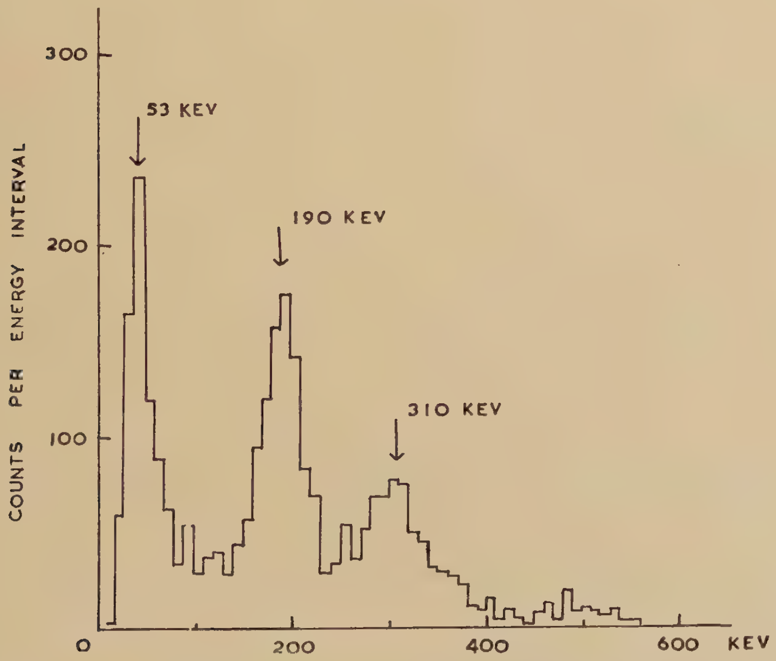

γ-ray spectrum from ^{176}Lu obtained with a scintillation counter (NaI).

In all the γ-ray experiments cylindrical NaI crystals ¾ in. diameter and ¾ in. length were used with standard 14-stage E.M.I. photomultipliers. The crystals, surrounded by the aluminium light reflectors, were placed in perspex containers and the source of Lu_2O_3 could be mounted in well defined positions in the ends. The crystals and photomultipliers were shielded from external radiations by 8 in. of lead on all sides and this reduced the background count rate from ~2000 C.P.M. to below 25 C.P.M. The thickness of perspex and aluminium was sufficient to stop the most energetic β-rays and the detection efficiency for the γ-rays was calculated from the known geometry of the source mounting.

Fig. 7

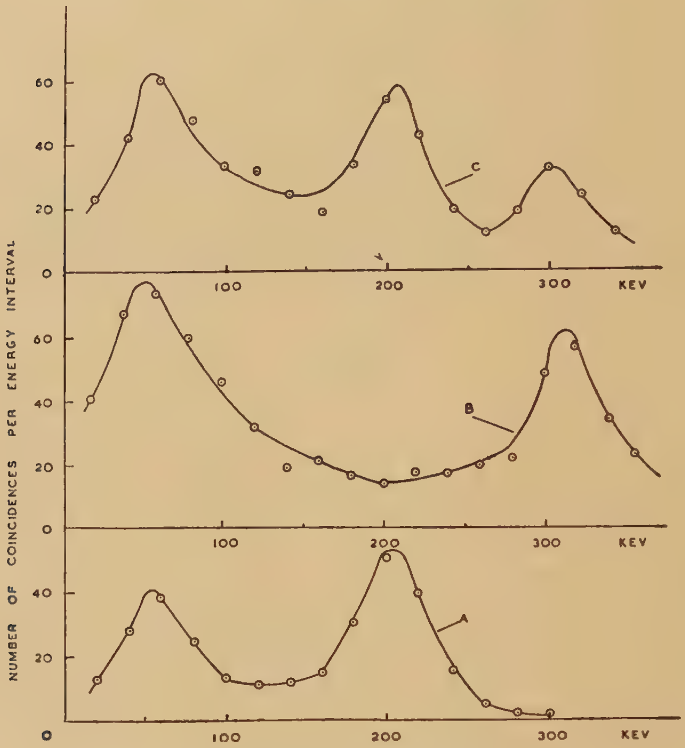

γ–γ coincidences obtained with ^{176}Lu.
Curve A—γ-ray spectrum in coincidence with 300–320 kev γ-rays.
Curve B—γ-ray spectrum in coincidence with 180–200 kev γ-rays.
Curve C—γ-ray spectrum in coincidence with 80–100 kev γ-ray.

The pulses from the photomultipliers after amplification were passed through a pulse lengthening and brightening circuit and then displayed on the screen of a cathode ray tube, photographed and the film subsequently analysed. The 280 kev γ-ray and the K x-rays from ^{203}Hg were used in the calibration of the scintillation counters.

The results of the film analysis are shown in fig. 6, where γ-ray peaks of 310±10 kev and 190±10 kev stand out clearly. A strong x-ray peak at 53 kev corresponding to Lu K x-rays was observed, arising principally from the absorption of the γ-rays in the source of thickness 0·45 g/cm^2.

The absence of 89 kev γ-rays confirms their high internal conversion. An evaluation was made of the number of 190 kev and 310 kev γ-quanta recorded in the experiment. Allowing for absorption, detection efficiency and the relative K and L internal conversion coefficients, agreement between them was obtained to within a few per cent of the value for the total number of disintegrations occurring in the same time.

The γ–γ coincidence experiments were undertaken to establish conclusively the occurrence of the 310 kev and 190 kev γ-rays in coincidence, as was strongly indicated from the determination of the individual absolute γ-ray counting rates. The source was mounted between two identical NaI crystals and the pulses from the photomultipliers were, as before, led through separate pulse lengthening and brightening circuits. The brightened pulse heads from each photomultiplier were displayed on the cathode ray tube using both X and Y deflection simultaneously. Each spot on the resulting pattern displayed the quantum energies of any two γ-quanta which were detected simultaneously. The full energy scan in both X and Y directions was employed to cover all possibilities in γ–γ, x–x, and γ–x coincidences. The resolving time of the electronic arrangement was $\sim 5\,\mu$sec, but with the low counting rates obtained ($\sim$180 C.P.M.) this resolution was satisfactory, and the whole γ–γ spectrum could be studied. Sections of the energy scan taken over ranges 80–100 kev, 180–200 kev, and 300–320 kev are shown in fig. 7, and the coincident γ-rays are clearly evident. The 89 kev γ-ray, too weak in intensity to be obvious in the γ-ray spectrum, are shown coincident with Lu K x-rays, due to γ-ray absorption, and with 190 kev and 310 kev γ-rays.

§ 7. DISCUSSION AND CONCLUSIONS

The excited states of ^{176}Hf have been used in support of the Bohr–Mottelson theory. In this respect the nucleus is of special value and it is particularly gratifying that the present rather detailed tests applied to the disintegration scheme have completely verified the picture, fig. 2. The degree of agreement between present results and theory is as close as indicated in the following table.

Excited states of ^{176}Hf	E.2	E.4	E.6
Experimental values	89 kev	279±10 kev	589±20 kev
Theoretical values given by $E_I = \hbar^2/2gI(I+1)$	(89 kev)	296 kev	623 kev

Measurements of the spin of ^{176}Lu gives the value 7 and 10±1, the latter value suggested by Klinkenberg (1951) from an analysis of the measured magnetic moment on the basis of j–j coupling. The continuous beta-spectrum seems of allowed shape and the log ft value 18·75 suggests 3rd or 4th forbiddenness. The assumption of a spin value of 10 for the ground state of ^{176}Lu together with even parity means that the beta transition corresponds to $\Delta I=4$, no. This would seem reasonable in view of the observed allowed shape and the measured high log *ft* value of 18·75. It appears unlikely that the transition corresponds to $\Delta I=3$, yes, which has been found to apply to the decay of ^{87}Rb (log $ft=17{\cdot}6$) and there to correspond to a shape requiring the 3rd forbidden correction (Tomozawa *et al.* 1952). It seems that the decay study is completely consistent with the allocation of the very high spin value of 10 to the ground state of ^{176}Lu.

The decay scheme, elucidated above, indicates that $3\pm1\%$ of the disintegrations proceed via K-capture to ^{176}Yb. Provided this nucleus is stable against β^--decay this process of K-capture in the decay of ^{176}Lu should be energetically possible. The measured K-capture intensity corresponds to a partial half-life of $1{\cdot}5\times10^{12}$ years.

We should like to thank Professor P. I. Dee for his interest and encouragement throughout the course of this research, and Mr. A. T. G. Ferguson for assistance in the γ-ray energy measurements. One of us (A.M.) is indebted to the D.S.I.R. for a financial grant.

REFERENCES

Arnold, J. R., and Sugihara, T., 1953, *Phys. Rev.*, **90**, 332.
Bohr, A., and Mottelson, B. R., 1953, *Phys. Rev.*, **90**, 717.
Cockroft, A. L., and Curran, S. C., 1951, *Rev. Sci. Instrum.*, **22**, 37.
Curran, S. C., Dixon, D., and Wilson, H. W., 1951, *Phil. Mag.*, **43**, 82.
Flammersfeld, A., 1947, *Z. Naturforsch.*, **2a**, 86.
Flammersfeld, A., and Mattauch, J., 1943, *Naturwiss.*, **31**, 66.
Goldhaber, M., unpublished.
Goldhaber, M., and Hill, R. D., 1952, *Rev. Mod. Phys.*, **24**, 179.
Hayden, R. J., Hess, D. C., and Inghram, M. G., 1950, *Phys. Rev.*, **77**, 299.
Kinsey, B. B., 1948, *Canad. J. Res.*, **26**, 404.
Klinkenberg, P. F. A., 1951, *Physica*, **17**, 715.
Libby, W. F., 1939, *Phys. Rev.*, **56**, 21.
McGowan, F. K., 1952, *Phys. Rev.*, **87**, 542.
Mihelich, J. W., and Church, E. L., 1952, *Phys. Rev.*, **85**, 691.
Rose, M. E., Goertzel, G. H., and Spinrad, B. I., 1951, *Phys. Rev.*, **83**, 79.
Schuler, H., and Gollnow, H., 1939, *Zeits. f. Physik*, **113**, 1.
Tomozawa, V., Umezawa, M., and Nakamura, S., 1952, *Phys. Rev.*, **86**, 791.

LXXVI. *Wave Motions and the Aerodynamic Drag on a Free Oil Surface*

By J. R. D. Francis
Imperial College, London*

[Received March 12, 1954]

Summary

Laboratory experiments are described in which air is blown over a viscous oil in a wind tunnel. At low windspeeds no waves at all appear on the surface, but at a sharply defined critical windspeed small ripples appear, some of which are unstable and grow quickly. The phenomenon is thought to be the instability predicted by Kelvin, which is not observed clearly on the sea. The sort of waves which grow by Jeffreys' 'sheltering' process do not appear until a higher windspeed than the critical one. The aerodynamic drag on the oil surface was also measured, and it appears that once the critical windspeed has been exceeded, the oil acts rather similarly to water, so far as drag forces are concerned.

§ 1. Introduction

The mechanism of the generation of waves on the sea by wind has been investigated by Kelvin and Helmholtz (quoted by Lamb 1932), and by Jeffreys (1925). The former, assuming two superposed perfect fluids of different densities in relative motion, examined the stability of a small perturbation wave at the interface. The wave shape in the lower fluid causes a local acceleration in the faster moving upper fluid, and consequently a local decrease of pressure. If the upward force due to this pressure is greater than the downward gravity force of the wave, then the wave will be unstable and will grow: It was found that for the water–air case the first waves to become unstable were those of 1·8 cm wavelength, travelling at 0·8 cm sec^{-1} when the windspeed is 660 cm sec^{-1}. These computed measurements are clearly at variance with the facts, for the first waves are seen on the sea at a windspeed of about 110 cm sec^{-1} and are about 8 cm wavelength. To account for the discrepancy, Jeffreys advanced his 'sheltering' theory in which the stability of a perturbation wave is again studied, this time by finding the energy passed into the wave by the wind pressures on it, and equating it to the energy dissipated in the wave by the viscosity of the water. Calculation of the former energy requires the assumption of an asymmetry of the pressure on front and rear of the wave; Jeffreys does this by assuming that a part of each wave is sheltered from the full wind velocity by the presence

---

* Communicated by the Author.

of the previous wave crest, giving a constant pressure there ; the proportion of the wave thus sheltered is defined by the 'sheltering' coefficient which cannot be directly measured. Instead, the observed wind at which waves just appear is used to find the coefficient, which proves to be about 0·3 of the whole wavelength, a not unreasonable proportion. Further, the use of this value gives a wavelength of 8 cm at the initiation, in close agreement with observation.

In view of the apparent success of the 'sheltering' theory, it seemed for some years that the Kelvin–Helmholtz instability was irrelevant, and for some reason absent from the water–air boundary. However, recently Munk (1947) and Roll (1951) have pointed out that the 660 cm sec^{-1} windspeed predicted as critical by Kelvin–Helmholtz is associated with several phenomena on the sea surface. The number of breaking waves ('white caps') suddenly increases ; the convection processes as shown by the soaring of sea-gulls seem to change ; and the evaporation suddenly increases. A fourth phenomenon, a sudden increase of wind drag, is disputed, and is discussed later. Tentatively, Munk ascribes all these to a sudden change taking place in the airflow over the waves, the interface becoming aerodynamically rough, with the troughs of the waves being filled by large air eddies ; and Munk further believes that the change of properties of the interface is due to the sudden initiation of unstable Kelvin–Helmholtz waves.

If this were so, and there were no trough eddies in the range of wind speeds from 110 cm sec^{-1} to 660 cm sec^{-1} the 'sheltering' theory would not be tenable, for a constant pressure on part of the wave implies the breakaway of the airflow, and an eddy. An easy test might seem to be to observe if trough eddies are present or not. This test is in fact a most difficult task, for the wind speeds are too high for the usual flow visualizers to be used ; further, both waves and water are moving relative to a fixed observer so the interpretation of photographs of the flow visualizers is much more complicated than in the usual solid boundary case. Finally, droplets of water on the glass walls of wind tunnels also confuse the records. Consequently, this direct method of determining the aerodynamic properties of a water surface has not yet given a definite answer. Some clues, however, can be obtained from wind tunnel experiments with an air-oil system, the viscosity of the oil being much greater than that of water. In this way, the 'sheltering' theory waves should not start until a much higher windspeed is reached ; so high indeed, that the Kelvin instability, if real, should occur first, and thus may be seen independently of 'sheltering' theory waves.

§ 2. Wind Tunnel Experiments

(*a*) *Observations on the Generation of Waves*

The experiments were carried out in a 7 m long wind tunnel, 7·6 cm wide and 38·1 cm deep with glass sides (Francis 1951). Air can be drawn through it by a fan at the lee end, and the wind speed was measured 4·2 m from the windward end by a Pitot-static tube, 0·3 cm head diameter, projecting from the roof. The oil was kindly given by the Shell Oil Company, and was defined as S2883 oil; the density was 0·875, the viscosity was 2·2 poise at room temperature, and the surface tension was 34 dynes cm^{-1}. The oil depth above the bottom of the tunnel was 15 cm and the difference of level of the oil surface along the tunnel when the wind blew was measured by two micrometer point gauges in stilling wells connected to pressure tappings in the floor.

At low windspeeds there were no waves on the oil surface at all, not even the small smooth-sided ripples seen on the sea. At a windspeed of 967 cm sec^{-1} at 8 cm above oil level a most remarkable instability shows itself, as follows :—

First it was noticed that a train of tiny ripples had started in a position near the lee end of the tunnel. They were about 1 cm wavelength, travelled at about 1 cm sec^{-1}, and their height was so small that their profile was obscured by the oil meniscus on the glass side of the tunnel; their presence could only be seen by the reflection of light from their sides. Then, quite suddenly, one of the ripples would become unstable and grow much larger, being accelerated by the wind action so that it rushed ahead of the original train of ripples. This is shown in the photograph, fig. 1 (Plate 21), which was taken obliquely, looking both through the glass side of the tunnel and also upwind. The succession of cine photographs in fig. 2 (Plate 22), shows how the unstable wave grows with explosive suddenness. The photographs were taken through the side of the tunnel, at a speed of 24 frames sec^{-1}, and it will be seen that the wave achieves its greatest height in about 6–8 frames, a time of about 0·25 sec. The single large wave thus generated runs on down wind to the lee end of the tunnel where it dissipates its energy on a shingle beach. There may or may not be a second single wave running in the tunnel at this moment; the spacing between waves seems to be entirely random and several seconds may elapse before another wave behaves similarly.*

With a slight increase of windspeed the point of instability moves rapidly upwind, and more than one unstable wave will be travelling at any instant of time. Increasing the wind speed still further transforms the single waves into a whole train of waves which have the same appearance as water waves, and which break if the wind is high enough (fig. 3, Plate 23). (Compare photos in Francis 1951.)

Under the conditions when the single unstable wave phenomenon was just occurring, the change of wind with height was measured with the Pitot-static tube, at a point about 40 cm upwind of the position where the wave became unstable (see table 1).

---

* The word ‘ solitary ’ is not used to describe the single unstable wave that was observed, as it did not appear to have the symmetry or shape of the solitary wave of Scott-Russell, which travels at a speed depending on the depth of the fluid.

Attempts were made to find the windspeed still closer to the oil surface, but when the Pitot tube was nearer than 0·5 cm, the local air accelerations round it caused unstable waves to be generated immediately underneath, so changing the conditions. However, the observed velocities can be plotted against the logarithm of the height (fig. 4), and extrapolated to a

Table 1. Wind Velocity Profile 40 cm Upwind of Single Unstable Waves

Height (cm) above mean oil level	Wind speed (cm sec^{-1})
9·4	980
7·9	967
6·65	949
4·4	921
2·9	914
2·4	902
1·4	839
0·5	744

Fig. 4

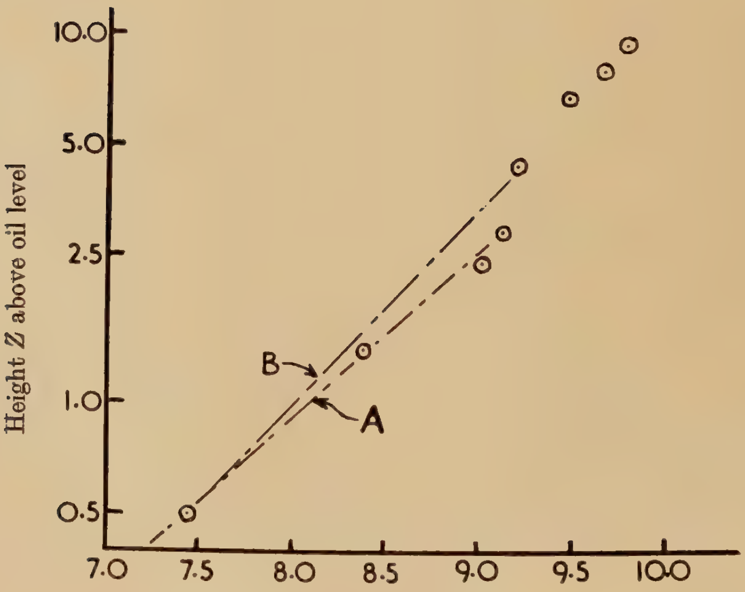

Windspeed u (m sec^{-1})

Air Velocity Profile over oil surface when single unstable waves are just being formed.

Line A extrapolates to 500 cm sec at 0·05 cm.
Line B extrapolates to 560 cm sec at 0·05 cm.

level of about 0·05 cm, approximately the height of the crests of the small ripple train. It will be seen that the velocity profile has a kink in it, and is not a straight line. Consequently, there is a little doubt as to the correct extrapolation, even if 0·05 cm is the correct height of the ripple train. The windspeed at the crests of the ripples is therefore computed to be in the range of 500 to 560 cm $\sec^{-1}$.

(*b*) *Observations of the Shear Stress of the Wind on the Oil Surface*

As in the case of a water surface, the wind force tangential to the oil surface causes both a piling up of liquid at the lee end, and also a return flow along the bottom. The former effect was measured with micrometer depth gauges working in stilling wells connected to points near the ends and middle of the tunnel; the same equipment had been used for similar experiments on a water surface. The observed change of depth δh in a length l of the tunnel is first corrected for the downwind change of air pressure, and then converted to the shear stress τ_0 by the equation

$$\tau_0 = gh\rho_{\text{oil}}\delta h/l$$

where ρ_{oil} is the density of the oil. The equation neglects the effect of the return flow creating a shear stress τ_b on the bottom of the wind tunnel. A sure correction could be applied if the oil flow was always laminar; under turbulent flow, which was observed in the oil when waves were being formed, the correction is uncertain; so no correction has been applied to the data for the effect of τ_b. τ_0 is thereby overestimated by the use of the above formula.

The stresses so obtained are expressed in terms of the shear stress coefficient $C=\tau_0/\rho_{\text{air}}u^2$ where u is the windspeed at 10 cm above oil level. The values of C are shown in fig. 5 plotted against u, and are compared to the corresponding values found for the water surface. Four sets of values are shown; two each for the leeward and windward halves of the tunnel with the waves produced in two ways; either by the air being drawn over the water by the fan alone; or by waves being made in a wave generator at the windward end, and then being subjected to wind action by the fan. In the last case the waves, if present, are much larger than those produced by the fan alone. It will be seen in fig. 5 that C appears to remain low and constant at small windspeeds; when the waves start to appear, starting with the single unstable wave, C now increases with u, at a somewhat similar rate to that applicable to a water surface.

§ 3. DISCUSSION

(*a*) *Generation of Waves*

The Kelvin–Helmholtz theory (quoted by Lamb 1932) predicts unstable waves on S2883 oil when the windspeed above the oil is 516 cm $\sec^{-1}$. The first waves to become unstable are predicted to be 1·27 cm wavelength, travelling at 0·67 cm $\sec^{-1}$. The observed phenomenon of the small ripples becoming a single unstable wave thus fits the theory fairly well; the errors of extrapolation to find the observed critical windspeed at wave level being quite enough to explain the discrepancy between the observed 500 to 560 cm sec^{-1}, and the predicted 516 cm sec^{-1}. The theoretical instability is thus shown to be real, and to take place without any other waves being present on the liquid surface.

Fig. 5.

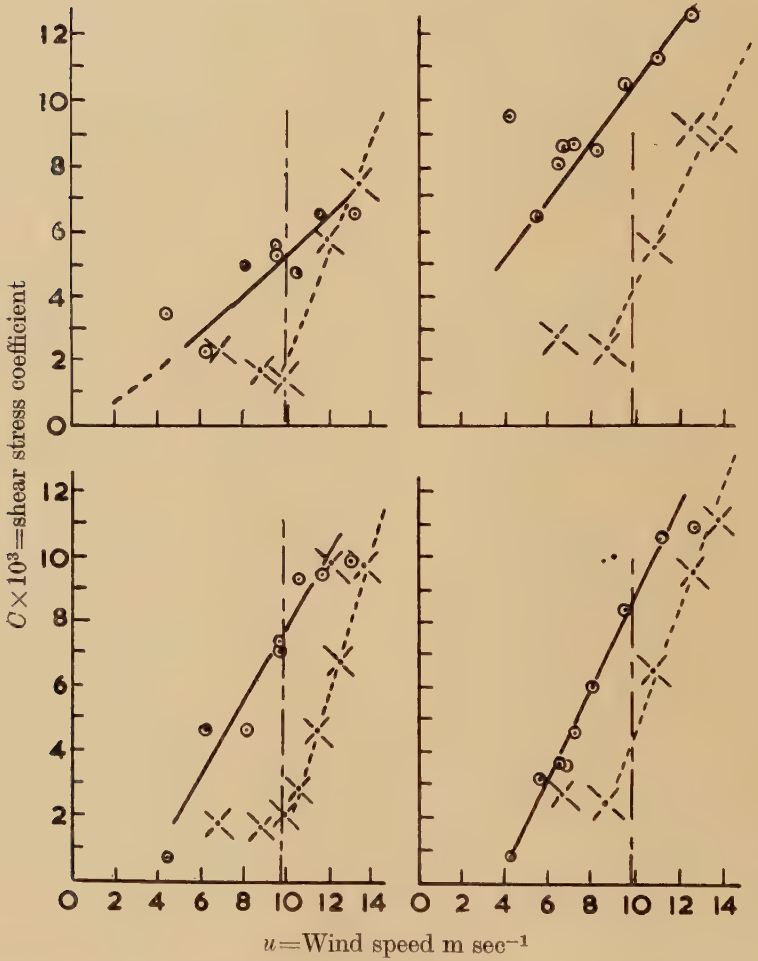

Shear stress coefficients based on wind at 10 cm above liquid level. Vertical dotted line represents critical wind speed for single unstable waves on oil. Circles mark water–air surface, crosses mark oil–air surface. Upper pair of graphs for windward end of wind tunnel; lower pair for leeward end. Left hand pair of graphs for conditions when waves made only by fan; right hand pair when waves made by both a generator and fan (see text). Water–air data from Francis (1951).

If the reality of the instability can now be conceded, it is logical to suppose that it occurs on a *water* surface at the predicted critical windspeed of 660 cm sec^{-1}; and that the observed changes of the sea surface at that windspeed are in fact the result of unstable wavelets being formed on waves already generated by another process, perhaps by Jeffreys' 'sheltering' process. Munk's views are thus to some extent vindicated. His surmise that the critical windspeed separated a low windspeed, aerodynamically smooth surface regime from a high windspeed, rough surface regime cannot, however, be reconciled with a sheltering theory with its lee eddies. Munk's evidence consisted of some early values of C, which showed a sharp discontinuity at $u=660$ cm sec^{-1}. Later evidence does not confirm this break (see for example Francis 1951), and the sea surface may therefore be always aerodynamically rough at windspeeds above 110 cm sec^{-1}, when Jeffreys' waves appear. The refuting of Munk's wind stress evidence does not detract from the value of his other evidence in favour of a critical windspeed—the white caps, the evaporation, the sea-gull's flight.

In assessing the significance of the Kelvin–Helmholtz instability on the sea it is somewhat surprising that the 660 cm sec^{-1} windspeed should, according to Munk, produce such a sharp discontinuity of the visible phenomena on the sea. Unstable wavelets would be expected first on the crests of Jeffreys' waves, when the locally accelerated wind there just becomes 660 cm sec^{-1}; the undisturbed general windspeed would be less than this. As the general windspeed increases, so would the wavelets be expected to cover more and more of the wave profile. Close examination of a water surface, in wind tunnel or on the sea, shows that such a progressive covering does occur; and that it is difficult to decide if waves are breaking and if 'whitecaps' have appeared. Slightly broken water and foam are observed to begin long before 660 cm sec^{-1}, and it may well be that such minor breaking does not photograph well, and so was missed in Munk's original data. Nevertheless, it cannot be denied by any practical observer that a change of appearance comes upon the sea at or near 660 cm sec^{-1}; it is only in doubt whether the change comes suddenly or gradually over a wide range of windspeed.

The prediction of the sheltering theory that the critical windspeed is raised by increasing the viscosity of the lower fluid has been previously checked by Keulegan (1951). He blew air over a viscous sugar solution (kinematic viscosity $\nu=0{\cdot}018$ to $0{\cdot}06$ cm^2 sec^{-1}) in a wind tunnel, and observed the windspeed at which waves just appeared. He found that this windspeed increased proportionately to $\nu^{1/3}$. The experiments that have been described extend Keulegan's work to a far greater viscosity ($\nu=2{\cdot}51$ cm^2 sec^{-1} for the S2883 oil). If the cube root law holds good from the pure water case ($\nu=0{\cdot}018$ cm^2 sec^{-1}, and critical windspeed 110 cm sec^{-1}) to the oil case, then the 'sheltering' theory waves on S2883 oil should occur at 570 cm sec^{-1} windspeed. But in the latter case the Kelvin instability waves have already appeared (calculated windspeed 516 cm sec^{-1};

observed 500 to 560 cm sec^{-1}), so that the critical windspeed for 'sheltering' waves is now obscured; a result directly opposite to the water–air case when the 'sheltering' waves obscured the Kelvin instability. The accurate prediction of the relative incidence of the two sorts of waves is additional evidence that the 'sheltering' theory cannot be far wrong, even though there has still been no direct observation of lee eddies.

(*b*) *Aerodynamic Drag of the Oil Surface*

The low and constant values of C at low windspeeds are consistent with what might be expected from a smooth unruffled surface moving slowly down wind; quite possibly the oil is then aerodynamically smooth. As soon as the critical windspeed is reached, and waves start to appear, then C starts to increase, nearly linearly with u. There is no great difference in the values of C obtained in the windward or leeward halves of the tunnel, nor with either method of producing waves; the size of the larger waves present at the lee end does not much affect C. A very similar result was obtained for the water–air interface, when the increase of C was ascribed to the growth in height and numbers of the small ripples and wavelets on the larger waves. The coincidence of the start of the increase of C with the critical windspeed for ripples on the oil surface, is perhaps an indication of the correctness of that idea.

ACKNOWLEDGMENT

The experimental work described above was carried out in the Civil Engineering Laboratories of Imperial College, London.

REFERENCES

FRANCIS, J. R. D., 1951, *Proc. Roy. Soc.* A, **206,** 387.
JEFFREYS, H., 1925, *Proc. Roy. Soc.* A, **107,** 189.
KEULEGAN, G. H., 1951, *J. Res. Bur. Stand., Wash.*, **46,** 358.
LAMB, H., 1932, *Hydrodynamics*, 6th edn. (Cambridge: University Press).
MUNK, W. H., 1947, *J. Marine Res.*, **6,** 203.
ROLL, H. U., 1950, *Ann. Met. Heft.*, **1–6,** 269.

LXXVII. *Isotopic Spin Selection Rules—V: Radiations from* ^{10}B

By G. A. Jones and D. H. Wilkinson
Cavendish Laboratory, Cambridge*

[Received March 30, 1954]

Abstract

The excitation function for the reaction ^{6}Li $(\alpha\gamma)$ ^{10}B has been investigated with alpha-particles of up to 1·3 Mev. States in ^{10}B are found at $4{\cdot}75\pm0{\cdot}02$ Mev and $5{\cdot}162\pm0{\cdot}008$ Mev; the known state at 5·11 Mev does not appear ($\omega\gamma<\sim0{\cdot}02$ ev). This paper confines its attention to the 5·11 and 5·16 Mev states; it is concluded that the former is probably (2−), $T=0$, and that the latter is (2+), $T=1$. The isotopic spin impurity of the ground state of ^{6}Li and the 5·16 Mev state of ^{10}B combined is $\sim6\times10^{-3}$; that of the 5·11 Mev state is $<2\times10^{-3}$. The isotopic spin rules are violated in permitting the formation of the 5·16 Mev $T=1$ state and operate in inhibiting the electric dipole transitions from the 5·11 Mev state.

§ 1. Introduction

Isotopic spin selection rules are liable to be encountered in two distinct guises if we bombard self-conjugate nuclei with alpha-particles: firstly we may encounter the isotopic spin discouragement if we attempt to form states of $T=1$; secondly, certain modes of decay of certain levels may be inhibited if the transitions involved are electric dipole between states of the same isotopic spin (Radicati 1952, Gell-Mann and Telegdi 1953). Both these considerations are of importance in the reaction ^{6}Li $(\alpha\gamma)$ ^{10}B that we have investigated using alpha-particles of energy up to 1·3 Mev.

§ 2. States of ^{10}B and ^{10}Be

The known levels of ^{10}B that concern the present work are shown in fig. 1. The energies of the levels are taken largely from the review of Ajzenberg and Lauritsen (1952) which also presents the evidence for the spin and parity assignments shown for ^{10}B. The computed corrections to the masses of the ground states of ^{10}Be and ^{10}C due to the Coulomb effect and the neutron–proton mass difference suggest that the state at 1·74 Mev in ^{10}B may be the analogue of the ground states of ^{10}Be and ^{10}C and is therefore the first state of $T=1$ in ^{10}B. That this surmise is probably correct is shown by the absence of inelastic deuteron scattering into this level (Bockelman, Browne, Sperduto and Buechner 1953) (see also Lauritsen 1952 and Sherr, Muether and White 1949). We therefore

---

* Communicated by the Authors.

place the ground state of ^{10}Be to correspond with the 1·74 MeV level of ^{10}B in fig. 1. This ground state is presumably (0+) as ^{10}Be is an even–even nucleus ; this assignment is supported by the lifetime and spectrum of the β-radiation between the ground states of ^{10}Be and ^{10}B ; even parity has been demonstrated by El-Bedewi (1952). The state at 3·37 MeV appears to be the first excited state of ^{10}Be (Ajzenberg 1952) ; it might therefore be expected to be (2+) in keeping with the general run of first excited states of even–even nuclei (Scharff-Goldhaber 1953). This latter assignment is supported by the observation of El-Bedewi (1952) that the state has even parity, by the observation of Cohen, Shafroth, Class and Hanna (1952) that the p–γ angular correlation in the reaction ^{9}Be (dpγ) ^{10}Be is consistent with $J=2$ and by the observation of Thomas and Lauritsen (1952) on internal positron formation from this level that suggests that the transition to the ground state is E2 though E1 or M1 cannot be excluded. We may then expect the second $T=1$ level in ^{10}B to be (2+)

Fig. 1

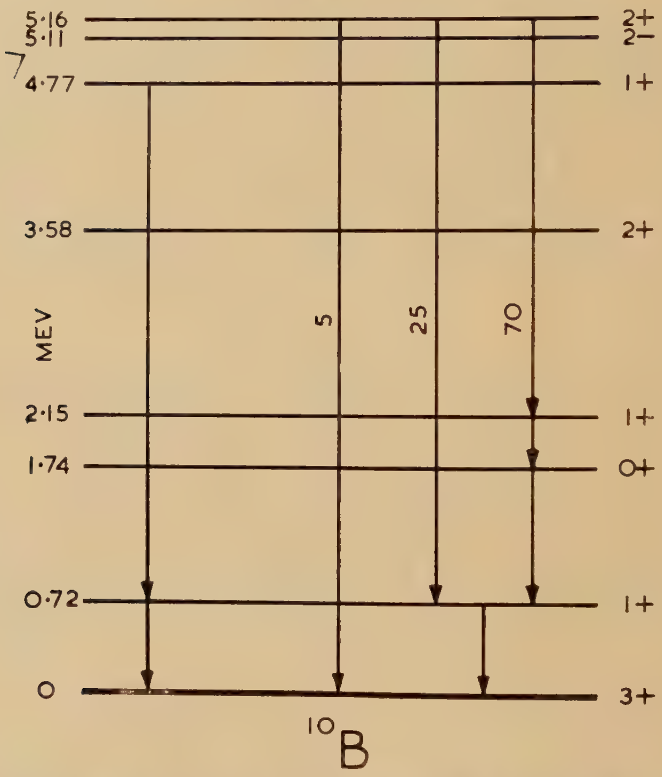

Energy levels of ^{10}B relevant to the present work and modes of decay as determined in the present investigation. (The figures on the arrows indicate the relative strengths of the initial transitions from the 5·16 MeV state.)

and to occur at about 1·74+3·37=5·11 MeV and to be therefore one or other of the doublet at 5·11 and 5·16 MeV. (The neighbouring states in ^{10}B are a doubtful one at 5·37 MeV and certain ones at 4·78 MeV and 5·58 MeV.) Although we cannot be sure that the $T=1$ state is to be found as a member of the doublet it seems likely and we shall make this assumption.

Now the excitation produced in ^{10}B by the addition of an alpha-particle to ^{6}Li is 4·45 MeV so the reaction ^{6}Li ($\alpha\gamma$) ^{10}B affords the possibility of preparing ^{10}B in the states at 4·78, 5·11 and 5·16 MeV of which the lowest has $T=0$ and the two highest are $T=0$ and $T=1$, though in which order we cannot say. If charge-independence were complete and isotopic spin consequently a good quantum number the reaction ^{6}Li ($\alpha\gamma$) ^{10}B should display the level at 4·78 MeV and one but not both the levels at 5·11 and 5·16 MeV.

From a study of the angular distribution of the neutrons leading to the (unresolved) 5·11–5·16 MeV doublet in the reaction ^{9}Be (dn) ^{10}B, Ajzenberg (1952) concludes that one or other member is (1−) or (2−). We therefore start our own investigations with the suggestion that the states at 5·11 and 5·16 MeV are (2+), $T=1$ and (1 or 2, −), $T=0$ in unknown order.

§ 3. THE EXCITATION FUNCTION FOR THE REACTION ^{6}Li ($\alpha\gamma$) ^{10}B

We have examined the excitation function for radiative capture of alpha-particles in ^{6}Li using an NaI(Tl) crystal, biassed at 0·8 MeV, in bad geometry at 0° to the alpha-particle beam. Figure 2 shows the excitation function taken with a target of ^{6}Li$_2$O of thickness about 10 μg per cm^2. The resonance occurs at an alpha-particle energy of 500±25 kev corresponding to a level in ^{10}B at 4·75±0·02 MeV. (The excitation due to ^{6}Li+α is 4·452±0·007 MeV which we derive from the Q-values of the reactions ^{10}B (nα) ^{7}Li, ^{6}Li (dp) ^{7}Li and the binding energy of the deuteron using the 'adjusted' values of Li, Whaling, Fowler and Lauritsen (1951).) Previous estimates of the energy of this level are: 4·78±0·04 MeV by neutron groups from ^{9}Be (dn) ^{10}B (Ajzenberg 1952) and 4·771±0·010 MeV from ^{10}B (pp′) ^{10}B (Bockelman, Browne, Sperduto and Buechner 1953). We find that this level decays principally to the 0·72 MeV state in ^{10}B and that $\omega\Gamma\sim 0{\cdot}15$ ev (Γ is the smaller of Γ_α and Γ_γ†). As we have detailed elsewhere (Wilkinson and Jones 1953), we believe this level to be (1+).

Figure 3 shows the excitation function similarly taken with a target of ^{6}Li$_2$O of thickness about 100 μg per cm^2; it represents the superposition of five separate runs which did not differ sensibly among themselves. A strong resonance is shown at an alpha-particle energy of 1183±5 kev corresponding to a level in ^{10}B at 5·162±0·008 MeV. There can be no doubt that this is the upper element of the doublet at 5·11 and 5·16 MeV; previous estimates are 5·159±0·010 MeV from ^{10}B (pp′) ^{10}B (Bockelman,

---

† More properly Γ is $\Gamma_\gamma\Gamma_\alpha/\Gamma_\gamma+\Gamma_\alpha$ of course.

Browne, Sperduto and Buechner 1953) and 5·165 ± 0·006 MeV from the slow neutron threshold in ^{9}Be (dn) ^{10}B* (Bonner and Butler 1951)—we have arrived at this figure from the reported threshold energy by using

Fig. 2

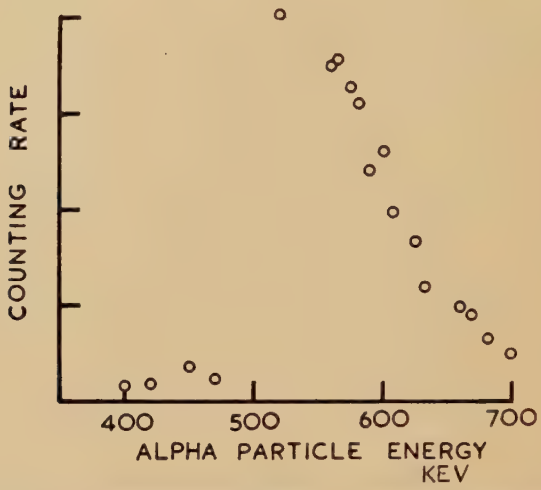

Excitation function for gamma-rays from ^{6}Li $(\alpha\gamma)$ ^{10}B taken with semi-thick target.

Fig. 3

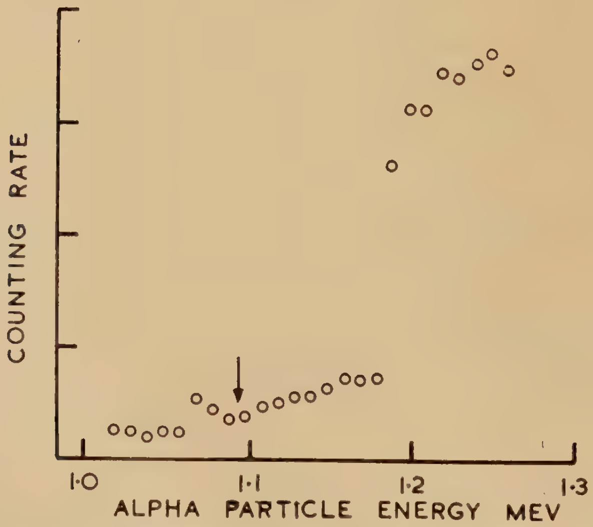

Excitation function of gamma-rays from ^{6}Li $(\gamma\alpha)$ ^{10}B taken with semi-thick target. The sharp resonance at 1068 kev is due to ^{13}C (αn) ^{16}O. The position of the arrow indicates where the resonance due to the 5·11 MeV level in ^{10}B is to be expected.

the 'adjusted' Q-values of Li, Whaling, Fowler and Lauritsen (1951) for the reactions ^{9}Be (dp) ^{10}Be and ^{10}Be (β) ^{10}B. These three estimates are of comparable precision and combine to fix the state at $5{\cdot}163 \pm 0{\cdot}005$ Mev. It appears from fig. 3 that the width of this level is less than about 10 kev. (Bonner and Butler remark that the width is less than about 3 kev.)

The rest of the excitation function of fig. 3 must be discussed in some detail. The sharp resonance at 1068 kev cannot be due to lithium as the target is thick; it is due to the neutrons from the reaction ^{13}C (αn) ^{16}O which we have reported earlier (Jones and Wilkinson 1951), the carbon coming from a very thin and patchy deposit on the surface of the lithium target. We have made a separate investigation of this latter reaction (Jones and Wilkinson 1953); both the sharp resonance and the gradual rise between it and the ^{6}Li resonance are due to ^{13}C (αn) ^{16}O.

It is clear that the 5·11 Mev level in ^{10}B is strongly suppressed relative to the 5·16 Mev level. We know quite accurately where the lower level should appear; Bockelman, Browne, Sperduto and Buechner (1953) locate it at $5{\cdot}105 \pm 0{\cdot}010$ Mev by ^{10}B (pp′) ^{10}B, i.e., 54 kev below the higher member of the doublet, the accuracy of the spacing probably being rather better than the ±10 kev of the individual level energies; Bonner and Butler (1951) locate it at $5{\cdot}112 \pm 0{\cdot}006$ Mev by the ^{9}Be (dn) ^{10}B threshold and give a doublet spacing of 53 ± 3 kev. We should thus expect the resonance corresponding to the 5·11 Mev level to appear 89 ± 4 kev in alpha-particle energy below that observed for the higher level; this point is indicated in fig. 3. Although the neutron background is an unfortunate obscuration, it appears from a comparison of fig. 3 and the appropriate section of the ^{13}C (αn) ^{16}O excitation function measured separately on a carbon target of similar thickness, that there is no room at the alpha-particle energy indicated by the arrow for a step in the excitation function as great as 2% of that at 1183 kev.

We find that, for the 5·16 Mev level, $\omega\Gamma \sim 1$ ev (Γ is the smaller of Γ_α and Γ_γ); we may then say that, for the 5·11 Mev level, $\omega\Gamma < \sim 0{\cdot}02$ ev.

§ 4. THE IDENTIFICATION OF THE STATES AT 5·11 AND 5·16 MEV

Since the 5·11 Mev state does not appear in our results it is natural to suppose that it is the (2+) $T=1$ state and that its formation is successfully inhibited by the isotopic spin rule. This interpretation implies that $\Gamma_\alpha < \sim 0{\cdot}012$ ev. It is also possible that it is the (2+) $T=1$ state but that its absence is due rather to low radiative widths for the various magnetic dipole transitions (see fig. 1) by which it may de-excite itself. It we take the predictions of the single-particle model as standard (Weisskopf 1951) we find $(2J+1)\,|\,M\,|^2 < 0{\cdot}01$. The lowest values of $(2J+1)\,|\,M\,|^2$ observed for magnetic dipole transitions in light elements are considerably greater than this (Wilkinson 1953) and it does not seem likely that all the possible magnetic dipole transitions involved here should be simultaneously so strongly discouraged.

We therefore reject this second possibility and consider the implications of the assumption $\Gamma_\alpha < 0{\cdot}012$ ev demanded by the first.

We first of all write

$$\Gamma_\alpha = 2kP\gamma_\alpha^2$$

where k is the wavenumber of the alpha-particle—^{6}Li pair ; P the penetrability and γ_α^2 the reduced width for alpha-particle emission. We then represent γ_α^2 in terms of the combined intensities α^2 of the $T=0$ contamination of this (2+), $T=1$ state and the $T=1$ contamination of the ^{6}Li ground state (Radicati 1953)

$$\gamma_\alpha^2 = \gamma_{\alpha c}^2\, \alpha^2$$

where $\gamma_{\alpha c}^2$ is a composite reduced width for the contamination states.

Finally we write

$$\gamma_{\alpha c}^2 = \theta_\alpha^2 \frac{3\hbar^2}{2Ma}$$

representing the reduced width as a fraction θ_α^2 of the Wigner limit $3\hbar^2/2Ma$ where M is the reduced mass of the system and a the channel radius (Teichmann and Wigner 1952).

So $$\theta_\alpha^2 = \frac{Ma\Gamma_\alpha}{3\hbar^2 kP\alpha^2}.$$

Now Radicati (1953) has shown that the ($T=0$) ground state of ^{6}Li contains about $2{\cdot}5 \times 10^{-3}$ parts or more in *intensity* of $T=0$ and so $\alpha^2 > 2{\cdot}5 \times 10^{-3}$. Our experimental limit on Γ_α then gives, taking $a = (4^{1/3} + 6^{1/3}) \times 1{\cdot}5 \times 10^{-13} = 5{\cdot}1 \times 10^{-13}$ cm,

$$\theta_\alpha^2 < 9 \times 10^{-4}.$$

This value is so small as to make this explanation of the absence of the 5·11 Mev level in our experiment appear rather unlikely—though we may not exclude it absolutely.

A further argument against accepting the 5·11 Mev state as (2+), $T=1$ concerns the behaviour (see fig. 1) of the 5·16 Mev state which we should then have to take, following Ajzenberg (1952)—see § 2, as (1−) or (2−), $T=0$: if (1−) were correct we should be faced with isotopic spin forbidden electric dipole transitions to the 0·72 and 2·15 Mev states, but with an isotopic spin allowed electric dipole transition to the (0+), $T=1$ state at 1·74 Mev which should therefore predominate but is, in fact, not seen at all ; if (2−) were correct the observed transitions would all be forbidden by the isotopic spin rule although for that to the 2·15 Mev state we find $(2J+1)\,|M|^2 > 0{\cdot}15$ and since the mean value of $(2J+1)\,|M|^2$ for allowed electric dipole transitions in light nuclei is about 0·2 (Wilkinson 1953) this would imply a complete break-down of the isotopic spin rules ; this seems to be rather unlikely at such low excitation.

We are therefore forced by several lines of argument to abandon the obvious suggestion that the 5·11 Mev state is that of $T=1$ and must ask whether the 5·16 Mev state may in fact be (2+), $T=1$. On the basis of its gamma-ray decay alone we should in fact have suggested (2+) ;

the decay spectrum suggests $J=1$ or 2; (1−) and (2−) are eliminated by the argument already made, while (2+) seems rather more probable than (1+) owing to the occurrence of the ground state transition.† With (2+) the $(2J+1)|M|^2$ values for the transitions to the 2·15, 0·72 and ground states become respectively $\geqslant 1{\cdot}2$, $\geqslant 0{\cdot}11$ and $\geqslant 0{\cdot}02$; with (1+) the ground state transition becomes electric quadrupole with $(2J+1)|M|^2 \geqslant 6$. Some support for the assignment $T=1$ to this 5·16 Mev state comes from the work of Chao, Lauritsen and Rasmussen (1949) who find that it emits gamma-rays in successful competition with alpha-particles. Using the results of these workers together with our own determination of the gamma-ray spectrum from the 5·16 Mev state and the rather scanty knowledge concerning the intensity of neutron groups (see Ajzenberg and Lauritsen (1952), Evans, Malich and Risser (1949)) we may estimate that, for the 5·16 Mev state $\Gamma_\alpha \sim \Gamma_\gamma$; this implies $\theta_\alpha{}^2 \sim 6\times 10^{-5}$—a most improbable low figure for a state not suffering the inhibition of the isotopic spin rule. If we assume that for the contamination states $\theta_\alpha{}^2=0{\cdot}01$—a figure unlikely to be wrong by more than a factor of 10—we find $\alpha^2 \sim 6\times 10^{-3}$; this figure must be compared with the value $\alpha_0{}^2(1) \sim 2{\cdot}5\times 10^{-3}$ suggested by Radicati for the contamination of the ground states of ^{6}Li that it includes and shows that the violation of the isotopic spin rule involved in the formation of this 5·16 Mev state is of the order expected.

It appears that a consistent explanation of the present and other results is obtained by supposing that the 5·16 Mev state is in fact the one of (2+), $T=1$.

We now return to the question of the 5·11 Mev state that we must suppose, after Ajzenberg (1952), to be (1−) or (2−) (and $T=0$). As before we may exclude its absence as being due to a small value of Γ_α‡ and so must explain why $\omega\Gamma_\gamma < \sim 0{\cdot}02$ ev. If the state is (1−) the isotopic spin allowed electric dipole transition to the (0+), $T=1$ state at 1·74 Mev must have $(2J+1)|M|^2 < 10^{-3}$ which is improbably small. If (2−) is the correct choice the electric dipole transitions to the $T=0$ states at 0, 0·72 and 2·15 Mev are all isotopic spin forbidden. That $\omega\Gamma_\gamma < 0{\cdot}02$ ev then suggests that the contamination of the $T=0$ state by $T=1$ is less than 2×10^{-3} in intensity; $\alpha_0{}^2(1) < 2\times 10^{-3}$ (using the mean value of 0·2 for $(2J+1)|M|^2$ for allowed electric dipole transitions in light elements).

§ 5. DISCUSSION

If we are correct in interpreting our results to suggest that the 5·11 Mev state is (2−), $T=0$ and the 5·16 Mev state is (2+), $T=1$ we have examples both of the isotopic spin selection rules in operation—inhibiting the electric dipole transitions from the 5·11 MeV state—and of their breaking down—allowing the formation of the 5·16 MeV $T=1$ state from two nominally $T=0$ particles.

---

† We do not regard this ground state transition as established with certainty, but we believe it to occur as reported in fig. 1.

‡ Indeed, Chao, Lauritsen and Rasmussen (1949) did not find any gamma-rays emitted by this level following ^{9}Be (dn) ^{10}B showing that probably $\Gamma_\alpha \gg \Gamma_\gamma$.

As we have already remarked, the isotopic spin impurity implied by our observed violation is of the order 6×10^{-3} in intensity† for the combined contributions of the ^{6}Li ground states ($T=1$ impurity) and the ^{10}B state at 5·16 MeV ($T=0$ impurity) and since Radicati has estimated $\alpha_0^2\,(1)\sim2{\cdot}5\times10^{-3}$ for the ^{6}Li ground state this violation is of the right order and cannot be taken to imply any departure from specifically-nuclear charge-independence.

If the 5·11 MeV state is indeed (2−) with $\alpha_0^2\,(1)<2\times10^{-3}$ we have an interestingly-high purity for a state that cannot be regarded as remote from possible $T=1$ contaminants. It is, of course, possible that the matrix element for electric dipole radiation by the contaminant state or states is unusually small and that our limit on α_0^2 (1) should be set correspondingly higher, but it is rather unlikely to be small for all the several electric dipole transitions involved. The nearest known (2−) state to this at 5·11 MeV is that at 7·48 MeV: since the latter decays by a strong electric dipole transition to the ground state ($(2J+1)\,|M|^2=0{\cdot}42$) we must suppose that it is $T=1$ and so forms a suitable contaminant for our state at 5·11 MeV. Setting then the separation in energy between state and contaminating state as $7{\cdot}48-5{\cdot}11=2{\cdot}37$ MeV we find for the matrix element of the Coulomb perturbation between the two $H^C_{10}<\sim0{\cdot}1$ MeV (assuming complete charge-independence for the specifically-nuclear forces). This is a rather low figure (though no lower than some examples computed by Radicati (1953)) and may perhaps be used to throw some light on the connection between the 5·11 and 7·48 MeV (2−) states. Radicati (1954) has calculated $H^C_{10}\sim0{\cdot}11$ MeV on the basis of this assignment of state and contaminating state under the assumption that the state belongs to the first Wigner super-multiplet. This suggests that the 5·11 MeV state might be expected to appear in an experiment of sensitivity only little greater than that of the present one.

ACKNOWLEDGMENTS

Part of this work was performed with the electro static generator of the Cavendish Laboratory; we would like to thank Mr. E. S. Shire for allowing us the use of this machine and Messrs. G. Lindsay Jones and J. Wormald for their patient operation of it.

We would like to thank Sir John Cockcroft and Dr. R. Dawton's division at the Atomic Energy Research Establishment, Harwell, for supplying the separated ^{6}Li with which this work was performed.

---

† It must be remembered that this estimate involves the guess $\theta_\alpha^2\sim0{\cdot}01$ for the alpha-particle decays allowed by the impurities and so may be considerably in error.

REFERENCES

AJZENBERG, F., 1952, *Phys. Rev.*, **88,** 298.
AJZENBERG, F., and LAURITSEN, T., 1952, *Rev. Mod. Phys.*, **24,** 321.
BOCKELMAN, C. K., BROWNE, C. P., SPERDUTO, A., and BUECHNER, W. W., 1953, *Bull. Amer. Phys. Soc.*, **28,** No. 1, 11.
BONNER, T. W., and BUTLER, J. W., 1951, *Phys. Rev.*, **83,** 1091.
BUECHNER, W. W., and STRAIT, E. N., 1949, *Phys. Rev.*, **76,** 1547.
CHAO, C. Y., LAURITSEN, T., and RASMUSSEN, V. K., 1949, *Phys. Rev.*, **76,** 582.
COHEN, L., SHAFROTH, S. M., CLASS, C. N., and HANNA, S. S., 1952, *Phys Rev.*, **87,** 206.
EL-BEDEWI, F. A., 1952, *Proc. Phys. Soc.* A, **65,** 64.
EVANS, J. E., MALICH, C. W., and RISSER, J. R., 1949, *Phys. Rev.*, **75,** 1161.
GELL-MANN, M., and TELEGDI, V., 1953, *Phys. Rev.*, **91,** 169.
JONES, G. A., and WILKINSON, D. H., 1951, *Proc. Phys. Soc.* A, **64,** 756; 1953, *Ibid.*, **66,** 1176.
LAURITSEN, T., 1952, *Annual Review of Nuclear Science* (Stanford: Annual Reviews Inc.).
LI, C. W., WHALING, W., FOWLER, W. A., and LAURITSEN, C. C., 1951, *Phys. Rev.*, **83,** 512.
RADICATI, L. A., 1952, *Phys. Rev.*, **87,** 521; 1953, *Proc. Phys. Soc.* A, **66,** 139; 1954, *Ibid.*, **67,** 39.
SCHARFF-GOLDHABER, G., 1953, *Phys. Rev.*, **90,** 587.
SHERR, R., MUETHER, H. R., and WHITE, M. G., 1949, *Phys. Rev.*, **75,** 282.
TEICHMANN, T., and WIGNER, E. P., *Phys. Rev.*, **87,** 123.
THOMAS, R. G., and LAURITSEN, T., 1952, *Phys. Rev.*, **88,** 969.
WEISSKOPF, V. F., 1951, *Phys. Rev.*, **83,** 1073.
WILKINSON, D. H., 1953, *Phil. Mag.*, **44,** 450.
WILKINSON, D. H., and JONES, G. A., 1953, *Phys. Rev.*, **91,** 1575.

LXXVIII. *The Propagation of Longitudinal Elastic Waves along Cylindrical Bars*

By H. Kolsky

Imperial Chemical Industries Limited, Butterwick Research Laboratories, Welwyn, Herts*

[Received March 15, 1954]

Abstract

The elementary theory of longitudinal waves in bars predicts that such waves travel with a constant velocity $c_0=(E/\rho)^{1/2}$. The Pochhammer theory shows that this is true only for waves of wavelength large compared with the diameter of the bar. Shorter waves travel more slowly, the limiting value being that of Rayleigh surface waves. When a disturbance is started at a point on one end-face of a cylinder, however, a spherical wave will travel out with the dilatational velocity c_1, and some energy should therefore travel along the bar with this velocity.

Minute explosive charges have been used to produce elastic pulses and the propagation of such pulses down steel cylinders of various diameters has been investigated. The waves arriving at the opposite end of the cylinder were recorded with a cathode-ray oscillograph. It was found that whilst most of the energy travels at a velocity less than c_0 there are also *precursor* waves of small amplitude which travel with velocities between c_0 and c_1. For long cylinders it was found that the pulse arriving at the detector had a tail of low frequency oscillations, indicating that higher modes of vibration are being excited.

§ 1. Introduction

By combining Newton's Laws of Motion with the elastic relations obtained from Hooke's Law the general equations of motion of an elastic solid can be obtained in terms of the particle displacements (see, for example, Love 1927, p. 293). These equations show that in an unbounded solid two different types of elastic wave can be propagated ; these two types of waves are generally termed dilatational and distortional respectively. Dilatational waves involve changes in volume of the material but no rotation, and travel with a velocity $c_1=[(k+4\mu/3)/\rho]^{1/2}$ where k is the bulk modulus, μ is the rigidity modulus and ρ is the density. Distortional waves on the other hand do not cause any changes in volume but result in both rotation and shearing of the medium and travel with a lower velocity, given by $c_2=(\mu/\rho)^{1/2}$. The particle motion in the case of a plane dilatational wave is along the direction of propagation and the wave is therefore often referred to as a *longitudinal* wave, whilst the motion in a distortional wave is at right angles to the direction of propagation and the wave is termed *transverse*.

---

* Communicated by the Author.

In attempting to apply this theory to the propagation of waves in bounded solids it is necessary to introduce the appropriate boundary conditions and in most cases this leads to equations which are mathematically intractable. In some simple cases exact solutions have been obtained and it is with one of these, namely the propagation of a longitudinal wave along an elastic cylinder, that this paper is concerned. Before discussing this, however, it should be mentioned that the reflection of an elastic wave at the free boundary of a solid is more complex than that of a sound wave at a fluid boundary, since in the case of a solid the boundary conditions cannot in general be satisfied on the assumption that a single reflected wave is generated. Thus when a dilatational wave is incident obliquely on a free surface both a dilatational and a distortional wave are generated, and similarly a distortional wave produces in general a wave of each type on reflection at a free surface. The conditions of such reflection have been studied by seismologists and relations between the amplitudes of the incident and the reflected waves are given by Knott (1899), Zoeppritz (1919), Macelwane and Sohon (1936) and Kolsky (1953). Now if a disturbance is started at some point on a bounded solid it is theoretically possible to trace the subsequent motion by considering the multiple reflection of the outgoing wave at the free boundaries of the solid. Where the length of the pulse produced by the disturbance is short compared with the dimensions of the solid the principles of geometrical optics can be used to trace the paths of separate 'rays' in the solid. When, however, the wavelength is comparable with the dimensions of the specimen diffraction effects will occur and ray tracing procedure will only give the positions of the wave-fronts. In general the detailed method is too complicated to give quantitative results but nevertheless is useful in describing the behaviour qualitatively. This will be illustrated later in considering the propagation of an elastic pulse along a cylinder.

The more usual method of treating the propagation of elastic waves in bounded solids is to find a solution to the equations of motion which will obey the boundary conditions. This was first done for elastic cylinders by Pochhammer (1876) and independently by Chree (1889). The type of solution assumed by these workers led to a *frequency equation* from which the phase velocity of a sinusoidal wave of known frequency in a cylinder of known diameter can be calculated. The computation is, however, rather heavy and it is only comparatively recently that calculations on the basis of these equations have been made. The results of these calculations have been published by Field (1931), Bancroft (1941), Czerlinsky (1942), Hudson (1943), Mindlin (1946), Davies (1948) and Hueter (1949). These calculations show that for the fundamental mode of vibration the phase velocity of plane sinusoidal waves along a cylinder is given by $c_0=(E/\rho)^{1/2}$ for waves of infinitely long wavelength and by the velocity of Rayleigh surface waves c_s for waves of infinitely short wavelength. Waves of finite wavelength travel at velocities between these two limits (see fig. 1, curve 1). The group velocity of the waves, which is more significant when considering the propagation of a pulse, has the same values as the phase velocity at the two extremes but shows a minimum in between (see fig. 2, curve 1).

For very long wavelengths the Pochhammer–Chree treatment is thus in agreement with the simple theory of the propagation of longitudinal waves along rods. The reason that the elementary treatment fails for shorter wavelengths is that it does not allow for the lateral inertia of the cylinder. This lateral inertia results in some of the kinetic energy of the motion being in the form of radial vibrations. Rayleigh (1894) showed that the effect of this was to make waves of shorter wavelength travel with velocities less than c_0 and gave an approximate expression for the magnitude of the correction. The curves obtained from the Pochhammer–Chree treatment show that for wavelengths large compared with the radius of the cylinder the Rayleigh correction is adequate but when the wavelength becomes comparable with the radius the Rayleigh

Fig. 1

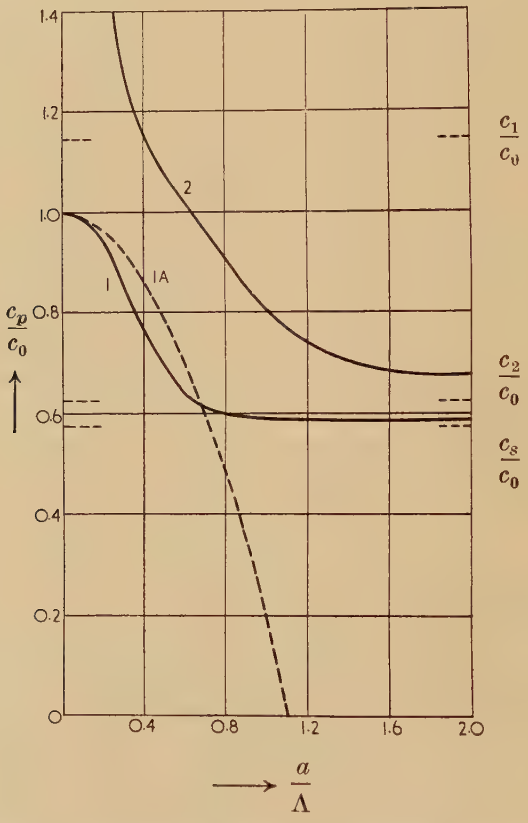

Phase velocity of extensional waves in cylindrical bars for $\nu=0{\cdot}29$.

correction results in very large errors, and in fact predicts that the phase velocity will become zero at a finite wavelength (see fig. 1, curve 1A).

Figures 1 and 2 show in a non-dimensional form the curves obtained for steel, assuming that this material has a value of Poisson's ratio $\nu=0{\cdot}29$. In fig. 1 the ratio of the phase velocity c_p to c_0 is plotted for various values of a/Λ where a is the radius of the cylindrical bar and Λ is the wavelength of longitudinal sinusoidal waves propagated along it.

Fig. 2

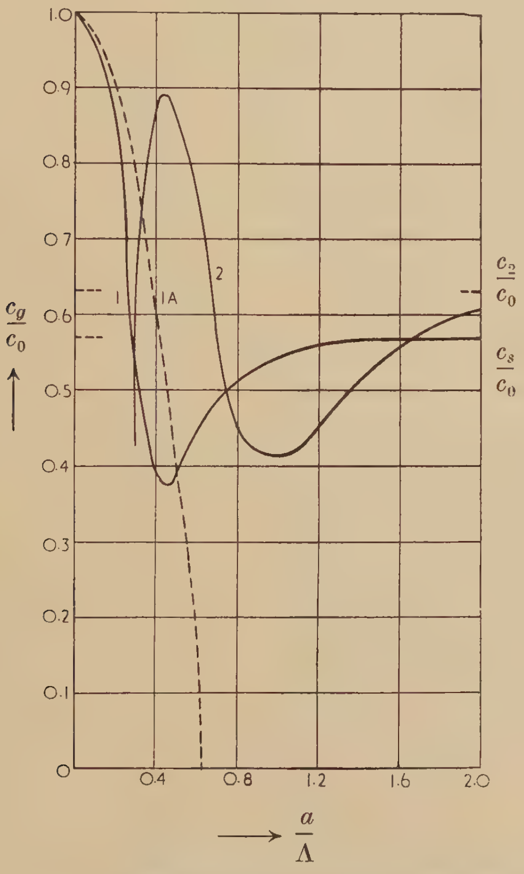

Group velocity of extensional waves in cylindrical bars for $\nu=0{\cdot}29$

c_1, c_2 and c_s are as before the velocities of dilatational, distortional and Rayleigh surface waves respectively. Curves 1 and 2 in the figure show the first and second modes of vibration, different modes corresponding to the presence of nodal cylinders in the vibration. Curve 1A corresponds to the curve obtained using the Rayleigh correction.

Figure 2 shows the group velocities (c_g) which have been obtained by differentiating the curves in fig. 1. It may be seen that in the first mode the group velocity has a minimum at $a/\Lambda=0{\cdot}45$, so that waves whose wavelength is 2·2 times the radius of the bar will have a group velocity lower than that of waves of any other wavelength. When a pulse is propagated down a steel bar it will be dispersed and the Fourier components whose wavelengths are around 2·2a will appear at the back of the pulse. Davies (1948) derived the curves shown in figs. 1 and 2 in order to interpret the transmission of elastic pulses down a Hopkinson Pressure Bar and he has shown that the dispersion of the pulses can be accounted for in terms of these curves. The curves marked 2 in both figures correspond to a higher mode of vibration in which there is one nodal cylinder for long wavelengths and two nodal cylinders for short wavelengths. It may be seen that although the phase velocity can have values greater than c_0, and in fact greater than c_1, the group velocity c_g is always less than c_0.

Several writers (Field 1931, Southwell 1941, Prescott 1942, and Cooper 1947) have pointed out, however, that the propagation of an elastic disturbance down a cylinder will only differ from propagation in an infinite medium in so far that the waves are being continually reflected at the sides of the cylinder and in between reflections they must travel with one of two velocities, i.e. c_1, the velocity of dilatational waves or c_2, the velocity of distortional waves. Thus if we consider a disturbance at a point in the interior of the cylinder a spherical dilatational wave will travel out from it with velocity c_1 and some part of this wave will travel down the cylinder without suffering any reflection. The amplitude will decrease inversely with the distance and for long cylinders the unreflected wave will be confined to a very narrow cone which has the point of the disturbance as its apex. Some energy nevertheless would appear to travel with a velocity which is considerably greater than c_0. The Pochhammer–Chree solutions apply strictly only to infinite trains of sinusoidal waves and are inadequate in accounting for this and the purpose of the experiments described below was to confirm that energy is in fact transmitted with a velocity greater than c_0 down elastic cylinders and to consider the effect of reflections at the free surface of the cylinder.

§ 2. THEORETICAL

The Elastic Equations

The equations of motion of an elastic solid expressed in terms of the particle displacement **s** is given in vector form by :—

$$\rho \frac{\partial^2 \mathbf{s}}{\partial t^2} = (k+\tfrac{4}{3}\mu) \text{ grad div } \mathbf{s} - \mu \text{ curl curl } \mathbf{s} \; . \quad . \quad . \quad . \quad . \quad . \quad . \quad . \qquad (1)$$

where ρ is the density of the medium. As mentioned earlier, eqn. (1) shows that waves can be propagated through a solid medium with one of two velocities, either with a velocity of $[(k+\frac{4}{3}\mu)/\rho]^{1/2}$ when curl **s** is zero, i.e. the motion is irrotational, or with a velocity of $(\mu/\rho)^{1/2}$ when div **s** is zero and the motion is equivoluminal. Pochhammer (1876) and Chree (1889) have applied eqn. (1) to the case of a cylindrical bar and to do this it is necessary to express it in terms of cylindrical polar coordinates (r, θ, and z). The displacement **s** has then three components u_r, u_θ and u_z along the axes and we have three scalar equations corresponding to (1) (see Love, p. 287). Pochhammer has considered the propagation of an infinite sinusoidal wave train down a cylinder so that for extensional oscillations u_θ is zero whilst u_r and u_z will both be of the form $[U \exp(ipt+\gamma z)]$ where p is 2π times the frequency and γ is 2π divided by the wavelength, U being in each case a function of r only. If the boundary condition that the curved surface of the bar is free from stress is then inserted, the frequency equation is obtained, and from this curves such as those shown in figs. 1 and 2 may be derived.

As pointed out by Love, it is impossible by the Pochhammer treatment to find an accurate solution for the free vibrations of a cylinder of finite length, since in this case the stress components must vanish along the flat end surfaces of the cylinder as well as on the curved surface and it is impossible to conform to all these boundary conditions simultaneously. When the radius of the cylinder is small compared with its length it can be shown that the residual stresses on the end surface are small so that the Pochhammer solution might be expected in this case to give a very close approximation to the velocity of propagation of longitudinal waves. Bishop (1953) has recently discussed this point and has suggested that the stress system at the ends of the cylinder which has a zero resultant does not propagate a disturbance down the cylinder, the argument involved being in the nature of a dynamical St. Venant Principle.

The Pochhammer treatment considers the propagation of an infinite train of sinusoidal waves down a cylinder and gives the phase velocity of such a train of waves. In order to determine what happens to a pulse we must consider it in terms of its Fourier components and this has been done by Davies (1948) who has treated the problem by two approximate methods. He has shown that for a long steel bar the experimental results are in good agreement with the theory and that no wave appears to travel with a velocity greater than c_0. This is, however, to be expected, since after having travelled some distance down the bar any unreflected dilatational waves will be very small in amplitude compared with those which have been reflected from the sides of the cylinder.

In order to treat the problem of the propagation of a pulse down a cylinder in terms of reflections from the sides we must use the relations for dilatational and distortional waves incident at free surfaces. A plane dilatational wave of amplitude A_1 incident on a free surface and travelling in a direction making an angle α with the normal to the surface is reflected partly as a dilatational wave of amplitude A_2 at an equal angle with the normal and partly as a distortional wave of amplitude A_3 at an angle β with the normal, where $\sin\alpha/\sin\beta=c_1/c_2$. The relations between the amplitudes are given by the equations :—

$$2(A_1-A_2)\cos\alpha\sin\beta-A_3\cos 2\beta=0. \qquad (2)$$

$$(A_1+A_2)\cos 2\beta\sin\alpha-A_3(\sin\beta\sin 2\beta)=0. \qquad (3)$$

From these equations the values of A_2/A_1 and A_3/A_1 can be obtained for different values of α and in fig. 3 these are plotted for steel, where Poisson's ratio ν has been taken as 0·29. It may be seen that no distortional wave is reflected at either normal or glancing incidence but that at all other angles waves of both types are produced on reflection; A_2 is here always negative so that there is a reversal of phase in the reflected distortional wave. As pointed out by Goodier and Bishop (1952), however, the theory breaks down at glancing incidence, since the solution implies that the incident and reflected waves are everywhere equal and opposite and the resultant motion is zero. The type of solution which applies at glancing incidence must clearly be different from this and Schardin (1950) has shown experimentally that a distortional wave of finite amplitude is produced under these conditions although the curves in fig. 3 imply that at glancing incidence its amplitude should be zero. This point is of importance in the study of the propagation of elastic waves in long bars, since the reflections at the surface of the bar will occur at angles very close to glancing incidence.

Fig. 3

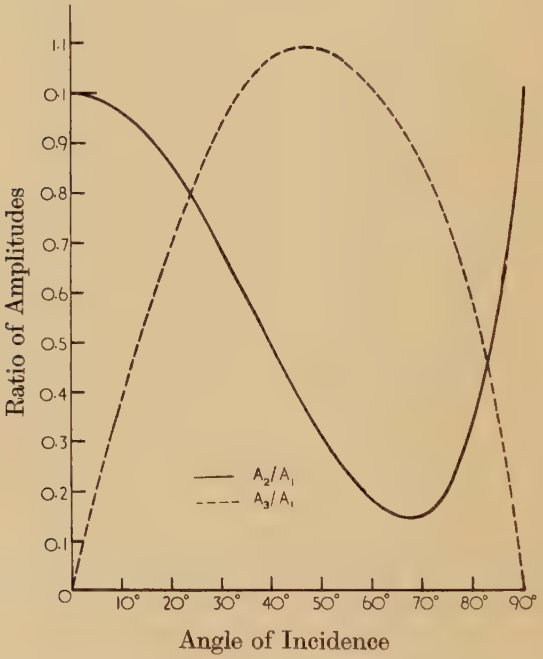

Amplitudes of reflected waves from longitudinal wave incident on free surface. $\nu=0{\cdot}29$.

For a distortional wave incident on a free surface with its vibrations in the plane of incidence there is a critical angle of incidence above which no dilatational wave is reflected, the phenomenon being similar to that of total reflection in the case of light. For steel ($\nu=0\cdot29$) this critical angle is 32° 57′ and fig. 4 shows the amplitude of the two reflected waves for angles of incidence up to this critical value. Equations similar to (2) and (3) apply here and if B_1 and B_2 are the amplitudes of the incident and reflected distortion waves and B_3 is the reflected dilatation wave the relations are :—

$$(B_1+B_2)\sin 2\beta \sin\beta - B_3 \sin\alpha \cos 2\beta = 0 \quad . \quad . \quad . \quad . \quad (4)$$

and

$$(B_1-B_2)\cos 2\beta - 2B_3 \sin\beta \cos\alpha = 0, \quad . \quad . \quad . \quad . \quad (5)$$

Fig. 4

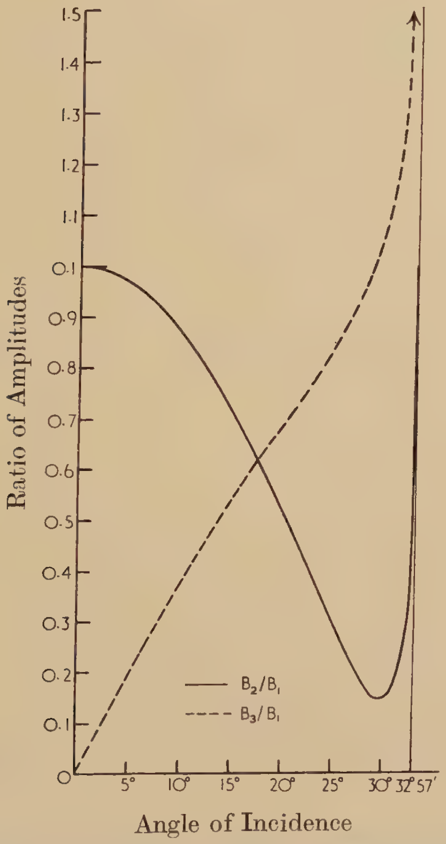

Amplitudes of reflected waves from transverse wave incident on free surface. $\nu=0\cdot29$.

β being the angle that the directions of propagation of the incident and reflected distortional waves make with the normal to the free surface and α being the corresponding angle for the reflected dilatational wave. A distortional wave with its vibrations perpendicular to the plane of incidence does not produce a dilatational wave on reflection at a free surface. The reflected distortional wave under these conditions is of equal amplitude and of opposite phase to the incident wave for all angles of incidence.

Now if a pulse is initiated at a point on one end-face of a cylinder so that it spreads out spherically from this point, the waves arriving at a point on the opposite end-face can have travelled by a series of different paths. This is illustrated in fig. 5, where the pulse is generated at the centre of one end-face of a short cylinder (ratio of length to radius being 1·37) and the pulses arriving at the centre of the opposite face are considered. It may be seen that, in this case after the direct pulse (1), the next pulse to arrive (2) is a dilatational pulse which has been reflected at the middle of the cylinder. The pulse after this (3) is a distortional pulse produced by the reflection of an outgoing dilatational pulse, and so on. In order to calculate the amplitudes of these separate pulses it is necessary to use the curves shown in figs. 3 and 4 at each reflection, allowing at the same time for the change in amplitude of the spherical waves as they diverge. This clearly cannot be carried out quantitatively beyond the first few reflections, but this type of approach is nevertheless useful in showing on a qualitative basis the type of behaviour expected from a pulse travelling in a short cylinder.

Fig. 5

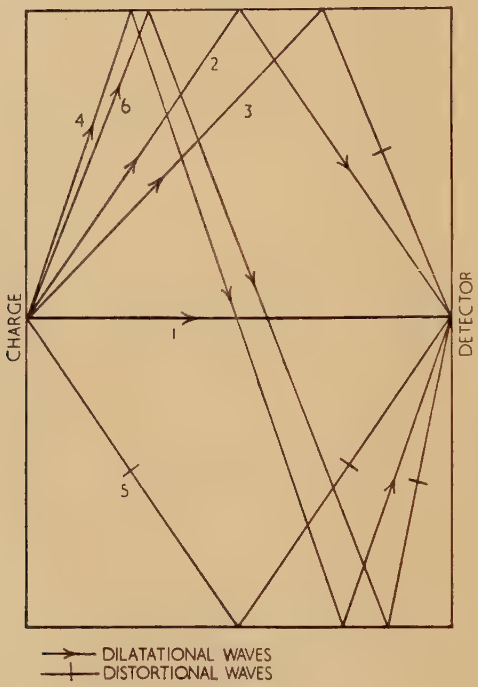

Reflection of waves in short cylinder. $\nu=0{\cdot}29$.

§ 3. Experimental

The experimental arrangement is shown diagrammatically in fig. 6. Steel cylinders of diameters between 1·25 cm and 15 cm were used and minute charges of lead azide or silver acetylide were employed to produce the pressure pulses. The charges were placed at the centre of one end-face of the cylinder and were detonated by means of an electrically heated wire. The pulses arriving at the other end of the cylinder were detected by means of a small condenser microphone. The insulated plate of the condenser microphone was set parallel to the end-face of the cylinder so that there was a gap of only a few thousandths of a centimetre between them. The output of the condenser microphone was fed into a high-gain wide-band amplifier and displayed and photographed on a high-speed cathode-ray oscillograph. The electrical circuits were similar to those used in earlier work (Davies 1948, Kolsky 1949). The single sweep time-base of the oscillograph was triggered by means of a photocell which received light from the detonating explosive. The delay between detonation and the beginning of the trace was found to be of the order of one microsecond. Timing traces were provided from either a 100 kc/s or a 10 kc/s crystal oscillator. With the long narrow cylinders (2·5 cm and 1·25 cm diameter) cylindrical condenser units which measured the radial displacement of the cylindrical surfaces were also used. The design of these has been described earlier (Kolsky 1949).

Fig. 6

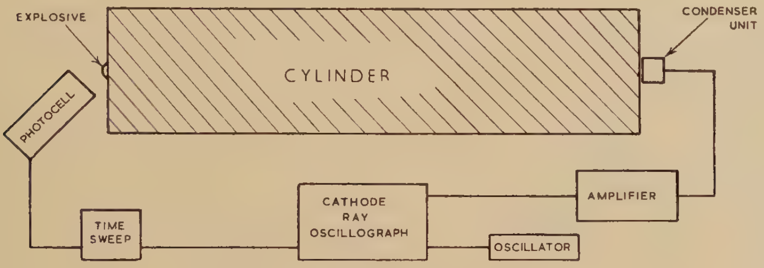

General experimental arrangement.

When the largest amplifications were used the condenser microphones were found to detect an electrical disturbance commencing at the instant of detonation. This was finally found to be due to electromagnetic radiation produced by the ionized explosive products and has been discussed elsewhere (Kolsky 1954). By the use of suitable earthed screens between the explosive and the detecting apparatus this extraneous effect was removed.

§ 4. Experimental Results

It was decided to see first whether when a charge is detonated at one end of a short narrow cylinder any energy is propagated along it with velocities greater than c_0. For this purpose a silver-steel cylinder 15 cm in length and 1·25 cm in radius was tried and charges of 0·1 g of lead azide were detonated at the centre of one end-face. In order to achieve the greatest sensitivity in these experiments the insulated plate of the condenser unit was of the same diameter as the bar and was charged to 240 v. The gap between it and the bar was set at 0·005 cm and the amplifiers were set to a maximum gain (voltage amplification=10 000). The velocity c_0 of longitudinal waves in this sample of steel was found to be 5320 m/sec. (This was measured by finding the resonant frequency of the bar in longitudinal oscillation and also by sending pressure pulses down a two-metre length of the same steel (cf. Kolsky 1949).) Poisson's ratio for this steel is found to be 0·29, so that the velocity of dilatational waves, c_1, is 6090 m/sec. In the experiments it was found that the opposite face of the 15 cm long bar began to move 25 μsec after the charge detonated, corresponding to a velocity of 6000 m/sec. Thus within experimental error some energy would appear to be communicated with the velocity c_1. When the sensitivity of the detector was decreased (by increasing the condenser gap or decreasing the amplification) the apparent velocity of the head of the pulse decreased and at considerably lower sensitivities the velocity of the head appeared to be about 5300 m/sec ($=c_0$).

The motion of the detecting end of the bar appeared to be quite continuous and showed no evidence of the arrival of separate pulses. The reason for this can be seen if the times of arrival of the pulses travelling by different routes are calculated (cf. fig. 5). Where the pulse is dilatational during the whole of its passage along the bar the calculation is quite straightforward ; where it is dilatational in some parts of its path and distortional for other parts (cf. routes 3 and 6 in fig. 5) the calculation involves the solution of a quartic equation. Taking $c_1=6090$ m/sec and the velocity of distortional waves $c_2=3310$ m/sec, the times of arrival of the first eight pulses are as follows :—

Pulse	1	2	3	4	5	6	7	8
Time of transit (μsec)	24·6	25·0	26·0	27·5	28·2	28·6	29·6	29·9

The first four pulses and No. 7 are dilatational throughout their passage and correspond to zero, one, two, three and four reflections at the curved surface of the bar. Since there is a reversal of phase in the stress on reflection at a free boundary, Nos. 1, 3 and 7 are compression pulses whilst 2 and 4 are tension pulses. Nos. 5, 6 and 8 correspond respectively to paths with one distortional section and one, two and three dilatational sections.

The initial compression pulse produced by the lead azide charge was 2–3 μsec in duration, so that the separate pulses would not be discriminated even if the detector is localized at the axis of the bar. Since the microphone in the experiments was the same diameter as the bar, there was a further blurring due to the differences in time of transit at different points on the end-face. Further, the conditions of geometrical optics hardly apply in this case, so that considerable diffraction of the pulses would be expected. In view of this it is not surprising that the motion observed appears to be continuous.

In order to observe the arrival of discrete pulses travelling by different routes a steel cylinder 10·4 cm in length and 7·6 cm in radius was used. Figure 5 shows the paths followed by the first six pulses in a cylinder having this ratio of length to radius. Taking $c_1=6090$ m/sec and $c_2=3320$ m/sec, the times of transit of these six pulses are as follows :—

Pulse	1	2	3	4	5	6
Time of transit (μsec)	17·1	30·3	42·2	52·9	55·7	63·7

There is also a pulse of small amplitude arriving at 51·3 μsec which has traversed path 1 three times. It will be seen in fig. 5 that path 5 corresponds to a distortional pulse travelling out from the seat of the charge. It may appear at first sight that no such pulse will be produced by the explosive, but as shown by Schardin (1950) and Christie (1952) both a dilatational and a distortional spherical pulse diverge from the seat of an explosion on a free surface, although the amplitude of the outgoing distortional pulse is zero along the direction of the axis of the cylinder (this is to be expected from considerations of symmetry). It may also be seen from the figure that where the paths involve both dilatational and distortional waves they can occur in more than one way for a given time of transit, e.g. the time of arrival for a pulse travelling path 3 is the same as that of a distortional pulse from the charge reflected as a dilatational pulse, the path being the mirror image of the one shown in the diagram.

Figure 7 (Plate 24, figs. 7 and 8) shows the record obtained from a small condenser microphone (1 cm diameter) placed at the centre of one flat face of the cylinder (length 10·4 cm, radius 7·6 cm) when a small charge was detonated at the centre of the opposite face. (It should be noted that this microphone measured the displacement of the surface and the stress is proportional to the particle velocity and therefore to the differential coefficient of the curve shown in the record.) The expected times of arrival of the different pulses and their sign are also shown in the figure and it may be seen that where the pulses can be discriminated there is good agreement between theory and experiment.

In order to calculate the relative intensities of the separate pulses four factors must be taken into account. These are :—

(1) The pressure amplitude of the pulse leaving the charge. This will vary with direction as a result of the free surface.

(2) The reflection coefficients and phase changes at each reflection. These can be obtained from figs. 3 and 4.

(3) The decrease in amplitude due to the wave diverging spherically from the charge so that the amplitude is inversely proportional to the distance travelled.

(4) The focussing effect after reflection at the cylindrical surface.

Clearly, even if the pulses were sufficiently short for diffraction effects to be ignored the analysis could not easily be carried out on a qualitative basis and the most that could be obtained is a general qualitative picture.

With very long bars the *precursor* pulses travelling with velocity c_1 will be small in amplitude and, as a result of the change in phase of stress on reflection pulses which have been reflected, an odd number of times will be of opposite sign to the generating pulse, whilst those reflected an even number of times will be of the same sign; consequently the net resultant will be very small. Under these conditions the Pochhammer treatment should be adequate in describing the propagation of a pulse down a bar.

Davies (1948) has shown experimentally that with pulses produced by the impact of bullets at one end of a long bar, curve 1 in fig. 2 gives a good representation of the displacements occurring at the opposite end. Now if the dispersion of a pulse is represented by curve 1, and the initial pulse is considered as infinitely sharp, it will contain Fourier components of all wavelengths. The group velocity of the low-frequency components will be c_0 and these appear at the head of the pulse. The very high frequency components travel with the velocity of Rayleigh surface waves, $c_s=0{\cdot}56c_0$, whilst the components for which $a/\Lambda=0{\cdot}45$ travel with the lowest group velocity and this is $0{\cdot}38c_0$. Thus if the head of the pulse takes a time t to reach a point along the bar, the very high-frequency components will take a time $1{\cdot}8t$ and the slowest components a time $2{\cdot}6t$. A pulse which was initially very short compared with t should thus take a time $1{\cdot}6t$ to pass the point. Some experiments were tried to test this. A 2·5 cm diameter steel bar 136 cm in length was used and a lead azide charge was detonated at the centre of one end-face, the waves arriving at the other end being detected with a condenser microphone. It was found that the main pulse is followed by a series of small oscillations which continue at least until time $3t$, when the head of the main pulse has traversed the bar twice again. Thus these oscillations cannot be accounted for in terms of curve 1 in fig. 2.

In this experiment observations at times beyond $3t$ were prevented by the return of the main pulse, and to overcome this limitation a cylindrical condenser microphone which could be placed at points along the bar was employed. Figure 8 shows the record obtained from such a microphone when it was placed 60 cm from the end at which the charge was detonated of a bar 183 cm in length. (This type of microphone measures the radial displacement of the bar which is proportional to the longitudinal stress when the latter is uniform across the section of the bar.) It may be seen from the record that high-frequency components arrive at times corresponding to about $1{\cdot}8t$ (t being the time of arrival of the head of the pulse) and that the amplitude of the oscillations decreases rapidly after about $2{\cdot}6t$. The pulse, however, does not then stop but shows rather lower frequency oscillations up to at least $5t$ when the reflection of the head of the pulse from the free end of the bar appears. In terms of the Pochhammer treatment these oscillations can only be accounted for if it is assumed that higher modes of vibration have been excited. It may be seen from curve 2 in fig. 2 that the group velocity of waves travelling in the second mode decreases steadily at low frequencies and this would account for the waves occurring at the tail of the pulse.

§ 5. CONCLUSION

The experimental results show that for cylinders in which the ratio of length to radius is of the order of unity the propagation of a short elastic pulse must be considered in terms of the separate routes by which energy may travel. For short cylinders a ‘ spectrum ’ of pulses is found to arrive at the opposite face of the cylinder and the Pochhammer theory is quite inadequate in describing the propagation. These results are similar to those observed by Hughes, Pondrom and Mims (1949) using ‘ wave packets ’ produced by piezoelectric crystals. The time of arrival of the first two pulses under these conditions depends on the value of c_1 for the medium, the first being the direct dilatational pulse and the second the dilatational pulse which has been reflected once at the surface of the cylinder ; from these times of arrival the value of c_1 and hence of $(k+4\mu/3)$ of the medium may be derived. The third pulse to arrive travels partly at a velocity c_1 and partly at a velocity c_2 (see fig. 5), hence from its time of arrival the value of c_2 can be calculated if the value of c_1 is known. From c_2 the value of μ can be obtained and hence the values of both k and μ may be derived separately. Hughes, Pondrom and Mims (1949) used this method for determining elastic constants.

For cylinders in which the ratio of length to radius is large the times of arrival of the separate pulses become closer and closer together and, except when outgoing pulses of very short duration are employed, the pressure changes continuously at the other end of the cylinder and is described adequately by the Pochhammer treatment. Most of the pulses which arrive at the other face of the cylinder under these conditions have spent part of their time as dilatational waves and the rest as distortional waves, so that their average velocity of propagation will lie between these two limits and it is in fact found that most of the energy travels with a velocity less than c_0. Nevertheless, the Pochhammer–Chree solutions, which strictly apply only to infinite sinusoidal trains of waves, are not complete in that they give no indication that energy can be communicated along a bar with a velocity greater than c_0 and there appears to be a need for an extension of the theory to account for the *precursor* waves which travel with velocities between c_0 and c_1 in cylinders of finite length.

ACKNOWLEDGMENTS

The author wishes to thank Miss P. M. Prince for her help with the experiments and Mr. D. G. Christie and Dr. F. C. Roesler for useful discussions.

REFERENCES

BANCROFT, D., 1941, *Phys. Rev.*, **59,** 588.
BISHOP, R. E. D., 1953, *Nature, Lond.*, **172,** 169.
CHREE, C., 1889, *Trans. Camb. Phil. Soc.*, **14,** 250.
CHRISTIE, D. G., 1952, *Trans. Soc. Glass Tech.*, **36,** 74.
COOPER, J. L. B., 1947, *Phil. Mag.*, **38,** 1.
CZERLINSKY, E. VON, 1942, *Akust. Z.*, **7,** 12.
DAVIES, R. M., 1948, *Phil. Trans.* A, **240,** 375.
FIELD, G. S., 1931, *Canad. J. Research*, **5,** 619.
GOODIER, J. N., and BISHOP, R. E. D., 1952, *J. Appl. Phys.*, **23,** 124.
HUDSON, G. E., 1943, *Phys. Rev.*, **63,** 46.
HUETER, T. F., 1949, *Z. angew. Phys.*, **1,** 274.
HUGHES, D. S., PONDROM, W. L., and MIMS, R. L., 1949, *Phys. Rev.*, **75,** 1552.
KNOTT, C. G., 1899, *Phil. Mag.*, **48,** 64.
KOLSKY, H., 1949, *Proc. Phys. Soc.* B, **62,** 676 ; 1953, *Stress Waves in Solids* (Oxford : Clarendon Press) ; 1954, *Nature, Lond.*, **173,** 77.
LOVE, A. E. H., 1927, *The Mathematical Theory of Elasticity*, 4th edition, (Cambridge : University Press).
MACELWANE, J. B., and SOHON, F. W., 1936, *Introduction to Theoretical Seismology* (New York : Wiley).
MINDLIN, J. A., 1946, *C. R. Doklady, U.R.S.S.*, **1,** 11.
POCHHAMMER, L., 1876, *J. Reine Angew. Math.*, **81,** 324.
PRESCOTT, J., 1942, *Phil. Mag.*, **33,** 703.
RAYLEIGH, 1894, *Theory of Sound* (London : Macmillan).
SCHARDIN, H., 1950, *Glastechn. Ber.*, **23,** 1.
SOUTHWELL, R. V., 1941, *Theory of Elasticity* (Oxford : Clarendon Press).
ZOEPPRITZ, K., 1919, *Nach. d. Konig. Gesell. d. Wissen. z. Göttingen, Math.-phys. Berlin*, pp. 66–84.

LXXIX. *Energy Band Shapes and Band Widths in Metals*

By S. Raimes
Department of Mathematics, Imperial College, London*

[Received April 14, 1954]

Abstract

The density of states curve given by the recent theory of Bohm and Pines is compared with those of the Sommerfeld and Hartree–Fock theories. It is found that the Bohm and Pines curve shows a rudimentary 'tail', and the effect of this on the interpretation of the experimental soft x-ray emission data is discussed, with particular reference to the metals sodium, magnesium and aluminium. Although the Bohm and Pines band width is a great improvement on that of the Hartree–Fock theory, it is still much larger than the observed width. It is suggested that this may be partly due to the neglect of the short-range correlation energy: a lower bound to the narrowing of the band from this cause is calculated, and found to be 0·1 ev for sodium.

---

§ 1. Introduction

Many properties of the conduction electrons in certain metals are satisfactorily explained by the Sommerfeld theory, in which the electrons are treated as non-interacting particles obeying Fermi statistics. However, when exchange interaction is taken into account, that is, when the Hartree–Fock theory of the electron gas is used instead of the Sommerfeld theory, the results of calculation are generally found no longer to agree with experiment. The reason for this may be seen in fig. 1, which shows the density of states as a function of energy according to the two theories. The curves represent metallic sodium in so far as the electron density has been chosen to be the same as in sodium, but it should be understood that the periodic field of the crystal has been neglected: the theories discussed in the present work are applied to a degenerate gas of free electrons, to which the conduction electrons in many metals, and particularly in sodium, approximate, and the effects of the ionic lattice must be superimposed on the results obtained here.

The density of states in the Hartree–Fock theory falls rapidly to zero at the Fermi surface and then rises again, but this does not happen in the Sommerfeld theory. It is apparent that the calculated values of any quantity which depends upon the density of states at, or near, the Fermi surface will be quite different in the two theories. This directly affects,

---

* Communicated by the Author.

for instance, the electronic specific heat, the paramagnetic and diamagnetic susceptibilities, and the thermal conductivity, as well as the temperature variation of such quantities.

The recent theory of Bohm and Pines (1953) satisfactorily resolves this situation. These authors take into account, as well as the exchange interaction, the effect of correlations between the positions of the electrons. These correlations are due to the Coulomb repulsion between the electrons and are neglected in the Hartree–Fock theory, which only includes an accidental correlation effect due to the Pauli Principle. It is shown that the long-range Coulomb interaction gives rise to *plasma oscillations*, or organized oscillations of the electronic system as a whole, and that the remaining interaction between the electrons may be described by a screened Coulomb potential of the form

Fig. 1

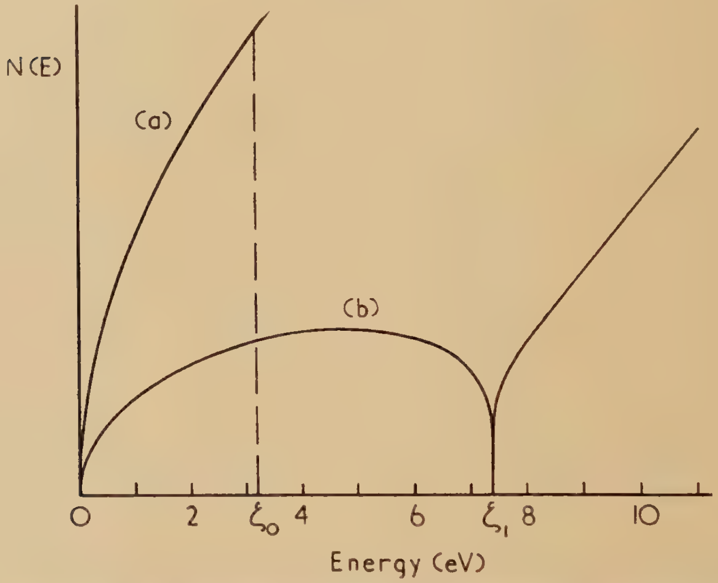

Density of states $N(E)$ for metallic sodium : (*a*) according to the Sommerfeld theory ; (*b*) according to the Hartree–Fock theory. ζ_0 and ζ_1 are the maximum energies at 0°K in the two cases.

$$\frac{e^2}{r}\left(1-\frac{2}{\pi}\int_0^{\beta k_0 r}\frac{\sin x}{x}\,dx\right), \qquad (1)$$

where k_0 is the radius of the occupied sphere in **k**-space, and the screening constant βk_0, of magnitude about 1 Å^{-1}, is the maximum wave number of the plasma oscillations. It is important to note that the energy of a quantum of plasma oscillation is much greater than the energy of an electron at the Fermi surface, so that these oscillations are not usually excited and may be disregarded in calculating many of the properties of metals at ordinary temperatures. When the exchange energy is calculated using the screened potential, the density of states curve, as shown in fig. 2, assumes a form very like that of the Sommerfeld theory, so that agreement with experiment is largely restored for quantities like those mentioned above.

Another discrepancy between the Sommerfeld and Hartree–Fock theories is very apparent in fig. 1. The Hartree–Fock band width is more than twice the Sommerfeld width, and, once again, it is the latter which is in closest agreement with experiment. Jones (1954) has pointed out that the Bohm and Pines theory is a great improvement on that of Hartree and Fock here also, and this may be seen in fig. 2. A large discrepancy remains, however, which it is important to explain, for any error in the band width will give rise to a similar error in the cohesive energy of the metal; yet very good calculated values of the cohesive energy, of sodium in particular, have been obtained by the Hartree–Fock method. or approximations to it, when the correlation energy has been added.

Although Koopmans's theorem (1933) does not strictly apply to the Bohm and Pines theory it is reasonable to suppose that, here also, the difference between the highest and lowest energies in the band should correspond to the width of a soft x-ray emission band. The band width given by the Bohm and Pines theory for sodium, using the value of β which minimizes the energy (Pines, 1953, eqn. 15), namely $\beta=0{\cdot}68$, is about 1·4 ev greater than the ' reduced ' band width obtained by Skinner (1940) from soft x-ray emission spectra. This is a large difference, and Jones shows that to eliminate it within the framework of the theory would require a value of β greater than 0·9. Unfortunately, as remarked by Jones, the validity of the Bohm and Pines theory becomes somewhat doubtful for values of β as large as 0·9.

It is the purpose of the present paper to show that this dilemma may not be inescapable, for two main reasons. First, short-range correlations between the electronic positions have been neglected. The minimum effect of these on the band width can be accurately determined, and the result shows that such correlations may account for a significant part of the discrepancy. Secondly, the density of states curve shows a rudimentary ' tail ', which suggests that the interpretation of the experimental soft x-ray data might be open to modification in such a way as to give rather larger values for the band widths than the ' reduced ' widths obtained by Skinner.

§ 2. The Density of States According to the Theory of Bohm and Pines

After the plasma oscillations have been accounted for, and the zero of energy suitably chosen, the energy E of an electron is found, as a function of $\alpha=k/k_0$, to be :

when $\alpha<1-\beta$,

$$E(\alpha)=\frac{\hbar^2k_0^2}{2m}\left(1-\frac{\beta^3}{6}\right)\alpha^2-\frac{e^2k_0}{2\pi}\left[2+\frac{1-\alpha^2}{\alpha}\log\left(\frac{1+\alpha}{1-\alpha}\right)-4\beta\right], \quad . \quad (2a)$$

and when $1-\beta<\alpha<1$,

$$E(\alpha)=\frac{\hbar^2k_0^2}{2m}\left(1-\frac{\beta^3}{6}\right)\alpha^2 -\frac{e^2k_0}{2\pi}\left[1+\frac{1-\alpha^2}{\alpha}\log\left(\frac{1+\alpha}{\beta}\right)+\frac{3\alpha^2+\beta^2-1}{2\alpha}-2\beta\right]. \quad . \quad . \quad (2b)$$

This allows for the effective mass, $m^*=m/(1-\beta^3/6)$, which the electrons possess as a result of the plasma oscillations. The use of m^* instead of the ordinary electronic mass m in the kinetic energy expression has the effect of increasing the density of states by a few per cent, and decreasing the band width by a similar amount. Pines (1953, eqn 36), in fact, uses the ordinary mass in calculating the ratio of the electronic specific heat C_v to the Sommerfeld value $C_v^{(0)}$: this yields the value

$$C_v/C_v^{(0)}=0{\cdot}89$$

for sodium (the value 0·82 given by Pines is a numerical error), whereas the use of the effective mass gives $C_v/C_v^{(0)}=0{\cdot}93$. The effect is hardly significant here, but it should be remembered that this calculation has been carried out with $\beta=0{\cdot}68$. The effective mass increases with β, so that it is of importance in deciding whether a larger value of β, which still remains within the range of validity of the theory, can give a band width in agreement with experiment.

The energy surfaces in **k**-space are spheres and the density of states $N(E)$ is given, in the usual way, by

$$N(E)=k^2/2\pi^2(dE/dk). \quad . \quad . \quad . \quad . \quad . \quad . \quad . \quad (3)$$

The resulting curve for sodium is shown in fig. 2. In both figs. 1 and 2, for purposes of comparison, the zero of energy has been taken to be the same in every case—in fact, the $N(E)$ curves for the Sommerfeld, Hartree–Fock, and Bohm and Pines theories should be displaced relative to one another. Thus the energy corresponding to curve (*b*) in fig. 2 is really $E(\alpha)-E(0)$, when $E(\alpha)$ is given by eqns (2*a*) and (2*b*).

The two expressions for E, with $\alpha<1-\beta$ and $\alpha>1-\beta$ respectively, give rise to two distinct sections of the curve of $N(E)$ against E, and the slope is discontinuous at $\alpha=1-\beta$. The first part of the curve, which constitutes the rudimentary tail mentioned above, is, apart from the slightly different effective mass, the same as the Hartree–Fock $N(E)$ curve, while the second part is very similar to the Sommerfeld curve. The pronounced kink in the curve is undoubtedly due to the assumption of a sharp cut-off for the plasma oscillations. Further refinements of the theory would probably result in a smooth curve, but the tail is so marked that is seems unlikely that the curve would return to the parabolic form of the Sommerfeld theory.

From eqns (2) the band width, $E(1)-E(0)$, is found to be

$$\frac{\hbar^2 k_0^2}{2m}\left(1-\frac{\beta^3}{6}\right)+\frac{e^2 k_0}{\pi}\left(1-\beta-\frac{\beta^2}{4}\right), \quad . \quad . \quad . \quad . \quad . \quad (4)$$

and the ‘ tail length ’, $E(1-\beta)-E(0)$, or the width of the first part of the $N(E)$ curve, is found to be

$$\frac{\hbar^2 k_0^2}{2m}(1-\beta)^2\left(1-\frac{\beta^3}{6}\right)+\frac{e^2 k_0}{2\pi}\left[2-\frac{2\beta-\beta^2}{1-\beta}\log\left(\frac{2-\beta}{\beta}\right)\right]. \quad . \quad . \quad . \quad (5)$$

Fig. 2

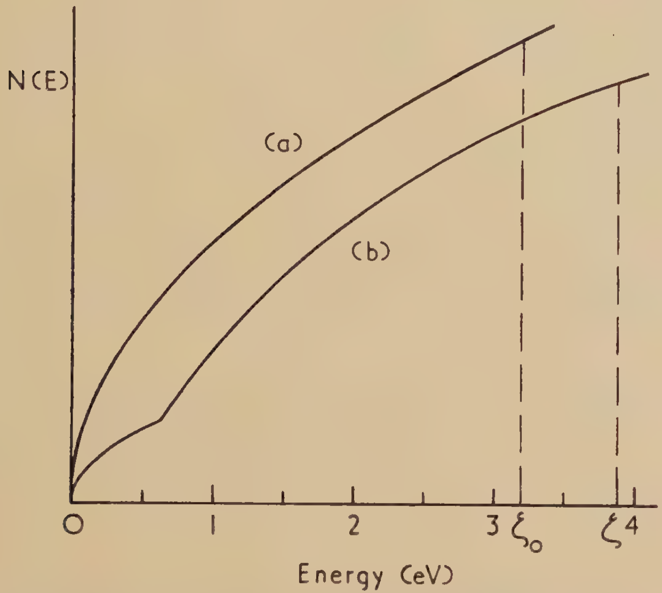

Density of states $N(E)$ for metallic sodium : (*a*) according to the Sommerfeld theory ; (*b*) according to the theory of Bohm and Pines. ζ_0 and ζ are the maximum energies at 0°K in the two cases.

	Na	Mg	Al
β_{min}	0·68	0·59	0·54
Bohm and Pines b.w.	3·9	8·9	14·5
Tail length	0·6	1·9	3·6
Sommerfeld b.w.	3·2	7·1	11·7
Empirical L_3 b.w.	$3·0\pm0·2$	$7·2\pm0·2$	$13·2\pm0·4$
Reduced b.w.	$2·5\pm0·3$	$6·2\pm0·3$	$11·8\pm0·5$

All values, except those of β_{min}, are in ev.

In the table the calculated values of these quantities are shown for the metals sodium, magnesium, and aluminium. The value of β chosen in each case was the value, called β_{min} by Pines, which minimizes the total energy. For magnesium and aluminium the required values were obtained from fig. 3 of Pines’s paper, giving β_{min} as a function of r_s, r_s being, in this connection, the radius of a sphere whose volume is equal to the mean volume per electron. Also shown in the table are the Sommerfeld band widths, and what Skinner (1940) calls the 'empirical' and 'reduced' widths of the soft x-ray emission spectra.

It may be worth noting that, if the length of the rudimentary tail is deducted from it, the Bohm and Pines band width reduces almost exactly to the Sommerfeld value.

The low energy limit of a band is very difficult to obtain empirically from the soft x-ray emission spectra, owing to the occurrence of very long tails, which are believed to result from line-broadening due to an Auger effect. It is a correction for the latter which accounts for the difference between the 'empirical' and 'reduced' band widths of Skinner. Very roughly, as shown in fig. 3, the low energy limit (A) which gives the 'empirical' band width is obtained from the experimental L_3 emission curve by a linear extrapolation to zero from that part of the curve immediately before the commencement of the long tail, while the low energy limit (B) which gives the 'reduced' band width is obtained by a parabolic extrapolation of the main part of the L_3 emission curve.

Fig. 3

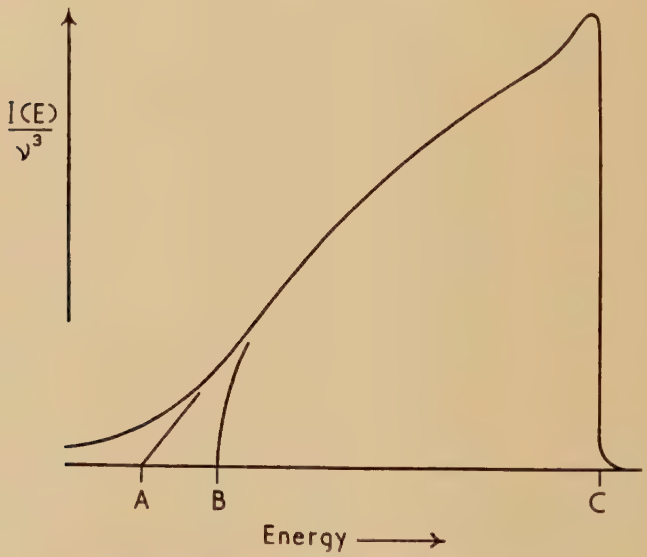

Soft x-ray L_3 emission band for sodium (after Skinner 1940). $I(E)$ is the intensity and ν is the emitted frequency; the quantity $I(E)/\nu^3$ is comparable with $N(E)$. AC is the 'empirical' band width, 3·0 ev, and BC is the 'reduced' band width, 2·5 ev.

Fixing the low energy limit is rendered even more hazardous by the appearance of a rudimentary tail, which has nothing to do with line-broadening, in the theoretical $N(E)$ curve. The occurrence of even a smoothed-out kink in the curve would represent a departure from the previously accepted parabolic form and hence lead to difficulties in the interpretation of experimental curves. It is clear from fig. 2 that a parabolic extrapolation of the upper part of the curve would cut off the rudimentary tail and hence give too small a band width. In fact, in such circumstances, a linear extrapolation to zero of the experimental curve at the base of the long tail might give more accurate results, so that the ‘ empirical ’ values may be more reliable than the ‘ reduced ’ values. The difference between the two sets of values given by Skinner is 0·5, 1·0, and 1·4 ev for Na, Mg, and Al respectively, and these quantities are comparable with the lengths of the rudimentary tails shown in the table.

§ 3. THE SHORT-RANGE CORRELATION ENERGY

There is a further effect which is not included in the theorectical $N(E)$ curve of fig. 2, namely, the short-range correlation energy. The long-range correlations between the electronic positions are accounted for by the plasma oscillations, but there remain the short-range correlations due to the screened Coulomb interaction. To calculate the exact effect of these on the $N(E)$ curve is hardly possible at this time, but it is relatively easy to abtain an accurate lower bound to the magnitude of their effect on the band width.

In table 1 of his paper Pines (1953) gives values of the *average* short-range correlation energy per electron, which we shall denote simply by $\epsilon(r_s)$. Over the range of r_s considered, that is for the alkali metals, these values are reproduced almost exactly by the function

$$\epsilon(r_s) = -\frac{0{\cdot}084}{r_s} - 0{\cdot}025, \qquad \ldots \ldots \quad (6)$$

where ϵ is in Rydberg units and r_s is in Bohr units.

If the number of electrons in the system is initially n, and this is reduced to x, the system remaining in its ground state, the *total* short-range correlation energy must become (cf. Seitz 1940, p. 343)

$$x\,\epsilon\{(n/x)^{1/3}r_s\} = G, \text{ say.}$$

The short-range correlation energy associated with an electron at the top of the band is thus

$$\left(\frac{\partial G}{\partial x}\right)_{x=n} = \epsilon(r_s) - \frac{r_s}{3}\epsilon'(r_s), \qquad \ldots \ldots \quad (7)$$

and the difference between this and the average value $\epsilon(r_s)$ for all the electrons represents the *minimum* narrowing of the band due to short-range correlations. This difference is

$$r_s\epsilon'(r_s)/3 = 0{\cdot}028/r_s, \qquad \ldots \ldots \quad (8)$$

and amounts to 0·1 ev for sodium. We therefore expect the theoretical band width to be reduced by at least 0·1 ev, and very probably by 0·2 ev or more when short-range correlation energy is included.

§ 4. CONCLUSION

We have seen that there are three factors which tend to improve the correspondence between theoretical and observed values of the band width, and which therefore alleviate to some extent the situation described by Jones (1954). These are (i) the effective mass the electrons possess as a result of the plasma oscillations, (ii) the effect of short-range correlations, and (iii) the appearance of rudimentary tails on the theoretical $N(E)$ curves. It may turn out, as a consequence of (iii), that Skinner's ' empirical ' band widths are more reliable than his ' reduced ' widths. However, if we take the ' empirical ' width, 3·0 ev, for sodium and assume that short-range correlations will reduce the theoretical width by 0·2 ev, then, using $\beta=0{\cdot}68$, there still remains a discrepancy of 0·7 ev between theory and experiment. It should be added, also, that the effect of the periodic field of the crystal has been neglected here, and there is reason to believe that this might increase the theoretical band width very slightly.

It would seem, therefore, that either the effect of short-range correlations is much greater than that assumed above, or a larger value of β must be taken. Here, however, a value of β less than 0·8 would suffice to produce exact agreement between theory and experiment, and such a value lies within the range of validity of the theory of Bohm and Pines.

It is a pleasure to acknowledge helpful correspondence with Professor H. Jones, F.R.S., and Professor D. Pines.

REFERENCES

BOHM, D., and PINES, D., 1953, *Phys. Rev.*, **92**, 609.
JONES, H., 1954, *Phys. Rev.*, **94**, 1072.
KOOPMANS, T., 1933, *Physica*, **1**, 104.
PINES, D., 1953, *Phys. Rev.*, **92**, 626.
SEITZ, F., 1940, *Modern Theory of Solids* (New York : McGraw-Hill).
SKINNER, H. W. B., 1940, *Phil. Trans. Roy. Soc.* A, **239**, 95.

LXXX. *The Forward Displacement of the Nitrogen Isotope of Mass* 13 *Produced by Bombardment of Aluminium with the Isotope* 14

By K. F. Chackett and J. H. Fremlin
Physics Department, University of Birmingham*

[Received March 22, 1954]

Abstract

The relative yields of ^{13}N produced in stacked foils bombarded by ^{14}N^{6+} ions in the Birmingham cyclotron have been studied. These show strong forward displacements of the ^{13}N compared with other radio-active products. The displacements are consistent with the hypothesis that the ^{13}N is formed by a reaction analogous to deuteron stripping in which the ^{13}N nuclei have a considerable proportion of the forward momentum of the bombarding ions.

§ 1. Introduction

As was reported in a previous communication (Chackett, Fremlin and Walker 1954), one of the many products found when aluminium is bombarded by ^{14}N^{6+} ions is ^{13}N.

Under our bombardment conditions, the energy spectrum of the bombarding particles is continuous. There is probably a peak in the region of 50 mev and beyond this there is a roughly exponential decrease in numbers of ions up to the highest energies. It follows, therefore, that at any point within a thick target, the majority of ions energetic enough to surmount the Coulomb barrier of the target nuclei have energies still not very far above the barrier. This state of affairs provides an explanation of the roughly constant ratio of the yields of nearly all the different products at all depths in the target. Resolutions of the complex decay curves of activities in aluminium foils from a stack bombarded by ^{14}N^{6+} ions showed, however, an excessively large component of abou tten-minute period in the deeper foils ; this activity we tentatively identified as due to ^{13}N. Such a product is unlikely to be formed from a compound nucleus heavier than ^{27}Al, or, in any quantity, from compound nuclei between ^{14}N and ^{27}Al. A much more likely mechanism would be the simple capture by the ^{27}Al nucleus of one neutron from the bombarding ion. If this were the case most of the ^{13}N nuclei so formed would retain a large forward momentum. There should, therefore, be a much higher yield of ^{13}N in the deeper foils in a stack than corresponds to the number of ^{13}N nuclei which are actually formed there. The present experiments with the beam of ^{14}N^{6+} ions do in fact show this effect.

---

* Communicated by the Authors.

In order to demonstrate most clearly the forward displacement of the ^{13}N, it is necessary to measure the distribution-in-depth of some other product or products formed simultaneously, for which forward displacement is not expected to be large. Such measurements may also serve as a monitor of the beam intensity, although only roughly so, since the yield of any product, summed over all the stack, will depend on the energy spectrum of the incident beam as well as on its intensity in numbers of ions. We have found it convenient to relate all the ^{13}N activities found either to ^{34}Cl, which has the advantage that it may be assayed from the same foil as that taken for the ^{13}N measurement, or to ^{32}P. The latter nuclide cannot easily be assayed in the same foil as that taken for the ^{13}N measurement. We have, therefore, adopted a procedure in which alternate foils are used for the ^{13}N determination, the remainder being counted, without any chemical treatment, after a lapse of time sufficient to allow all activities other than ^{32}P to have decayed. While the method involving the ^{34}Cl is rapid and enables one to appreciate immediately the trend in any one experiment, we prefer on the whole to relate all our work to the ^{32}P yield. This is partly because we have accumulated more data on the ^{32}P distribution, since many bombarded foils have been kept without chemical treatment from other series of experiments as well as this.

Fig. 1

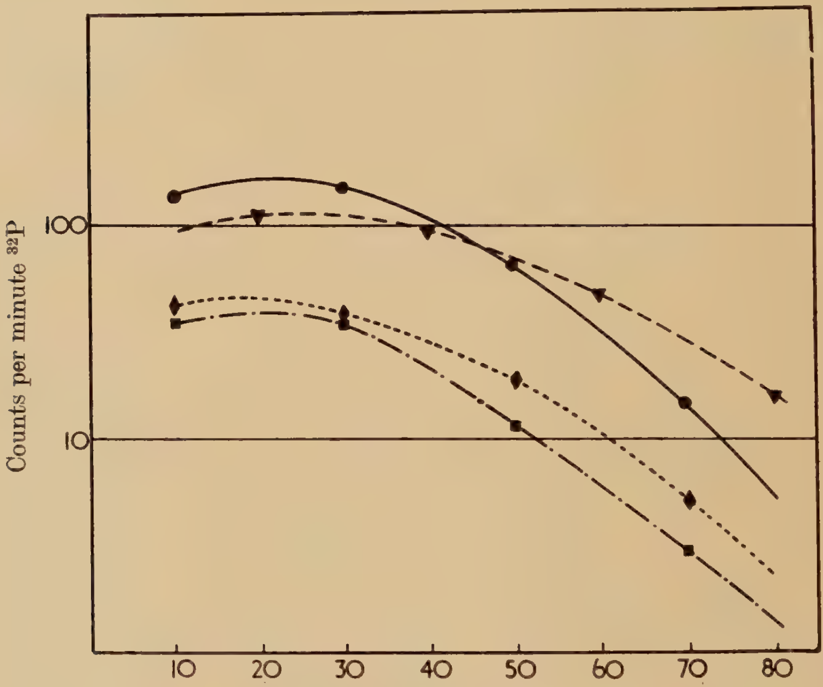

Typical distribution of ^{32}P yield in a stack of Al foils.

More importantly, the shape of the curve of ^{32}P yield versus target thickness appears to vary from experiment to experiment rather less than does that of ^{34}Cl, which may indicate a smaller dependence on initial energy spectrum of the ^{14}N beam. Although in general ^{32}P yields, expressed in terms of counts per minute for a standard geometrical arrangement, are obtained only on alternate foils, the curve of activity versus depth (or foil number) shows a rather rounded maximum (see fig. 1), enabling interpolations to be made for the missing foils with some confidence. We have therefore, in what follows, expressed our ^{13}N yields as counts per minute

Fig. 2*

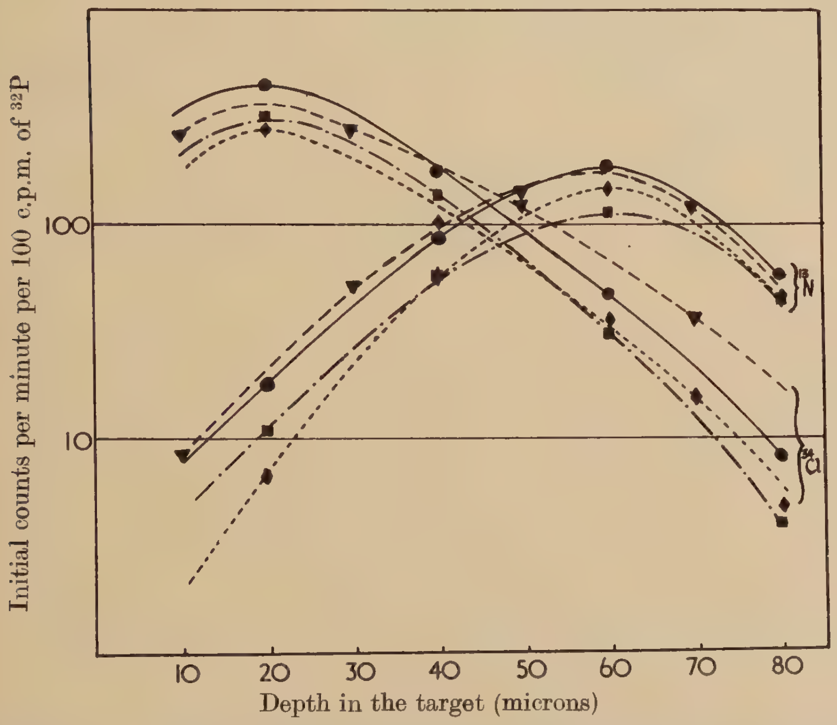

Distribution of yields of ^{13}N and ^{34}Cl in a stack of aluminium foils bombarded by ^{14}N^{6+} ions under resonance conditions.

relative to 100 counts per minute of ^{32}P in an 80 μ thickness (i.e. eight 10 μ foils) of aluminium below a ‘ cover foil ’ of 5 μ (see § 2). Due corrections have been made for radio-active decay.

For comparison we give in addition to the ^{13}N results those obtained for ^{34}Cl (fig. 2). These were derived from the same experiments. These results, and those for some other products, will be discussed in more detail in a later paper.

---

* *Note added in proof.*—Ordinate scale in fig. 2 should be multiplied by 10.

§ 2. EXPERIMENTAL

The bombardment conditions were those previously described (Chackett *et al.* 1954), a stack of about 10 foils of 10 μ thickness being bombarded under a 5 μ cover foil at a radius of 63·5 cm. Bombardment times were uniformly exactly 10 minutes, after which selected foils were analysed both for ^{13}N and ^{34}Cl.

Each selected foil was dropped into a cold alkaline solution containing KCl and NH_4OH carriers in a small reaction tube of special design (see fig. 3). The tube was plugged loosely at the top to prevent droplets of liquid from being splashed out, and then fitted into a hole cut into a square of perspex carrying a pad of gauze soaked in dilute sulphuric acid. The joint was made reasonably gas-tight with Plasticine. The tube was then dipped into hot water which caused rapid solution of the target, after which a fine stream of air was bubbled through the solution for 60 seconds, the evolved ammonia, carrying ^{13}N as $^{13}NH_3$, being trapped on the gauze pad. The tube was detached and the perspex square slid into a standard Geiger counter source-holder. By this technique six foils could be treated and counting begun within 20 minutes of the end of bombardment. Decay curves were followed in some cases for five half lives ; no activities other than the ten-minute ^{13}N were detected.

Fig. 3

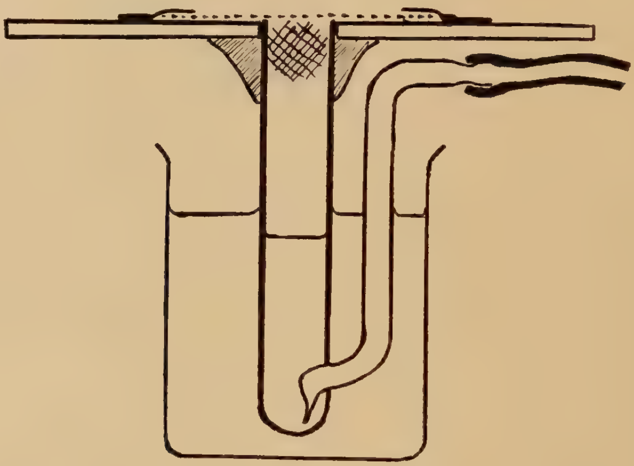

Apparatus for ^{13}N estimation.

The remaining solution was acidified with nitric acid and a radiochemically pure silver chloride sample carrying ^{34}Cl was obtained from each ; these were counted on the same counters as the ^{13}N samples, in as nearly the same geometrical conditions as could be conveniently achieved.

The inherent inaccuracies in the ^{13}N and ^{34}Cl assays are very small compared to the variations found from foil to foil. The chemical yield of the ^{13}N procedure was checked in a special experiment by using a second gauze pad, immediately after the first, and bubbling air through the same solution for a further two minutes ; the activity found on the second pad was less than 5% of that on the first, indicating that the standard procedure gave an efficiency of at least 95%. Much more important, probably, was the effect of possible lateral displacement of the active atoms on the pad, which would introduce errors due to inconstant geometrical efficiency in different experiments. Such an effect is difficult to allow for and has been neglected ; it is hardly likely to affect the result by more than 10% or so. The straightness of the decay curves indicated that the geometrical counting efficiency did not change during counting, as might happen if diffusion through the pad took place. The errors in the ^{34}Cl determination would be very small, since chemical yields, always close to 95%, were determined by direct weighing and were allowed for. Errors due to placement of the sources under the counter would not be appreciable. In the case of the chlorine self-absorption effects would be negligible and in the case of nitrogen would be closely the same in all experiments, the factor of loss being about 1·5 times.

§ 3. RESULTS

The results of seven runs with ^{14}N bombarding ions may be summarized by the following statements.

(*a*) In four runs with $^{14}N^{6+}$ ions in which the magnetic field of the cyclotron was adjusted to exact resonance for the ion beam, the ^{13}N yield showed a well marked maximum in the sixth of ten 10 μ foils, the counting rate at the peak being a factor of about ten greater than that from ^{13}N in the second foil (fig. 2). This is in contrast to the results for ^{34}Cl, shown in the same figure, the peak in this case occurring at a depth of only 20 microns.

(*b*) In two runs with $^{14}N^{6+}$ ions the magnetic field was deliberately held too high (by about 0·4%) for exact resonance, the beam current recorded during the bombardment being about 30% of the resonant maximum. In this condition it is known (Walker *et al.* 1954) that the beam is relatively richer in high energy particles, and should therefore show greater average penetration. The observed ^{13}N yield, and the ^{34}Cl yield, were in fact slightly enhanced in the deeper foils. A run in which the magnetic field was kept a little below exact resonance conditions, however, gave a ^{13}N distribution with a maximum in the sixth foil and not of significantly different shape from the four similar curves from the exact resonance runs. It appears, therefore, that such variations in the initial energy spectrum of the beam as may be produced by slight changes in the magnetic field of the cyclotron have only a minor effect on the distribution in depth of the reaction products.

(*c*) There are quite significant variations in the total yield of ^{13}N (and of ^{34}Cl) summed over all the foils, from experiment to experiment, in the group of ‘ resonance runs ’. Thus, again normalizing to 100 c/m of ^{32}P initially summed over eight 10 μ foils, the corresponding counts for ^{13}N, summed over the same foils, vary from 4300 to 6500 : the counts for ^{34}Cl vary from 8200 to 14 600. These figures are not very accurate, as the ^{32}P counting rate was often low. The variations are, however, in part real, being perhaps due to variation in conditions at present outside our control, such as the pressure inside the cyclotron tank. Such variable factors might well have the effect of changing the shape of the initial energy spectrum of the beam.

§ 4. Discussion

The results are very suggestive of a type of neutron stripping reaction, giving ^{13}N, in which a large part of the forward momentum remains with the nitrogen nucleus. If the initial kinetic energy of the ^{14}N ions involved is large and the interaction energy is small, the product ^{13}N nucleus can be deflected through only a small angle from the direction of the ^{14}N beam. It will therefore reach a depth in the stack comparable with that which would have been reached by the original ^{14}N ion if undeflected. The large displacement observed would therefore be expected. The ^{32}P and ^{34}Cl produced, however, whatever the reactions involved, will on simple kinematical grounds have only a small kinetic energy and a correspondingly small displacement in the direction of the beam. An approximate quantitative treatment is being worked out.

It is of interest to try to relate the yield of the ^{13}N in all the foils to that of the other nuclear fragments produced simultaneously. In the case of the ^{14}N bombardments this would be ^{28}Al if the neutron-exchange mechanism is correct ; however, some of these nuclei may be left in an excited state and may emit a particle such as a neutron, alpha particle or proton ; of these processes alpha emission alone will lead to an observable product, viz. ^{24}Na. From the present experiments under resonance conditions we calculate a yield of ^{13}N atoms, per 100 ^{34}Cl atoms, of about 25 ; this is to be compared with the yield, per 100 ^{34}Cl atoms, of 12 for ^{24}Na and 150 for ^{28}Al given previously (Chackett *et al.* 1954). It appears, therefore, that most of the ^{28}Al, and perhaps also some of the ^{24}Na, is made in processes which do not lead also to ^{13}N. This may mean either that fragmentation of the ^{13}N frequently occurs after neutron loss, or that ^{28}Al is produced also in processes such as alpha-particle emission from excited states in ^{32}P. The reaction $^{13}N \rightarrow 3\alpha + p$ requires only about 9 MeV, and in fact another way of explaining the strong forward displacement of the ^{13}N atoms observed might be that large deflections would involve a strength of interaction much above this, so that any product ^{13}N nuclei would rarely remain intact.

To conclude, we believe that the data presented confirm conclusively that the ^{13}N is produced by a form of stripping reaction, and give a strong indication that the neutron transfer occurs at interaction energies well below the potential barrier as usually calculated. An important point is also clearly demonstrated for any future work on excitation functions, done by stacked-foil techniques, with heavy ions. This is that careful consideration is required of the displacement from their point of origin of the products observed. Particular care must be observed in the interpretation of results obtained by the use of beams whose energy has been much reduced by absorption methods, when active products formed in the absorber and travelling on with the beam may make large contributions to activities subsequently observed in the target. Conversely, such effects might be utilized in closer studies of reaction mechanisms.

ACKNOWLEDGMENTS

The authors would like to thank Professor P. B. Moon and several other members of the laboratory for useful discussions, and others for technical assistance.

REFERENCES

CHACKETT, K. F., FREMLIN, J. H., and WALKER, D., 1954, *Phil. Mag.*, **45,** 173.

WALKER, D., FREMLIN, J. H., LINK, W. T., and STEPHENS, K. G., 1954, *Brit. J. Appl. Phys.*, **5,** 157.

LXXXI. *The Angular Distributions of α-Particles from the* ^{14}N(d, α) *Reaction at Low Bombarding Energies*

By D. Cartwright, L. L. Green and J. C. Willmott
Nuclear Physics Research Laboratory, University of Liverpool*

[Received April 2, 1954]

Abstract

The angular distribution of the α-particles from the ^{14}N(d, α) reaction proceeding to the ground and first excited states of ^{12}C have been studied at low bombarding energies. The results show that in the region of 21 mev excitation energy ^{16}O has states 1^-, 2^+, 3^-, but there is no state of zero spin and even parity.

§ 1. Introduction

The angular distributions of the two α-particle groups from the ^{14}N(d. α) reaction which leave ^{12}C in its ground state and first excited state respectively, have previously been studied by Gibson and Thomas (1952) using 7·9 mev deuterons. These authors used a photographic plate method and the results they obtained were extremely complex and they were unable to analyse them. This, and the fact that the excitation energy of the compound nucleus is rather high (20·7 mev) suggest we may be in a region of many overlapping levels. Hence it was considered worth while to study this reaction at low bombarding energies where penetration factors would perform a certain amount of selection in the levels of the compound nucleus which can take part.

§ 2. Apparatus and Measurements

A beam of deuterons was accelerated in a 1 mev Philips H.T. set electronically stabilized to within one Kilovolt, and then bent and analysed by a variable field permanent magnet built by the magnet division of Mullards. The beam then passed through a collimator into the angular distribution chamber shown in fig. 1. The target was insulated from the base of the chamber to enable the beam current to be measured, and its position was adjustable in height and laterally. The position of the target was adjusted by means of sighting tubes to be in the middle of the chamber for all positions of the base plate. The whole apparatus was then checked, (*a*) by placing a natural Thorium α-particle source in the position of the target and observing that an isotropic angular distribution was obtained, and (*b*) by using the ^{7}Li(p, α) reaction. In this way it was found that the measured angular distribution was within 1% of the true distribution.

---

* Communicated by Professor H. W. B. Skinner, F.R.S.

The reaction products were detected in a large proportional counter filled with 60 cm of argon and 1 cm of carbon dioxide. The particles entered the counter through a thin mica window (about 1·6 milligram/cm^2) and their maximum residual range in the counter was equivalent to about 10 cm of air at N.T.P. The window of the counter subtended a solid angle at the target of 0·15%. An absorber wheel, which was mounted on the counter, and which carried various thicknesses of aluminium foil, enabled the residual range to be adjusted to the most suitable value. The energy resolution was about 3%. After amplification the resultant pulses were counted by a 30-channel pulse amplitude analyser, and a smaller proportional counter mounted at 90° to the beam direction acted as a beam monitor.

Fig. 1

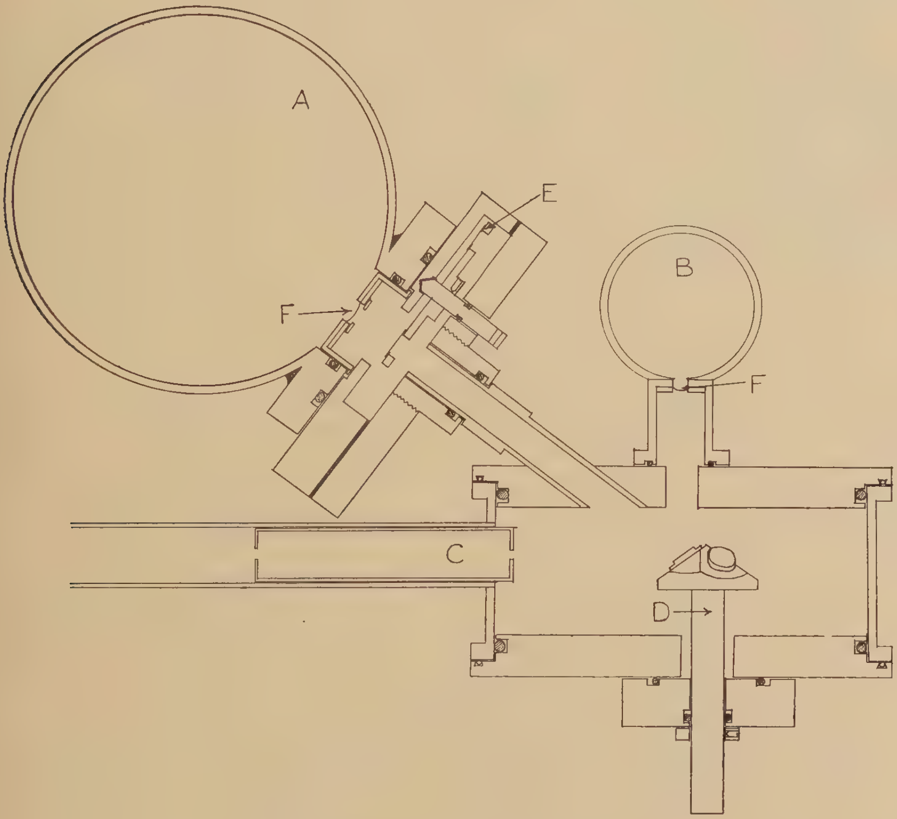

Target chamber and counters.

A—Proportional counter.
B—Monitor counter.
C—Coltimator.
D—Target pillar.
E—Absorber wheel.
F—Mica windows.

The target consisted of adenine evaporated on to a copper backing. The uniformity and thickness of the targets could be judged by the interference colours seen under white light. For the measurement of the angular distributions small area targets less than 20 kev thick were used, while for the measurement of the yield-curve a special thin, large area target was used, the area of completely uniform coloration in this case being more than ten times the area covered by the incident beam of deuterons.

First, the excitation function was measured in the energy range from 450 kev to 900 kev, in order to discover if there are any resonances in this region. Due to the high excitation of the compound nucleus and the energy of the outgoing α-particles, only broad resonances would be likely to occur; hence the excitation curve was taken at approximately 50 kv intervals. After the yield had been measured at each of the energies, the yield at 716 kev bombarding energy was measured to check that the target conditions had remained unchanged. The large proportional counter was placed at 135° to the beam and both groups were measured together. This means that a weak resonance in the higher energy group could have been missed, but this is not very likely in view of the fact that the ratios of the total cross sections for the two groups are very nearly the same at 595 and 730 kev.

Fig. 2

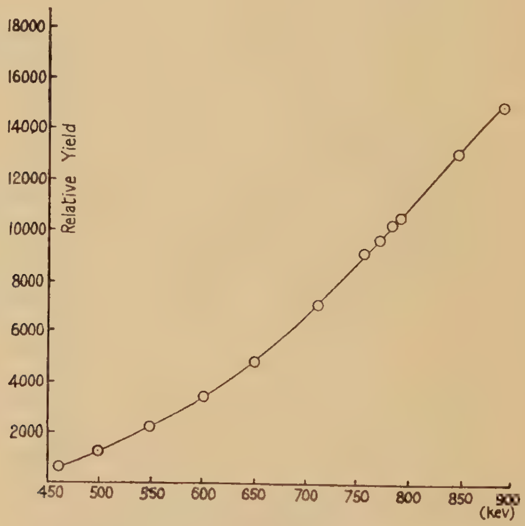

Deuteron bombarding energy (kev).

The relative yield against energy for both groups together is shown in fig. 2. It will be seen that the yield is a steadily rising function of energy, and, in view of this, it was decided to measure the angular distributions at two energies in the region from 450 kev to 900 kev.

§ 3. RESULTS

The results for the α-particles going to the ground state and to the 1st excited state of ^{12}C are shown in figs. 3 and 4 for bombarding energies of 595 kev and 730 kev respectively. It will at once be seen that the yield to the 1st excited state is much greater than the yield to the ground state, and more isotropic. The ratios of the total cross sections at the two energies, calculated from the fitted curves are

Fig. 3

595 kev bombarding energy

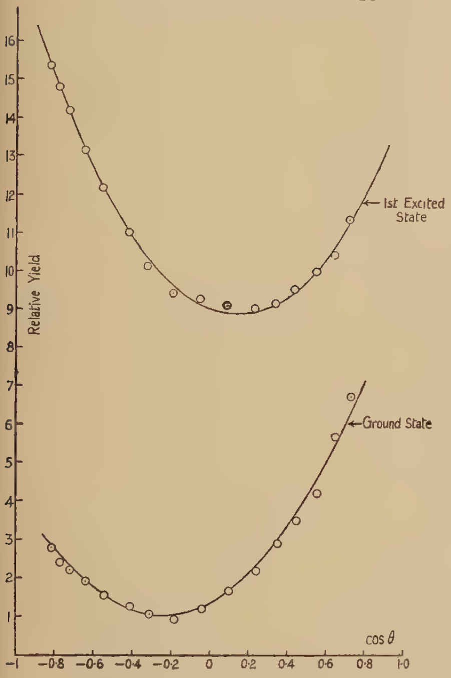

θ=centre of mass angle.

Fig. 4

730 kev bombarding energy

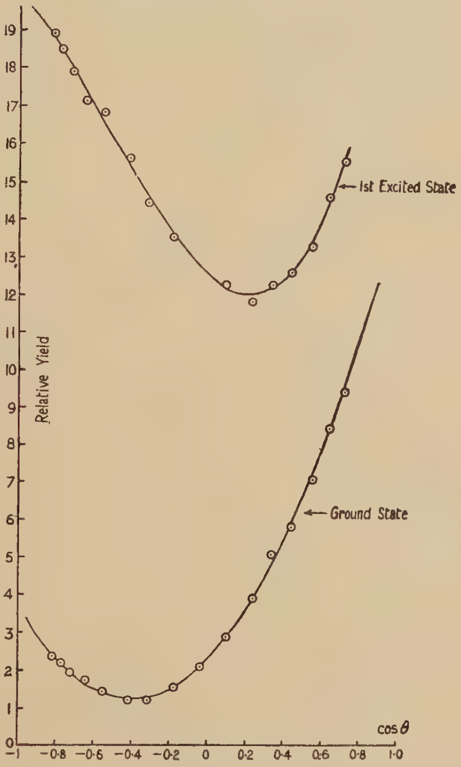

θ=centre of mass angle.

$$595 \text{ kev } \sigma_{T'}/\sigma_T=3{\cdot}5, \qquad 730 \text{ kev } \sigma_{T'}/\sigma_T=3{\cdot}4$$

where $\sigma_{T'}$ is the total cross section for the emission of α-particles to the 1st excited state of ^{12}C and σ_T is the total cross section for emission to the ground state.

The angular distribution for these α-particles have been analysed in terms of Legendre polynomials: the coefficients in the equation

$$\gamma_\theta=\gamma_{90}[P_0(\cos\theta)+aP_1(\cos\theta)+bP_2(\cos\theta)+cP_3(\cos\theta)]$$

are given in table 1 together with their probable errors.

It will be seen that except for a fairly small term in P_3 in the angular distribution of the 1st excited state at 730 kev the distribution is of the form

$$P_0(\cos\theta)+aP_1(\cos\theta)+bP_2(\cos\theta)$$

This form is largely governed by the penetrability of the ingoing waves, which have been calculated in table 2 from the data given by Bloch *et al.* (1951). It will be seen that only ingoing waves up to $l=2$ need be considered, and even the $l=2$ wave will largely make itself felt by its interference with $l=0$ waves, as this term is proportional to $\sqrt{p_0p_2}$ rather than to p_2.

Table 1

Energy	Ground state		
	a	b	c
595 kev	$0·846\pm0·013$	$1·173\pm0·021$	—
730 kev	$1·174\pm0·031$	$0·979\pm0·024$	—
	1st excited state		
	a	b	c
595 kev	$-0·174\pm0·008$	$0·416\pm0·016$	—
730 kev	$-0·056\pm0·007$	$0·368\pm0·011$	$0·138\pm0·016$

Table 2. Relative Penetrability p_L for d on ^{14}N

Radius	Energy	p_0	p_1	p_2	p_3
5×10^{-13} cm	595 kev	1	0·27	0·024	$0·95\times10^{-3}$
5×10^{-13} cm	730 kev	1	0·30	0·031	$1·5\times10^{-3}$
6×10^{-13} cm	730 kev	1	0·31	0·050	$3·3\times10^{-3}$

The outcoming α-particles are too high above the potential barrier for there to be any discrimination against high l-values.

The asymmetry of the distributions about 90° in the centre of mass system indicates that at least two states of opposite parities in the compound nucleus must be considered. The angular distributions for the two α-particle groups have been compared with the results to be expected according to the theory of angular distributions as given by Blatt and Biedenharn (1952) in their review article. The spin of the residual nucleus in the ground state is zero and the state is of even parity. Consequently, only states 0^+, 1^-, 2^+, etc. in the compound nucleus can decay by α-emission to this state. Owing to penetrability considerations, 4^+ is the highest level which is likely to take part at these bombarding energies, and, except where it interferes with levels of lower angular momentum, its contribution will be small. The simplest assumption that can be made is that just two states of opposite parity partake in the reaction, and initial calculations were made assuming the states in the compound nucleus to be 0^+ and 1^-, and then 0^+ and 3^-; both these assumptions led to angular distributions in which the coefficient of P_1 was far too small and further calculations showed that indeed any combination of two or three levels which included among them a 0^+ state led to a similar result. A combination of 1^- and 2^+ again gives too low a value for the coefficient of P_1 at 730 kev bombarding energy, though agreement can be obtained at 595 kev if one makes some artificial assumptions about the combinations of channel spin and orbital angular momentum which take place. In particular, the probability, after removal of geometrical factors, of a state 1^- being formed from channel spin $s=1$ and orbital angular momentum $l=1$ must be more than an order of magnitude greater than the probability of formation from $s=0$ and $l=1$, or $s=2$ and $l=1$, and the relative phase for $s=1$ and $l=1$ combination must have an extreme value.

The addition of a 3^- state to the 1^- and 2^+ states for the compound nucleus leads quite satisfactorily to the desired result at both energies without the introduction of the assumptions required before.

In the case of the first excited state there are no parity restrictions on the levels in the compound nucleus which can take part in the reaction. Consequently other levels would be expected to take part as well as the states 1^-, 2^+ and 3^- which are necessary to explain the results for the ground state. Thus a higher yield would be expected for this state as has been found to be the case. As a result of the high spin of the final nucleus in this state ($J=2$), a fit of the experimental results could probably be obtained for almost any set of assumed levels, owing to the large number of parameters available for adjustment, and so no information on how many further levels exist can be obtained from this treatment of the data. However, the experimental results are similar to those obtained using Wolfenstein's (1951) method for the calculation of angular distributions when there is a statistical density of energy levels in the compound nucleus. This method leads to the result that the coefficients of the odd Legendre polynomials are zero, the coefficient of P_2 is of the same order as found in this experiment and higher even terms have coefficients decreasing by at least an order of magnitude. The coefficients of the odd terms obtained by us are not zero, but they are small.

We should like to thank Professor H. W. B. Skinner for his encouragement and advice and also Dr. R. Huby for many interesting discussions and for the calculations based on the statistical model of Wolfenstein. One of us (D.K.C.) is grateful to the Department of Scientific and Industrial Research for a research grant.

References

Blatt, J. M., and Biedenharn, L. C., 1952, *Rev. Mod. Phys.*, **24**, 241.
Bloch, I., Hull, M. M., Broyles, A. A., Bouricius, W. G., Freeman, B. E., and Breit, G., 1951, *Rev. Mod. Phys.*, **23**, 147.
Gibson, W. M., and Thomas, E. E., 1952, *Proc. Roy. Soc.*, **210**, 543.
Wolfenstein, L., 1951, *Phys. Rev.*, **82**, 690.

LXXXII. *On the Relation between Čerenkov Radiation and Bremsstrahlung*

By J. D. Lawson
Atomic Energy Research Establishment, Harwell*

[Received April 14, 1954]

In his paper on Čerenkov radiation, Tamm (1939) calculates the angular distribution of radiation intensity obtained when the track of the radiating particle is of finite length. This radiation he then divides into two parts, one of which is identified with true Čerenkov radiation, the other being associated with the acceleration of the charge at the beginning and end of the track. This separation into two components is somewhat arbitrary, and it is not in general possible to associate the radiation in a specific direction with either component. The implications of this fact will now be studied, taking Tamm's purely classical analysis as a starting point.

In Tamm's analysis the particle is represented by a δ-function of current, which is then Fourier analysed into a spectrum of current waves of the form

$$I=I_0 \cos \omega(t-x/\beta \mathbf{c}) \quad . \quad . \quad . \quad . \quad . \quad . \quad (1)$$

where $\mathbf{c}$ is the velocity of light in free space and $\beta\mathbf{c}$ the velocity of the particle. The radiation field from each component may then be calculated and the total radiation found by integrating over ω. It is interesting to note that the problem is just that of finding the polar diagram of an array of Hertzian dipoles placed end to end, and fed in such a way that there is a progressive change of phase along the array.

The radiation intensity per unit solid angle from a single frequency component may be written

$$R(\theta)=\frac{K^2a^2\sin^2\theta}{\lambda^2}\left\{\frac{\sin\left[\frac{\pi a}{\lambda}\left(\frac{1}{\beta n}-\cos\theta\right)\right]}{\frac{\pi a}{\lambda}\left(\frac{1}{\beta n}-\cos\theta\right)}\right\}^2 \quad . \quad . \quad . \quad (2)$$

where K is a constant proportional to the current, a=the length of the track, n=the refractive index of the medium and λ=the wavelength in the medium. This formula is implied in Tamm's eqns. 7·6 and 7.9, but not explicitly stated in the above form. In order to study the characteristics of the radiation as a and β are varied, we write eqn. (2) in the form

$$\frac{2\lambda^2R(\theta)}{K^2a^2\sin^2\theta}=\frac{\lambda^2}{\pi^2a^2(1/\beta n-\cos\theta)^2}\left\{1-\cos\left[\frac{2\pi a}{\lambda}\left(\frac{1}{\beta n}-\cos\theta\right)\right]\right\}. \quad (3)$$

This may be further simplified to

$$S(y)=y^{-2}(1-\cos 2y) \quad . \quad . \quad . \quad . \quad . \quad . \quad (4)$$

where

$$y=\frac{\pi a}{\lambda}\left(\cos\theta-\frac{1}{\beta n}\right). \quad . \quad . \quad . \quad . \quad . \quad . \quad . \quad (5)$$

---

* Communicated by the Author.

From eqn. (4) it will be seen that θ is only real in the range

$$1 > \lambda y/\pi a + 1/\beta n > -1,$$

and that the width of that part of $S(y)$ which corresponds to real angles is $2\pi a/\lambda$. $S(y)$ is plotted in the figure, and the range of real angles shown for the special case when $a = 4\lambda$ and $1/\beta n = 1/2$. It is evident that the maximum of the curve only occurs at a real angle if $\beta n > 1$. According to the distinction drawn by Tamm we get Čerenkov radiation and acceleration radiation if $\beta n > 1$, but only acceleration radiation if $\beta n < 1$.

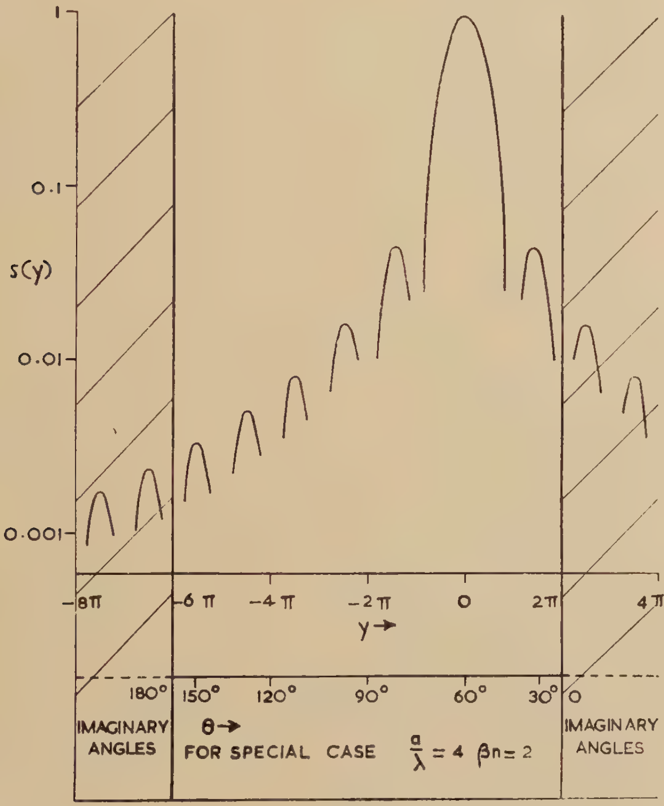

The function $S(y)$, real and imaginary regions are shown for a special case

However there is no physical discontinuity as βn passes through unity, the curve in the figure just moves bodily to the right as βn increases. This argument shows clearly that it is not possible to make a sharp distinction between Čerenkov radiation and the radiation caused by accelerating the electron.

So far we have only considered a finite track; as a increases, that part of $S(y)$ corresponding to a given angular range increases, and in the limit of an infinite track a sharp transition does indeed occur at $\beta n = 1$. However in any practical material the track is broken up into a series of short lengths by scattering. The curve $S(y)$ therefore has a finite width which is determined by the statistics of the scattering. Now since $S(y)$ has a finite width some radiation will occur when $\beta n < 1$. This radiation may be identified with bremsstrahlung. When $\beta n > 1$ the distinction between Čerenkov radiation and bremsstrahlung is not sharp.

Returning to the consideration of a single finite track we note that for relativistic particles in free space $\beta n = \beta \approx 1 - E^2/2\boldsymbol{m}^2\mathbf{c}^4$, so that for small θ eqn. (3) may be written

$$\frac{8\pi^2 R(\theta)}{K^2} = \frac{\theta^2}{(\theta^2 + \boldsymbol{m}^2\mathbf{c}^4/E^2)^2}\left\{1 - \cos\left[\frac{\pi a}{\lambda}\left(\theta^2 + \frac{\boldsymbol{m}^2\mathbf{c}^4}{E^2}\right)\right]\right\}, \quad . \quad (6)$$

The overall angular distribution will not be affected appreciably by the second factor of the right hand side, provided that the oscillation of the cosine term is sufficiently rapid. As a rough criterion we might say that there should be many cycles between $\theta = 0$ and $\theta = \boldsymbol{m}\mathbf{c}^2/E$. This will be so if

$$a/\lambda \gg 2E^2/\boldsymbol{m}^2\mathbf{c}^4 \quad . \quad . \quad . \quad . \quad . \quad . \quad . \quad . \quad (7)$$

If this condition holds the overall angular distribution and intensity of the radiation are independent of a and λ (since they only occur in the cosine term) and the maximum intensity occurs at an angle $\theta_1 = \boldsymbol{m}\mathbf{c}^2/E$. If it does not hold, the radiation is not so strongly beamed forward and the maximum occurs at an angle greater than $\boldsymbol{m}\mathbf{c}^2/E$. In the limit when a/λ becomes small $S(y)$ is constant throughout the real range and $R(\theta)$ is proportional to $\sin^2\theta$.

The radiation just discussed is very similar to bremsstrahlung, and similar criteria for ensuring that the radiation does travel forward as predicted by the Bethe-Heitler theory are likely to apply. If the distance between scattering centres is of order $\lambda E^2/\boldsymbol{m}^2\mathbf{c}^4$ or less the distance a is not clearly defined, but might be taken as roughly that length of track from which the radiation adds coherently at a distant point. Such a length cannot easily be defined since the degree of coherence between the radiation from one element of track and another progressively deteriorates as the distance between them increases, and furthermore it depends on the angle to the track at which the radiation is measured (even this cannot be clearly defined since the direction of the track varies), so the problem is of great complexity. An indication of this may be seen in a paper by Dedrick (1952), where some calculations of this nature are carried out.

The considerations in this note emerged after discussions with Dr. J. V. Jelley, to whom I am indebted for suggesting the problem.

REFERENCES

Dedrick, K. G., 1952, *Phys. Rev.*, **87**, 891.
Tamm, I., 1939, *J. Phys. U.S.S.R.*, **1**, 439.

LXXXIII. *Neutron Scattering and the Weak-Interaction Model of the Nucleus*

By J. M. C. Scott
Cavendish Laboratory, Cambridge*

[Received April 8, 1954]

Summary

Data on the scattering of slow neutrons are examined, using the theory of a previous paper, to see whether a size-resonance effect exists (of the kind which can be pictured qualitatively in terms of the crystal ball model). It is concluded that the effect is real, and that the resonances occur at the predicted values of the mass-number.

It is also found that a single-particle wave function for the incident neutron in the nucleus suffers less perturbation with medium weight nuclei than it does with heavy or light nuclei ; there seems to be no obvious explanation.

§ 1. Introduction

The results obtained in experiments on the coherent scattering of slow neutrons (Hughes 1953) give us the coherent scattering lengths, $a=\pm\sqrt{(\sigma_{\text{coh}}/4\pi)}$, of about 70 isotopes or elements, if we exclude the lightest elements. Some properties of these scattering lengths have been discussed in a previous paper (Scott 1954 a, which will be referred to as I). The present paper is concerned with the question of how far they exhibit a ‘ size resonance ’ effect, depending on the distance from the surface of the nucleus to the centre and back measured in wavelengths of the neutron. This question is intimately related to the question whether the weak-interaction model or the medium-interaction model outlined in I is the more appropriate. Although the answer does not affect the main conclusions of I, the distinction between the two models is important for the understanding of other properties of medium and heavy nuclei.

§ 2. Partial Reflection and Transmission Properties of a Boundary Layer

It was shown in I that the statistical distribution of the known values of

$$a-R=a-(r_0A^{1/3}+\text{const}) \quad . \quad . \quad . \quad . \quad . \quad . \quad (1)$$

is not consistent with the hypothesis of a simple potential-well model of the nucleus with a sharply defined surface, since the well depth would be required to have the impossibly low value of 7 Mev. The constant r_0 here, which determines the nominal radius, may be taken as

$$r_0=12\times10^{-14}\,\text{cm}\,; \quad . \quad . \quad . \quad . \quad . \quad . \quad . \quad . \quad (2)$$

---

* Communicated by the Author.

the exact value chosen for r_0 turns out to be rather unimportant.

The partial reflection and transmission properties of a boundary layer which is not sharp can be conveniently formulated as follows. In the internal region of the nucleus (fig. 1), the well depth $-V(r)$ is W (some 45 or 50 Mev) and the neutron wavelength is $2\pi/K$. The wave equation for the wave function $r^{-1}f(r)$ of an s neutron has solutions $f^{(i)}(r)$ in the interior region which can be taken either as

Fig. 1

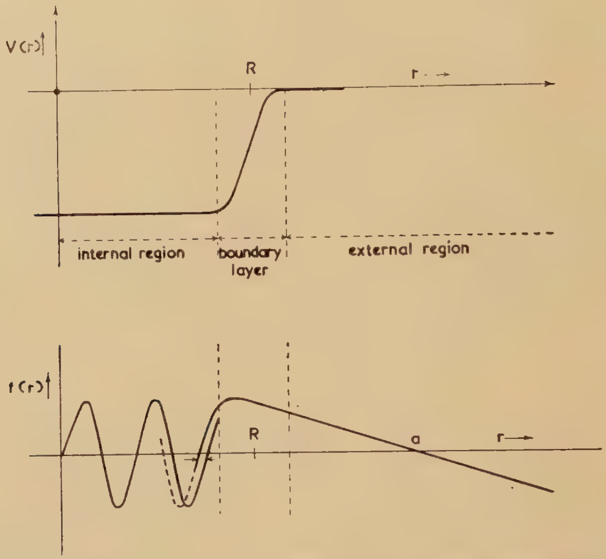

The phase-shift indicated by the arrows in the lower diagram is the angle β which is plotted in fig. 2.

$$f^{(i)}=a_1 \sin Kr+a_2 \cos Kr$$

or as

$$f^{(i)}=b_1 \exp (iKr)+b_2 \exp (-iKr).$$

There are similar solutions $f^{(e)}$ for the external region. The properties of the boundary layer at any given energy could be specified by a 2×2 matrix which connects (a_1, a_2) or (b_1, b_2) with the corresponding constants for the continuation $f^{(e)}$ of the same function in the external region.

Consider now a small range of energies, say 1 kev, corresponding to slow neutrons outside the nucleus. The internal wave number K varies little in this range of energies, and can be taken equal to its zero-energy value K_0, but the great variation of the external wavelength would make the partial-transmission matrix sensitive to energy if it were taken in this form. It is preferable to work instead with the matrix $\{c_{st}\}$ (defined below) which connects the values of the wave function and its derivative just inside with their values just outside. To avoid introducing unnecessary symbols we suppose the wave functions inside and outside to be extrapolated sinusoidally as far as $r=R$ and evaluated there. They are connected by the relations

$$f^{(e)}(R)=c_{11}K^{1/2}f^{(i)}(R)+c_{12}K^{-1/2}f^{(i)\prime}(R) \quad . \quad . \quad . \quad . \quad . \quad (3\,a)$$

$$f^{(e)\prime}(R)=c_{21}K^{1/2}f^{(i)}(R)+c_{22}K^{-1/2}f^{(i)\prime}(R). \quad . \quad . \quad . \quad . \quad . \quad (3\,b)$$

Then (i) the matrix $\{c_{st}\}$ is evidently real, (ii) it is approximately independent of energy in a small range of the order of 1 kev, and (iii) the constancy of the Wronskian of any two solutions requires that the determinant of the matrix should satisfy

$$c_{11}c_{22}-c_{12}c_{21}=1\,; \quad . \quad . \quad . \quad . \quad . \quad . \quad . \quad . \quad . \quad . \quad (4)$$

(iii) and (i) in effect ensure the conservation of neutron flux through the layer.

The matrix $\{c_{st}\}$ evidently needs three real parameters to specify it completely. These will be chosen as follows. If we define a length S, by

$$S=1/(c_{21}{}^2+c_{22}{}^2)$$

c_{21} and c_{22} can be written in the form

$$c_{21}=S^{-1/2}\sin\alpha, \quad c_{22}=S^{-1/2}\cos\alpha\,;$$

and then one other real parameter Y, besides S and α, suffices to specify the most general relations (3) that are consistent with (4):—

$$\begin{pmatrix} c_{11} & c_{12} \\ c_{21} & c_{22} \end{pmatrix}=\frac{1}{\sqrt{S}}\begin{pmatrix} S\cos\alpha-Y\sin\alpha & -S\sin\alpha-Y\cos\alpha \\ \sin\alpha & \cos\alpha \end{pmatrix}. \quad . \quad . \quad (5)$$

§ 3. RELATION OF THE CONSTANTS TO NEUTRON SCATTERING

The usefulness of the constants S, Y and α for describing the boundary layer lies in their physical interpretation in elastic scattering. If the wave function of an incident slow neutron just inside the nucleus can be described by

$$f^{(i)}(r)=\sin(Kr+\beta) \quad . \quad . \quad . \quad . \quad . \quad . \quad . \quad . \quad (6)$$

then according to (3) the scattering length of the nucleus for neutrons of that energy is

$$a=R-\frac{f^{(e)}(R)}{f^{(e)\prime}(R)}=R+Y+S\tan\theta \quad . \quad . \quad . \quad . \quad . \quad (7)$$

where

$$\theta=-KR+\alpha-\beta. \quad . \quad . \quad . \quad . \quad . \quad . \quad . \quad . \quad . \quad (8)$$

Thus S determines the extent of the spreading of the values of the scattering-lengths above and below the value of the apparent nuclear radius; Y is a minor correction to the radius, scarcely greater than the present uncertainties in R; and α is a phase angle which (together with KR) fixes the place at which the size-resonances should come in the periodic table.

The value of β depends on the internal structure of the nucleus and raises deeper questions. In the extremest form of the weak-interaction model (' zero interaction '), the wave-function can be decomposed exactly into a single particle wave-function and the parent wave-function of the target or residual nucleus ; and then β in (6) must be zero. In the weak-interaction model proper, β (which is to be evaluated just inside the internal region) is a small angle, determined by perturbations, unless there happens to be a resonance level of the compound nucleus at an energy very close to that of the actual system. It may be, on the other hand, that β is effectively random : this happens in the case which we have called medium interaction.

§ 4. METHOD OF ANALYSING THE DATA

If $a-r_0A^{1/3}$ be plotted against $A^{1/3}$, then the extreme weak-interaction model predicts that the points should fall on a curve which is the graph of $y=-\tan x$ drawn with a suitable scale and origin, whereas the medium interaction model predicts an irregular collection of points, with ordinates randomly distributed in a distribution depending on S, and uncorrelated with the abscissa $A^{1/3}$. One can study the data better, however, by estimating the θ of (7) and (8) from

$$\theta=\tan^{-1}\frac{a-(r_0A^{1/3}+Y)}{S} \quad . \quad . \quad . \quad . \quad . \quad . \quad . \quad (9)$$

and plotting this against $A^{1/3}$. As θ is multiple–valued, being indeterminate by an arbitrary multiple of π, the extreme weak-interaction model would predict a series of parallel lines separated by a vertical interval of 180°, descending with a gradient $-Kr_0$; the total descent as far as the thorium region should be about 600°. The extent to which the points are crowded towards these lines will furnish a criterion of the weakness of the interaction, and of the reality of the suggested size-resonance effect in the slow neutron cross sections.

Instead of doing this, we have added KR to θ, in order to get rid of the linear change of phase with radius, and have plotted

$$\theta+Kr_0A^{1/3}=\alpha-\beta \quad . \quad . \quad . \quad . \quad . \quad . \quad . \quad . \quad . \quad . \quad (10)$$

against $A^{1/3}$ in fig. 2. Except for α, which is constant, this diagram is essentially a plot of β, which can be thought of as the discrepancy between the phase of the standing wave just inside the nuclear surface and the phase it ought to have if it extended right in to the centre without suffering any perturbation by admixture with neighbouring resonance levels of the compound nucleus.

§ 5. VALUES OF CONSTANTS USED ; EFFECT OF ANY INACCURACY

The following form was chosen for the potential in the boundary region :

$$V(r)=-\tfrac{1}{2}W\left\{1-\tanh\frac{r-R}{2b}\right\}. \quad . \quad . \quad . \quad . \quad . \quad . \quad (11)$$

It was one of the profiles considered in I, and is perhaps the simplest reasonably realistic transition from the well-depth W to zero. For the important constant b, determining the thickness of the transition layer, the value

$$b = 6 \times 10^{-14} \text{ cm} \quad . \quad . \quad . \quad . \quad . \quad . \quad . \quad . \quad . \quad (12)$$

was used; this is slightly greater than the experimental value (I, eqn. (52)) and slightly less than the theoretical estimate (I, § 3.2), but consistent with both. S is almost entirely determined by the value of b, and is $S = 18{\cdot}9 \times 10^{-14}$ cm according to eqn. (38).

The radius at which the potential falls to half value was taken as

$$R = r_0 A^{1/3} = 12 A^{1/3} \times 10^{-14} \text{ cm.} \quad . \quad . \quad . \quad . \quad . \quad (13)$$

The value of r_0 adopted affects the results in two ways: $R + Y$ appears in (9) as a sort of median value, above or below which the scattering length is equally likely to fall. The uncertainty in r_0 produces little effect in this way because S is so large; and $Y = 7{\cdot}5$ is known accurately enough. But the influence of the choice of r_0 on the optical path-length to the centre of the nucleus is more important: for r_0 also appears in (10), where Kr_0 determines the change of internal phase-angle with increasing radius, and K depends on the well-depth which must therefore be considered too.

Fig. 2

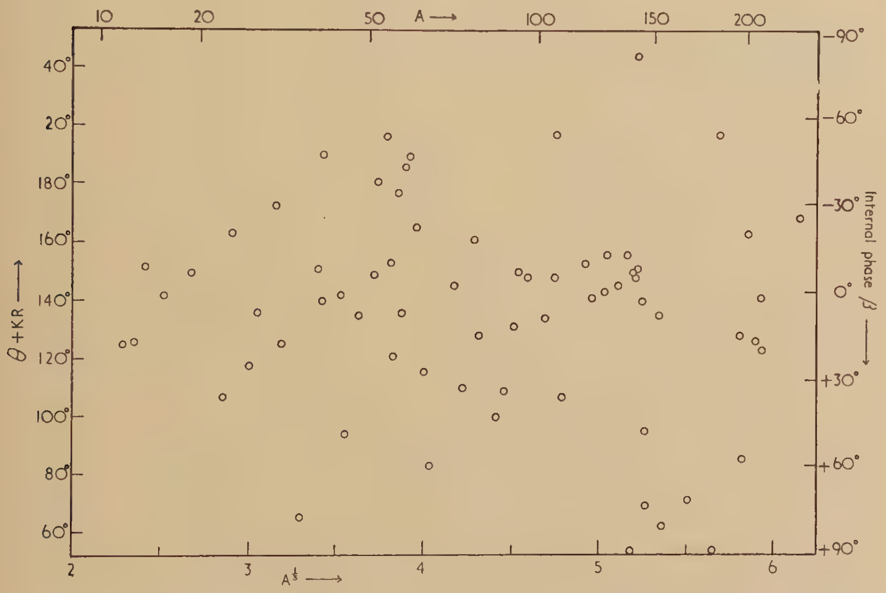

The value of the well depth deduced from the picture of a Fermi–Dirac gas of nucleons (I, § 3.1) is too rough because (i) the sides of the well were taken infinitely high, (ii) they do not slope as in (11), and (iii) the number of particles is not large. We therefore turn to the shell model, and consider a nucleus half way between $N = 50$ and $N = 82$ (to avoid any risk of fluctuations of R associated with magic numbers); from the slope of the mass-defect curve near ^{113}Cd we estimate that a neutron in a $3s$ orbit has a binding energy between 7 and 8 MeV. Using the explicit $3s$ wave function for the field (11) and treating the hypergeometric functions as in I (§ 4.41), we find

$$W = 51 \text{ MeV} \qquad . \quad . \quad . \quad . \quad . \quad . \quad . \quad . \quad (14)$$

and

$$KR = 108\, A^{1/3} \qquad . \quad . \quad . \quad . \quad . \quad . \quad . \quad (15)$$

reckoned in degrees. A larger radius than (13) would require a smaller well depth and vice versa, but the value (15) of the phase shift per unit of $A^{1/3}$ would be little affected.

The value of α can be obtained from the analysis in I, and is

$$\begin{aligned}\alpha &= 2 \arg \Gamma(1+iKb) - \arg \Gamma(1+2iKb) + \pi \qquad . \quad . \quad . \quad (16)\\ &= 143^\circ.\end{aligned}$$

The principal effect of assuming a form of potential different from (11), but with an exponential tail given by the same value of b, would be to change the value of α slightly.

Fig. 3

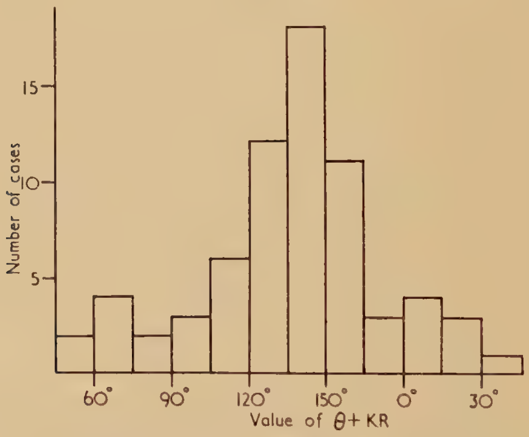

Distribution of values of $\theta + KR$.

§ 6. RESULTS AND DISCUSSION

On examining fig. 2 it is clear that the points are appreciably concentrated towards a horizontal line, the position of which agrees well enough with that predicted by the theory (143°). In fact more than half the points lie within a range of 32° out of the possible 180° (namely 125° to 156° inclusive). This may be taken as evidence supporting the weak-interaction model, and as showing that the size-resonance effect is real. In the limit of zero interaction (pure refraction model), this resonance would make the scattering cross section very large at mass-numbers 10, 56 and 164.

With weak interaction the values of β would be expected (Scott 1954 b) to follow a statistical distribution

$$dP=\frac{\sinh 2\sigma}{2\pi}\frac{d\beta}{\sinh^2\sigma+\sin^2\beta} \quad . \quad . \quad . \quad . \quad . \quad . \quad (17)$$

which varies from a narrow peak if σ is small to a uniform distribution in the limit $\sigma\to\infty$ (i.e. medium interaction). The data taken as a whole give a value of $\sigma=0{\cdot}31$ approximately, and a χ^2 test indicates a good fit to the distribution (17).

There is however a strong suggestion of inhomogeneity. The values of β for nuclei which lie in the region $4{\cdot}5<A^{1/3}<5{\cdot}2$, say zirconium to praseodymium, are much more closely crowded together than the values of β in other parts of the periodic table. This region seems to coincide with the filling of the neutron shell $N=50$ to 82, although no reason is known for expecting the weak-interaction model to be better here than elsewhere. The conspicuous change at $A^{1/3}=5{\cdot}2$ might be thought to indicate an abrupt increase in radius by some 15% at a neutron number of 82; but, quite apart from other evidence against such a substantial increase, a closer examination shows that it would not account for the present data, which seem to demand an increased scatter (σ) in the values of β.

If we divide the nuclei into three groups, with $N\leqslant 50$, $50<N\leqslant 82$, and $N>82$ (the statistics do not justify any finer subdivision), we obtain estimates of 0·37, about 0·16, and 0·8 respectively for the parameter σ which measures the strength of the interaction.

The statistical scatter of the calculated internal phase-angles β can be attributed, in part at least, to the influence of resonance levels of the compound nucleus which happen to lie very near the binding energy. It is natural to consider whether the present analysis could be refined and improved by correcting for the effect of any of these slow-neutron resonance levels for which the parameters are known. But the levels at negative kinetic energies will be just as important as the observable ones, so that the advantage gained would be slight. A better method would be to take the scattering cross section half-way between the lowest two observed resonances, and to apply corrections for those resonances (I am indebted to Professor D. J. Hughes for this remark). It is doubtful if this would be practicable except for separated isotopes of spin zero.

REFERENCES

HUGHES, D. J., 1953, *Neutron Cross Sections* (AECU 2040 and supplements), U.S. Dept. of Commerce.

SCOTT, J. M. C., 1954 a, *Phil. Mag.*, **45**, 441; 1954 b, unpublished.

LXXXIV. *A Note on the Divergence of the Perturbation Method in Field Theory*

By S. F. EDWARDS*
Department of Mathematical Physics, The University of Birmingham†

[Received May 14, 1954]

ABSTRACT

After certain approximations are made, the divergence of the perturbation series expressing the radiative corrections to the motion of a nucleon, is related to the divergence of the Born approximation to the motion of a bare nucleon in a given field.

§ 1. INTRODUCTION

SEVERAL authors (Hurst 1952, Thirring 1953, Petermann 1953, Utiyama and Imamura 1953) have performed calculations on the perturbation expansion to show that this, regarded as a power series in the coupling constant, is not a convergent series, using the method of actually summing the series and finding its lower bound to be infinite. This result persists after renormalization, and is also present in those ‘ super renormalizable ’ theories, where renormalization difficulties do not occur. Hurst suggested that the series was asymptotic, so that whereas in meson theory with large coupling constant the series was of no value, in electrodynamics it was; and this accords with the agreement with experiment of electrodynamics. No mathematical indication of how these difficulties arise has been proposed though a physical argument has been given by Dyson (1952), and this note sets out to show how an asymptotic expansion is to be expected, though for reasons which will become evident later cannot apply rigorously except to theories free from renormalization difficulties.

§ 2. CALCULATION

The formulation of Edwards and Peierls (1954) is adopted, and the case of the one nucleon Green function considered, in say neutral pseudoscalar theory. The argument goes through in just the same way for other Green functions and other meson theories. The approximation is made that there is no meson–meson interaction, directly or via pair production. This is expressed by $\delta\Delta/\delta\phi=0$ where Δ is the meson Green function and ϕ an external field. Then the formulation shows that if $G(\Omega)$ satisfies

---

* I.C.I. Research Fellow.

† Communicated by the Author.

$$[-i\gamma_\mu\,(\partial/\partial x_\mu)+m+g\gamma_5\Omega(x)]\,G\,(x,x';\;g\Omega)=\delta\,(x-x'), \quad . \quad . \quad (1)$$

then S, the propagator including radiative corrections satisfies

$$S(x-x')=\frac{\int\delta\Omega G(x,x';\;\Omega)\exp\left\{-\frac{i}{2}\int(\Omega\Delta^{-1}\Omega)\,d^4yd^4y'\right\}}{\int\delta\Omega\exp\left\{-\frac{i}{2}\int(\Omega\Delta^{-1}\Omega)d^4yd^4y'\right\}} \quad . \quad (2)$$

where $\delta\Omega=\prod_{\text{all }x}d\Omega(x)$ and all integrations are over the range $-\infty$ to ∞. The mathematics of such integrals is rather difficult and so to discuss their properties certain restrictions will be placed upon the integrations. Firstly on integrating over all potentials it is clear that only those contribute which give a finite value to $\int\Omega(x)\Delta^{-1}(xx')\Omega(x')d^4xd^4x'$. This suggests that Ω be represented by a suitable complete discrete set of functions ϕ_n, with the ortho-normality condition chosen so that

$$\tfrac{1}{2}\int\phi_n(x)\Delta\ {}^{1}(x,x')\phi_m(x')d^4xd^4x'=\delta_{nm}. \quad . \quad . \quad . \quad . \quad (3)$$

In momentum space this becomes

$$\Sigma a_n\phi_n(p)=\Omega(p) \quad . \quad . \quad . \quad . \quad . \quad . \quad . \quad (4)$$

where

$$\int\phi_n(p)\Delta^{-1}(p)\phi_m(-p)d^4p=2\delta_{nm} \quad . \quad . \quad . \quad . \quad . \quad (5)$$

$\phi_n(p)$ being the Fourier transform of $\phi_n(x)$. The functions are chosen so that the values of p^2 for which they are large increase with n, i.e. the values of x^2 for which they are large decrease with n. This choice amounts to saying that curtailing the series to $n<N$, amounts to a cut-off in momentum space, e.g. a Feynman cut off. S now becomes

$$S=\frac{\int\prod_0^\infty da_n\,G(x,x';\;ga_1,ga_2\ldots)\exp\left\{-i\sum_0^\infty a_n{}^2\right\}}{\int\prod_0^\infty da_n\,G(x,x';\;ga_1,ga_2\ldots)\exp\left\{-i\sum_0^\infty\ {}^2\right\}} \quad . \quad . \quad . \quad (6)$$

where

$$\left(\frac{\gamma_\mu}{i}\frac{\partial}{\partial x_\mu}+m+\gamma_5\sum_0^\infty ga_n\phi_n(x)\right)G\,(x,x';\;ga_1\,ga_2\ldots)=\delta(x-x'). \quad . \quad (7)$$

At this point a serious assumption is made: that the set can be cut off at a certain N, i.e. the dependence of G upon $G_{N+1},\ldots$ may be neglected. This means that the insertion of a cut off into the integrals of the perturbation expansion does not seriously alter the value of the series, and is not a valid assumption in theories containing divergent integrals which have to be renormalized. Absorbing the g into the definition of the a's, S is now

$$\frac{\int_{-\infty}^{\infty}\ldots\int_{-\infty}^{\infty}da_1\ldots da_NG\,(x,x';\;a_1\ldots a_N)\exp\left\{-\frac{i}{g^2}\sum_0^N a_n{}^2\right\}}{\int_{-\infty}^{\infty}\ldots\int_{-\infty}^{\infty}da_1\ldots da_N\exp\left\{-\frac{i}{g^2}\sum_0^N a_n{}^2\right\}} \quad . \quad (8)$$

S is now in a form which has been discussed rigorously by Watson (1918) for the case of one variable, the treatment immediately extending to several variables. The form of Watson's lemma convenient to our purpose has been given by Jeffreys and Jeffreys (1949). Watson shows that if within its radius of convergence

$$G(a)=G_0+aG_1+a^2G_2+\ldots+a^{2n-1}G_{2n-1}+R_{2n}(a) \quad . \quad . \quad . \quad (9)$$

and if G is analytic at $a=0$ and has singularities only at isolated points which have principal values or are otherwise integrable, then

$$S=\int_{-\infty}^{\infty}\exp\{-\tfrac{1}{2}\,a^2/g^2\}G(a)da \quad . \quad . \quad . \quad . \quad . \quad (10)$$

$$\sim g\sqrt{(2\pi)}\,(G_0+g^2G_2+1\cdot 3g^4G^4+$$
$$\ldots+1\cdot 3\ldots(2n-3)\,g^{2n-2}G_{2n-2}+\ldots) \quad (11)$$

provided that the integral exists.

A necessary (but not sufficient) condition for this series to converge is that $G(a)$ has an infinite radius of convergence; otherwise the series is asymptotic in the sense of Poincaré. The case above differs from the lemma only by having several variables, and a Fresnel rather than a Gaussian type of integral, neither of which affect the argument. Writing the Born expansion of G,

$$G(x,x';\,a_1\ldots a_N)=G^{(0)}(x,x')+\Sigma a_iG_i^{(1)}(x,x')+$$
$$\Sigma a_ia_jG_{ij}^{(2)}(x,x')+\ldots \quad . \quad . \quad . \quad . \quad (12)$$

and considering x, x' as fixed, this is a power series like (9) and gives

$$S\sim G^{(0)}(x,x')+g^2\left(\frac{\pi^2}{16}\right)\sum_{i=0}^{N}G_{ii}^{(1)}(x,x')+\ldots \quad . \quad . \quad (13)$$

the usual perturbation expansion, cut off at N. This expansion is asymptotic unless the expansion of $G(x,\,x';\,a_1\ldots a_N)$ is absolutely convergent with an infinite radius of convergence. Now the condition that $\int\Omega\Delta^{-1}\Omega d^4p$ is bounded implies that for large p, $\Omega\sim(\Delta^{-1}(p)p^4)^{-\frac{1}{2}-\delta}$ with $\delta>0$. The justification for cutting off the series of a_n's was that $\Delta^{-1}(p)\sim p^{2+\epsilon}$, $\epsilon>0$ for large p, and so this gives $\Omega\sim p^{-3-\delta-\epsilon/2}$. The condition $\Omega\sim p^{-3-\eta}$, $\eta>0$ is precisely that given by Matthews and Salam (1953) which ensures that (1) i.e. (7) is soluble by the Fredholm method, when considered as the integral equation

$$(\gamma p+m)\,G\,(p,x';\,a_1\ldots a_N)+g\gamma_5\int\sum_{1}^{N}a_n\phi_n(p-q)\,G\,(q,x';\,a_1\ldots a_N)\,dq$$
$$=\exp(ipx'). \quad . \quad . \quad . \quad . \quad . \quad . \quad . \quad . \quad . \quad . \quad . \quad (14)$$

It must be noted, however, that for electrodynamics etc., $\Delta^{-1}(p)=p^2$ and the Matthews and Salam criterion is only just satisfied, implying as before that in these theories the neglect of certain a_n's is not justified. In the valid case, however, the solution can be written

$$S=\frac{\int_{-\infty}^{\infty}\cdots\int_{-\infty}^{\infty}da_1\ldots da_N\,[H(x,x';\;a_1\ldots a_N)/K(a_1\ldots a_N)]\exp\left\{-\frac{i}{g^2}\sum_0^N a_n^2\right\}}{\int_{-\infty}^{\infty}\cdots\int_{-\infty}^{\infty}da_1\ldots da_N\exp\left\{-\frac{i}{g^2}\sum_0^N a_n^2\right\}}\quad\ldots\quad(15)$$

where both H and K are expressed as absolutely convergent expansions for all values of the a's. K will in general have a series of (complex) roots, the first of which gives the radius of convergence of the expansion (12), and since in general this root is finite, the lemma leads to the result that S is asymptotic in g^2. As has been pointed out, the physically realistic cases require a cut-off before they can be brought into the above scheme, but the above result might suggest that the divergence of the perturbation method does not rule out sensible solutions to eqn. (1).

ACKNOWLEDGMENTS

The author wishes to thank Professor Peierls, Dr. G. Feldman, and Dr. P. T. Matthews for many valuable discussions of this work.

REFERENCES

EDWARDS, S. F., and PEIERLS, R. E., 1954, *Proc. Roy. Soc.* A, 000, 000.
DYSON, F. J., 1952, *Phys. Rev.*, **85**, 631.
HURST, C. A., 1952, *Camb. Phil. Soc.*, **48**, 625.
JEFFREYS, H., and JEFFREYS, B., 1946, *Methods of Mathematical Physics* (Cambridge, 1949), Ch. 17.
MATTHEWS, P. T., and SALAM, A., 1953, *Phys. Rev.*, **90**, 690.
PETERMANN, A., 1953, *Helv. Phys. Acta*, **26**, 291.
THIRRING, W., 1953, *Helv. Phys. Acta*, **26**, 33.
UTIYAMA, R., and IMAMURA, T., 1953, *Prog. Theor. Phys.*, **9**, 431.
WATSON, G. N., 1918, *Proc. Lond. Math. Soc.* (2), **17**, 133.

LXXXV. *The* d-^{6}Li *Reactions*

By F. Hirst, I. Johnstone and M. J. Poole
Atomic Energy Research Establishment, Harwell*

[Received April 22, 1954]

Abstract

The cross sections for two of the d-Li reactions (namely ^{6}Li(dα)^{4}He and ^{6}Li(dn)^{7}Be) have been measured in the energy range 60 to 450 kev. No evidence has been found for resonances in this region, and the branching ratio between the reactions remains substantially constant over much of the energy range.

§ 1. Introduction

The reaction ^{6}Li(dα)He^4 has previously been studied in the energy range from 200 kev to 3·5 mev (Heydenburg, Hudson, Inglis and Whitehead 1948, Whaling and Bonner 1950) with an energy resolution of about 60 kev. Little quantitative information is available about the parallel reaction ^{6}Li(dn)^{7}Be, particularly in the low energy region. The object of the experiments to be described was to extend existing measurements to a lower energy, with improved energy resolution.

§ 2. Method

Deuteron beams with energies from 150 kev to 450 kev were provided by a Cockcroft–Walton accelerator. Measurements with energies below 150 kev were taken by making use of diatomic and triatomic beams.

Targets of ^{6}LiF and ^{6}Li$_2$O were prepared, the former by evaporation and the latter by direct deposition of ^{6}Li in the electromagnetic separator of the establishment. The amount of ^{6}Li on the latter could not be determined accurately, but because of their greater lithium content oxide targets were used for all low energy points in the ^{6}Li(dα)^{4}He investigation (where it is most important to have a thin target). The amount of ^{6}LiF in the fluoride targets was determined by weighing on a micro-balance. These weighed targets served to give a measurement of cross section at one or two higher energies, which were then used to put an absolute scale on the curves obtained with oxide targets. The amount of material on the oxide targets was about 5 μg/cm^2 of Li$_2$O and most of the fluoride targets were about three times as thick. Fluoride targets were used in all cases for the ^{6}Li(dn)^{7}Be experiment.

The yield of α-particles from the ^{6}Li(dα)^{4}He reaction at 90° was determined using a side-window proportional counter. Alpha-particles and protons are produced from the d-Li reactions and protons, tritons and ^{3}He ions from the D–D reactions (caused by deuterium contamination of the target). Only the α-particles and protons had enough energy to pass through the counter window, and these were clearly resolved as separate groups when the amplified pulses from the counter were analysed in a 30-channel pulse-analyser. The current falling on the target during a run was measured with a simple current integrator.

---

* Communicated by the Authors.

To make the counter sensitive enough for the lowest energy points the solid angle subtended by the counter was large and somewhat badly defined ; therefore only relative excitation curves were taken with this apparatus. A second target chamber was constructed in which the α-particles were allowed to pass through a very carefully located and measured aperture (dimensions known to better than 1%) on to a thin sodium iodide scintillator. This chamber was used with ^{6}LiF targets to obtain absolute cross section values at a few high energy points as already mentioned.

The ^{6}Li(dn)^{7}Be reaction was studied by bombarding a ^{6}LiF target placed normally to the beam with a known amount of deuterons and observing the ^{7}Be activity with a sodium iodide scintillation γ spectrometer The 479 kev γ line was clearly resolved.

This spectrometer was calibrated absolutely by comparing one of the bombarded targets with a standard ^{198}Au source using an organic scintillator whose sensitivity could easily be calculated as a function of γ-ray energy. To obtain values of the cross section for the reaction from the γ-ray intensities a correction had to be made for the motion of the c.m. of the compound system (^{7}Be nuclei recoiling in 2π solid angle backward in laboratory space will be lost). For the purposes of this correction only the angular distribution was assumed isotropic in c.m. space.

§ 3. Discussion of Results

The differential cross section at 90° for the reaction ^{6}Li(dα)^{4}He is shown in fig. 1 and the total cross section for the reaction ^{6}Li(dn)^{7}Be in fig. 2. For the first reaction the angular distribution has been shown to be nearly isotropic (Heydenburg, Hudson, Inglis and Whitehead 1943, Dunbar and Hirst 1951). In consequence of the even intrinsic parity of all particles concerned in this reaction, and the zero spin of the outgoing α-particles only even incident angular momenta are effected. At these low energies this effectively means that only ingoing s-waves need be considered. (At 200 kev the d-wave penetrability is only 0·3% of the s-wave penetrability.) Accordingly the cross section $\sigma(E)$ has been written

$$\sigma(E)=\pi\lambdabar^2 G\alpha(E)P_0(E)$$

where $\lambdabar$ is the Dirac wavelength of the incoming particle, $\alpha(E)$ is the intrinsic reaction probability, $P_0(E)$ the s-wave penetrability and G a statistical spin factor (equal to $\frac{1}{9}$ or $\frac{5}{9}$ according as $j=0$ or 2). The solid curves on fig. 1 show $\pi\lambda\kern-0.5em\raise0.6ex\hbox{-}^2 P_0(E)$ calculated for reaction distances of $4{\cdot}0 \times 10^{-13}$ cm and $4{\cdot}5 \times 10^{-13}$ cm, and normalized to fit the experimental curve at 150 kev. Tables of exact Coulomb wave-functions published by Bloch *et al.* (1951) were used to calculate these curves. Values of $\alpha(E)$ derived from the ratio between the experimental and theoretical curve are also shown. These decrease monotonically towards the higher

Fig. 1

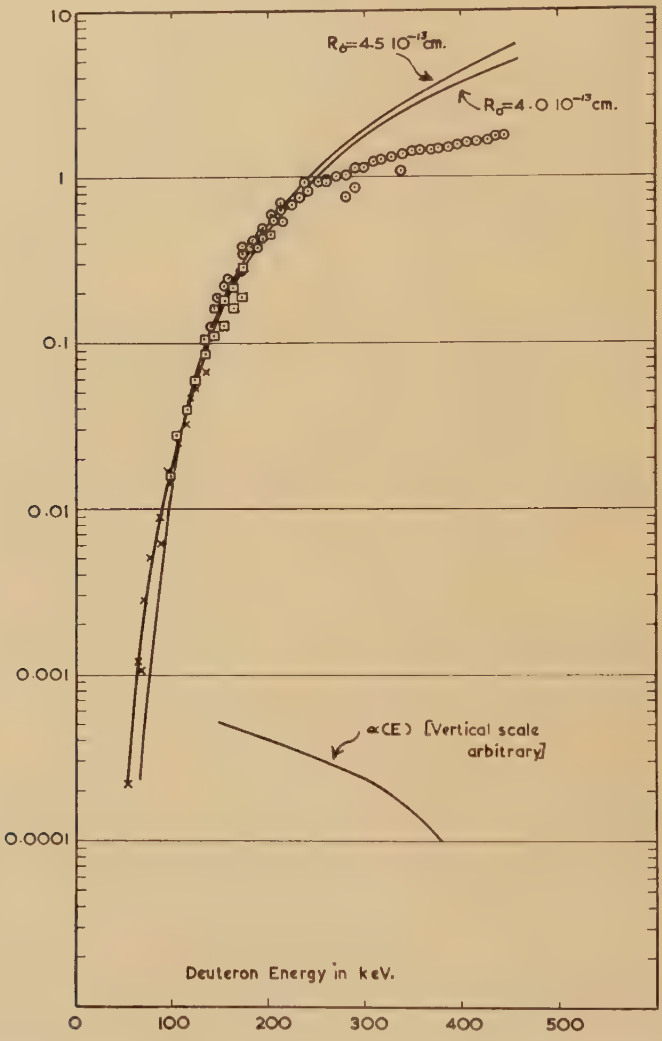

90° differential cross section for the reaction ^{6}Li(αd)^{4}He. [Points are experiment ; solid lines theory.]

energies, showing no sign of the resonance at 347 kev reported by Whaling and Bonner (1950).*

The reaction ^{6}Li(dn)^{7}Be, although proceeding via the same compound nucleus, has no symmetry restrictions on the incoming orbital momentum and p-waves would be expected to contribute. (The angular distribution is anisotropic: Whaling, Evans and Bonner 1949.) However, in fig. 2

Fig. 2

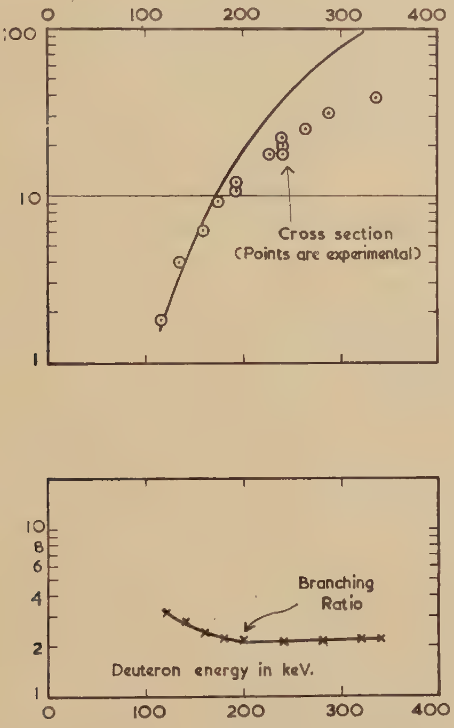

Cross section for the reaction ^{6}Li(dn)^{7}Be and branching ratio between ^{6}Li(dn)^{7}Be and ^{6}Li(dα)^{4}He.

the s-wave penetrability has also been plotted, and the experimental points show divergences from the theoretical curve very similar to those observed in the previous reaction (fig. 1). This is brought out more clearly by the second graph in fig. 2, which shows the branching ratio r between neutron and α-particle emission. The nearly constant value of r suggests that the same states of the compound nucleus may be involved in the two reactions.

---

* Since this work was undertaken Sawyer and Phillips (1953) have published further work on this reaction in the energy range 30 kev to 240 kev. Their cross sections are within 20% of the results of this work and also show no appreciable variation in $\alpha(E)$.

§ 4. ERRORS

The following is a list of the principal sources of error in the two experiments :—

Target Thickness

The weighings are accurate to ±3 μg and 3 cm^2 were weighed, giving an error of ±1 μg/cm^2 for any target. In the ^{6}Li(dα)^{4}He experiment targets of both 3·5 μg/cm^2 and 15 μg/cm^2 were used, while for the ^{6}Li(dn)^{7}Be experiment only targets of ~15 μg/cm^2 were used.

Measurements of the thickness of one of our targets were made by D. L. Allan by an independent method which determined the ^{6}Li content. His results agreed to within ±10% with the weighings and gave the additional information that even after several hours bombardment the amount of ^{6}Li on the target was unchanged.

Beam Current

Separate current integrator calibrations agreed to ±2%.

Counting Errors

In both experiments statistical errors of the counts varied from ±10% at the lowest energy to better than ±1% at the highest. At energies above 100 kev all counts were better than ±3%.

Absolute Calibration of ^{7}Be *Counter*

Successive determinations showed sensitivities differing by up to 10%. This error will affect the ^{7}Be curve as a whole but will not affect the shape of the curve.

ACKNOWLEDGMENTS

The authors wish to thank Mr. R. N. Hall and Dr. M. L. Smith who were responsible for the preparation of the targets. Dr. Howlett and members of the computing section assisted with tedious calculations of barrier penetrability.

REFERENCES

DUNBAR, D. N. F., and HIRST, F., 1951, *Phys. Rev.*, **83**, 154.
HEYDENBURG, N. P., HUDSON, C. M., INGLIS, D. R., and WHITEHEAD, W. D., 1948, *Phys. Rev.*, **74**, 405.
SAWYER, G. A., and PHILLIPS, J. A., 1953, *Declassified report* L.A. 1578.
WHALING, W., EVANS, J. E., and BONNER, T. W., 1949, *Phys. Rev.*, **75**, 688.
BLOCH, I., HULL, M. M., BROYLES, A. A., BOURICIUS, W. G., FREEMAN, B. E., and BREIT, G., 1951, *Rev. Mod. Phys.* **23**, 2, 147.

LXXXVI. CORRESPONDENCE

The Thermal Conductivity of Gallium Single Crystals at Low Temperatures

By H. M. Rosenberg
Clarendon Laboratory, Oxford

[Received May 16, 1954]

Gallium is known to exhibit considerable anisotropy in its electrical and thermal resistances at room temperature (Powell 1951) and the electrical anisotropy has been found to persist to low temperatures (Olsen-Bär and Powell 1951). It was therefore of interest to see whether the thermal resistance was also anisotropic at low temperatures. Three single crystals have been measured in the temperature range 2 to 40°K. These had their axes parallel to the directions of high, low and intermediate electrical resistivity and they were all made from the same batch of metal.

The experiments show that the thermal resistance at low temperatures exhibits as strong an anisotropy as does the electrical resistance. This applies both above the region of the thermal conductivity maximum (about 8°K for these specimens), where the electronic thermal conductivity is limited mainly by lattice scattering, and below the maximum, where impurity scattering is the dominant mechanism.

The thermal resistivity, W, is of the usual form at low temperatures, $W=AT^2+B/T$. The lattice scattering parameter, A, has been calculated for the three crystals and the ratio of the values obtained is very similar to the ratio of the electrical resistances at 20°K. The electrical resistances are in the ratio 1 : 2·7 : 8·9 whereas the values of A are in the ratio 1 : 4 : 10·5. The impurity scattering parameters, B, also show a similar anisotropic effect, although the correspondence between them and the ratio of the electrical resistances is not so satisfactory. This may in some degree be due to the fact that the value of B can be modified by slight damage to the crystals. Since they are very fragile this could easily occur whilst they were being mounted. Nevertheless it is clear from the results that the anisotropy is present for both the impurity scattering and the lattice scattering mechanisms. At 40°K the thermal resistances are in the ratio 1 : 2·3 : 5·2. Thus the experiments show that there is a broad agreement between the anisotropy in both the thermal and electrical resistance, although this does not seem to be strictly quantitative. Further details of the results will be published in due course.

I should like to thank Dr. K. Mendelssohn, F.R.S. for the interest he has taken in this work, and Dr. R. W. Powell of the National Physical Laboratory for very kindly preparing the specimens.

References

Olsen-Bär, M., and Powell, R. W., 1951, *Proc. Roy. Soc.* A, **209**, 542.
Powell, R. W., 1951, *Proc. Roy. Soc.* A, **209**, 525.

The Angular Correlation between Gamma-Rays and Alpha-Particles from ^{7}Li (pγ) ^{8}Be (α) ^{4}He

By E. K. Inall
Research School of Physical Sciences, Australian National University, Canberra*

[Received May 12, 1954]

The detection of alpha-particles in coincidence with gamma-rays from the 17·63 Mev level of ^{8}Be, formed by the resonant capture of 441 kev protons by ^{7}Li, was reported by Inall and Boyle (1953). The energy of the alpha-particles showed that gamma-ray transitions occurred to energy levels of ^{8}Be at 4·09, 5·3 and 7·5 Mev, in addition to the transitions to the 2·9 Mev level as observed by Burcham and Freeman (1950).

Measurements of the cross section for the elastic scattering of protons by ^{7}Li have shown that p-wave protons form the 17·63 Mev level of ^{8}Be. This level therefore has a spin of one and even parity. Thus radiation to levels of even spin greater than two would be of high multipole order and of too low intensity to be observed. Therefore the spins of the levels identified in the gamma-alpha coincidence experiments, viz. those at 4·09, 5·3 and 7·5 Mev, were known to be zero or two, and since the parities were known to be even, the radiation would have been magnetic dipole or electric quadrupole. Gamma-alpha angular correlations have now been measured, using apparatus similar to that described earlier (Inall and Boyle 1953), to give a definite value of the spin for each level.

A natural lithium target 100 kev thick was bombarded with 450 kev protons. The alpha-particle counter was fixed at 81° to the beam (90° in the c of m system) and the angle θ, between the axes of this counter and gamma-ray counter, was varied from 210° to 80° in the plane normal to the beam. Each counter had a square acceptance aperture which subtended an angle of 17° at the target.

The coincidences between the gamma-rays and the three groups of alpha-particles from the 4·09, 5·3 and 7·5 Mev levels were identified by range measurements, the results of which are plotted in fig. 1. From this the anisotropy of the correlation for the 4·09 and 5·3 Mev levels and the apparent isotropy for the 7·5 Mev level are clear. When $\theta=180°$ the recoil energy, received by the ^{8}Be from the gamma-ray, increased the energy of the associated alpha-particles by a greater amount than when $\theta=90°$. The consequent changes in range are apparent in fig. 1. These are about three-quarters of those calculated, but still they provide additional evidence that the coincidences observed were between alpha-particles and gamma-rays.

Further angular correlation data were obtained by taking alternate coincidence counts at two ranges suitable to give the ‘ height of one step ’ of the range curve (fig. 1) for various values of θ. The results are plotted in fig. 2. The best fit between the observations and a correlation function of the form $W(\theta) \sim 1 + A\cos^2\theta$ was obtained when $A = 0{\cdot}85$ for the transitions through the levels at 4·09 MeV and 5·3 MeV, and $A = 0$ for those via the 7·5 MeV level. The full lines in fig. 2 represent these functions after they have been modified to allow for the finite solid angles of the counters.

---

* Communicated by Professor E. W. Titterton.

Devons and Lindsay (1950) have shown that since p-wave protons on ^{7}Li form the 17·63 MeV state of ^{8}Be, the isotropy of the gamma-rays at the 441·5 kev resonance implies that a channel spin of two (spin of ^{7}Li parallel to spin of the proton) occurs five times as frequently as a channel spin of one (spins anti-parallel). Using this mixing of channel spins, and assuming the radiation to be pure magnetic dipole from the spin one even parity state at 17·63 MeV to a spin two even parity state the correlation function was calculated to be $W_m(\theta) \sim 1 - 0{\cdot}6\cos^2\theta$. Further calculations assuming the radiation to be a mixture of magnetic dipole and electric quadrupole gave

Fig. 1

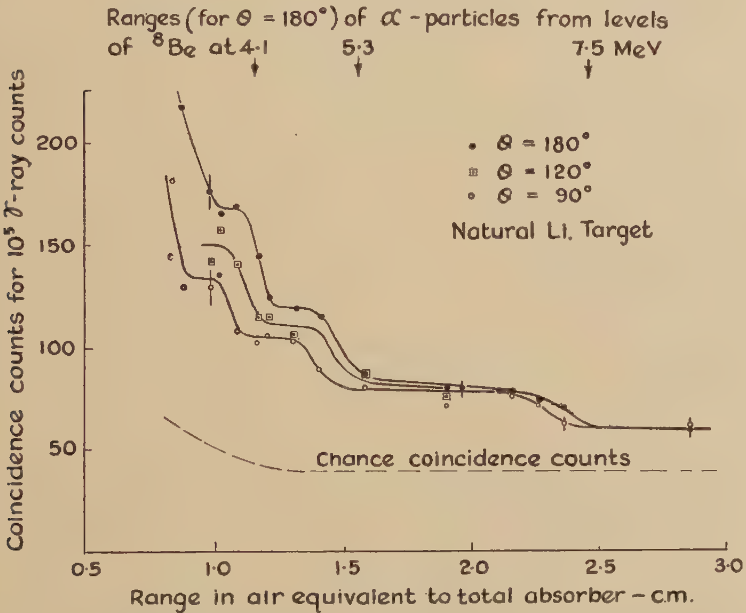

Showing the change in the range of the alpha-particles due to change in the angle between the counters.

$$W(\theta) \sim (1 - 0{\cdot}6\cos^2\theta) + (2c/\sqrt{5})\,(1 - 3\cos^2\theta) + c^2\,(1 - 3\cos^2\theta + 4\cos^4\theta), \quad . \; . \; . \; . \; . \; (1)$$

where the total intensity of the electric quadrupole component was c^2 times that of the magnetic dipole component. This function can be fitted to the experimental results by taking $c = -0{\cdot}42$.

Then

$$W(\theta) \sim 1 - 0{\cdot}004\cos^2\theta + 0{\cdot}9\cos^4\theta. \quad . \; . \; . \; . \; . \; . \; (2)$$

which, after correction for the finite aperture of the counters, has been plotted as the broken curves in figs. 2 (*a*) and (*b*). The observations therefore imply that the spins of the 4·09 Mev and 5·3 Mev levels are two and that there is a significant electric quadrupole component in the radiation.

Because only a small fraction of the transitions lead to the 7·5 Mev level, it was necessary to run the experiment for a long time to collect angular correlation data on these transitions. Effort was therefore concentrated on observations at $\theta=180°$ and 90° where equal intensities

Fig. 2

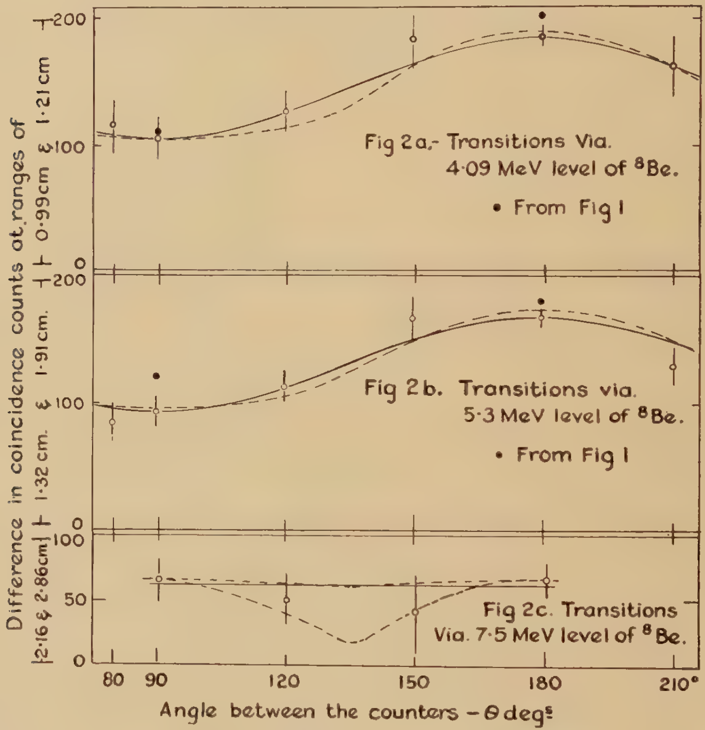

In (*a*) and (*b*) the solid curves represent the function $W(\theta)\sim 1+0{\cdot}85\cos^2\theta$ corrected for the finite solid angle of the counters. The broken curves represent $W(\theta)\sim 1-0{\cdot}004\cos^2\theta+0{\cdot}9\cos^4\theta$, calculated for a mixture of electric quadrupole and magnetic dipole radiation. Similarly the broken curves in (*c*) represent $W(\theta)\sim 1-2{\cdot}8\cos^2\theta+2{\cdot}8\cos^4\theta$ and $W(\theta)\sim 1-0{\cdot}2\cos^2\theta+0{\cdot}2\cos^4\theta$.

were observed, with the result that, although the readings at intermediate angles were consistently low, the statistical accuracy was such that the correlation could be isotropic. This would imply that the spin of the 7·5 Mev level is zero as found by Steigert and Sampson (1953). On the other hand, a spin of two is not ruled out since an approximately isotropic correlation could result from a mixture of magnetic dipole and electric quadrupole transitions. For example when $c=2{\cdot}88$

$$W(\theta)\sim 1-2{\cdot}8\cos^2\theta+2{\cdot}8\cos^4\theta \quad . \quad . \quad . \quad . \quad . \quad . \quad (3)$$

and when $c=0{\cdot}21$

$$W(\theta)\sim 1-0{\cdot}2\cos^2\theta+0{\cdot}2\cos^4\theta. \quad . \quad . \quad . \quad . \quad . \quad . \quad (4)$$

These functions are plotted as the broken curves in fig. 2 (*c*). It is clear that (3) fits the experimental points better than an isotropic correlation. The apparatus is therefore being modified to enable data to be collected more rapidly so as to obtain an accurate measure of the angular correlation.

In view of the comparatively high energy of the gamma-rays, values of c in the region of 0·2 to 0·5 are not inconsistent with theoretical estimates. Even the value $c=2{\cdot}88$ used in (3) is not so large as to be ruled out by present knowledge.

The coincidence counts recorded during the recent experiments were slightly greater than those reported previously. The weighted averages, and the measured angular correlations, were used to calculate the intensities of the transitions via each level of ^{8}Be, as a percentage of the total gamma-radiation. These intensities were $1{\cdot}8\pm0{\cdot}3\%$ for the 13·5 MeV gamma-ray, $1{\cdot}7\pm0{\cdot}3\%$ for the 12·2 MeV, and $1{\cdot}0\pm0{\cdot}3\%$ for the 10·1 MeV gamma-ray.

I wish to thank Professor E. W. Titterton for his comments and suggestions, Dr. F. C. Barker for his assistance in calculating the angular correlation, and Mr. A. J. F. Boyle who helped with the experimental work.

REFERENCES

BURCHAM, W. E., and FREEMAN, JOAN M., 1950, *Phil. Mag.*, **41,** 921.
DEVONS, S., and LINDSAY, G. R., 1950, *Proc. Phys. Soc.* A, **63,** 1202.
INALL, E. K., and BOYLE, A. J. F., 1953, *Phil. Mag.*, **44,** 1081.
STEIGERT, F. B., and SAMPSON, H. B., 1953, *Phys. Rev.*, **92,** 660.

The Temperature Dependence of the Critical Shear Stress and of Work-hardening of Metal Crystals

By ALFRED SEEGER
Max-Planck-Institut für Metallforschung und Institut für theoretische und angewandte Physik der Technischen Hochschule Stuttgart, Stuttgart, Germany

[Received May 26, 1954]

IN a recent theoretical study of the plastic properties of crystalline solids (Seeger 1954), particular attention was given to the dependence of work-hardening and critical shear stress in close-packed lattices on temperature and strain-rate. It was found that the following model is able to explain quantitatively the rather extensive experimental results on hexagonal metals (Schmid and Boas 1935) and also the far less complete data so far available for cubic metals.

There are two main contributions to critical shear stress and work-hardening of single crystals :

(1) The elastic stresses round dislocations, which depend on temperature only through the temperature variation of elastic constants. This contribution will be denoted by $\tau_G(\epsilon)$.

(2) The stress necessary for pushing a dislocation past other screw dislocations threading the glide plane, thereby forming jogs.

The strain rate under an external resolved shear stress τ in this model is

$$\dot{\epsilon}=NAb\,\nu_0 \exp\left\{-\frac{U_0-v(\epsilon)(\tau-\tau_G)}{\boldsymbol{k}T}\right\}, \quad . \quad . \quad . \quad . \quad (1)$$

where

$$v(\epsilon)=bd\,l'_0(\epsilon). \quad . \quad . \quad . \quad . \quad . \quad . \quad . \quad . \quad . \quad . \quad . \quad . \quad . \quad . \quad (2)$$

Here

N=number of dislocations per unit volume held up by intersecting dislocations,

A=area swept out by dislocation after cutting an intersecting screw,

b=dislocation strength,

ν_0=Debye's frequency,

$\boldsymbol{k}$=Boltzmann's constant,

U_0=activation energy for intersection (jog formation) at zero stress,

d=' diameter ' of dislocations threading the glide plane. In hexagonal metals $d\sim b$, in Al $d\sim 2{\cdot}5\,b$, in Cu $d\sim(6\text{–}13)\,b$.

The differences in the magnitude of d/b of various metals is connected with the possibility of forming extended dislocations.

l'_0=distance between dislocation lines acting as obstacles for slip.

The stress required for deformation with the strain-rate $\dot{\epsilon}$ is

$$\tau=\tau_G(\epsilon)+\frac{U_0-\boldsymbol{k}T\log\left(NAb\nu_0/\dot{\epsilon}\right)}{v(\epsilon)} \qquad T\leqslant T_0(\dot{\epsilon}) \quad . \quad . \quad . \quad (3)$$

$$\tau=\tau_G(\epsilon) \qquad T>T_0(\dot{\epsilon}) \quad . \quad . \quad . \quad (4)$$

The critical temperature T_0, below which the critical shear stress increases linearly with decreasing temperature (eqn. (3)), and above which it is practically constant (eqn. (4)), is given by

$$U_0=\boldsymbol{k}T_0\log\left(NAb\nu_0/\dot{\epsilon}\right). \quad . \quad . \quad . \quad . \quad . \quad . \quad . \quad . \quad (5)$$

This law agrees very well with experiment in Zn, Cd, Mg, Bi. Due to the large numerical value of v the temperature variation of critical shear stress in Cu is too small to be detectable. The numerical value of l'_0 deduced from the experimental data on T_0 fit the data obtained from other sources.

There are two ways in which the coefficient of work-hardening $\theta = d\tau/d\epsilon$ depends on temperature :

(1) If the temperature is high enough to allow recovery (e.g., climbing of dislocations), the dislocated state of the crystal (measured by τ_G) will no longer be uniquely determined by ϵ, but depends on strain-rate and temperature as well.

(2) In f.c.c. metals l'_0 is constant only in the easy glide region. Beyond easy glide $l'_0(\epsilon)$ decreases with increasing strain due to the production of dislocations in secondary glide systems and introduces a linear temperature dependence in θ. This is the explanation why θ shows less temperature variation in the easy glide region than at larger strains.

References

Seeger, A., 1954, *Z. Naturforschung*, **9a**, in press.
Schmid, E., and Boas, W., 1935, *Kristallplastizität* (Berlin : Springer).

Paramagnetic Resonance in Plutonyl Rubidium Nitrate, and the Spin of ^{239}Pu

By B. Bleaney, P. M. Llewellyn, M. H. L. Pryce
Clarendon Laboratory, Oxford
and
G. R. Hall
Atomic Energy Research Establishment, Harwell

[Received May 24, 1954]

Paramagnetic resonance has been observed at wavelengths of 3·2 cm and 1·5 cm at a temperature of 20°K in a single crystal of the uniaxial salt $PuO_2\,Rb\,(NO_3)_3$, magnetically diluted with the isomorphous uranyl salt $UO_2\,Rb\,(NO_3)_3$. The concentration of plutonium relative to uranium was estimated at about 6%. The isotopic constitution was ^{239}Pu 98%, ^{240}Pu 2%. The resonance consists of two lines of equal intensity, which are interpreted as the components of a hyperfine structure doublet, indicating that the spin of ^{239}Pu is $I=\frac{1}{2}$, confirming the optical observations of van den Berg, Klinkenberg and Regnaut (1954). The contribution from the ^{240}Pu was too weak to be observed.

The behaviour of the resonance lines as the magnetic field is rotated relative to the crystal axis is compatible with the assumption that all the plutonyl ions in the crystal lattice are magnetically equivalent and uniaxial, with spectroscopic splitting factors $g_{\parallel}=5{\cdot}4\pm0{\cdot}2$, $g_{\perp}=0{\cdot}0\pm0{\cdot}4$. This is in accordance with theoretical expectations (Eisenstein and Pryce 1954), which indicate that the ground level of the PuO_2^{++} ion in crystal surroundings possessing a threefold axis of symmetry, as is the case in this crystal, is a degenerate doublet with $g_{\parallel}\sim6$, $g_{\perp}=0$. This agreement lends further support to the hypothesis that the magnetic electrons in the actinide series of elements are in the 5f state.

In an ideal crystal lattice at the absolute zero of temperature resonance absorption would be forbidden under these conditions, but strains and thermal fluctuations will cause a small splitting of the doublet and a breakdown of the selection rules. The observed absorption is strongest when the radio-frequency magnetic field is parallel to the axis, as would be expected if $g_\perp$ were very small, but a splitting of the doublet were present. This, though small compared with the measuring frequency (0·3 cm^{-1}) is enough to provide a mechanism for absorption. In this respect the situation is similar to that encountered in praseodymium ethylsulphate (Bleaney and Scovil 1952).

With the d.c. magnetic field parallel to the crystal axis the half width of the lines at half intensity is about 40 gauss, and the separation of the two components is 340 ± 20 gauss. From this figure a provisional value of $0{\cdot}5 \pm 0{\cdot}2$ nuclear magnetons for the absolute value of the nuclear magnetic moment can be derived. The sign of the nuclear moment is not determined in these experiments.

The resonance results are summarized in the spin Hamiltonian

$$g_\parallel \beta H_z S_z + A S_z I_z$$

in which S is the fictitious spin associated with the electronic doublet, $g_\parallel$ has the value quoted and $A = 0{\cdot}11\ \mathrm{cm}^{-1}$.

References

Bleaney, B., and Scovil, H. E. D., 1952, *Phil. Mag.*, **43,** 999.
Eisenstein, J. C., and Pryce, M. H. L., 1954, to be published.
van den Berg, M., Klinkenberg, P. F. A., and Regnaut, P., 1954, *Physica*, **20,** 37.

[*The Editors do not hold themselves responsible for the views expressed by their correspondents.*]

Fig. 1

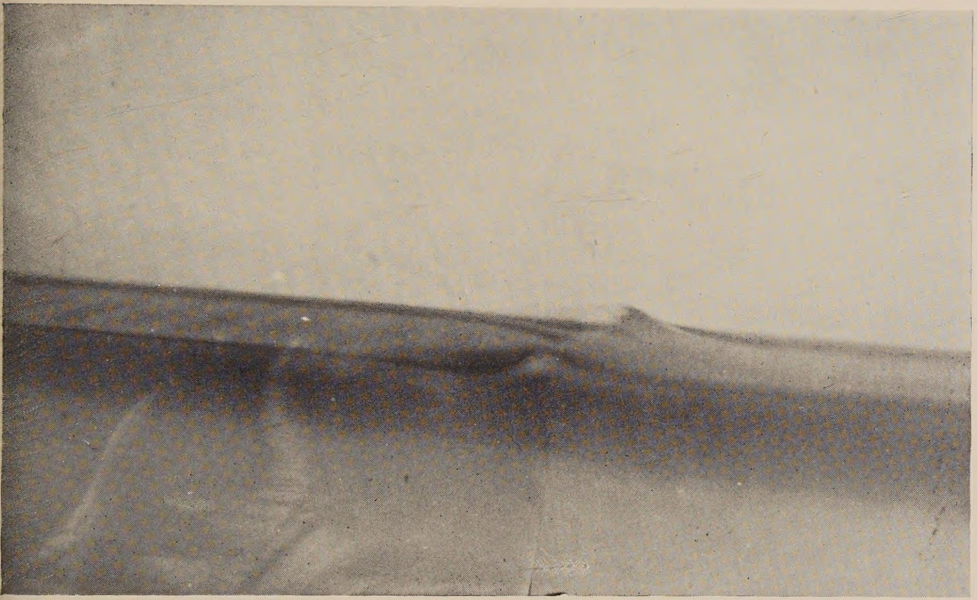

Photograph of unstable wave having just grown from small ripples. Wind from left to right; camera looking slightly upwind, and downward on to oil surface. Ripples show as transverse bars of light.

Fig. 2

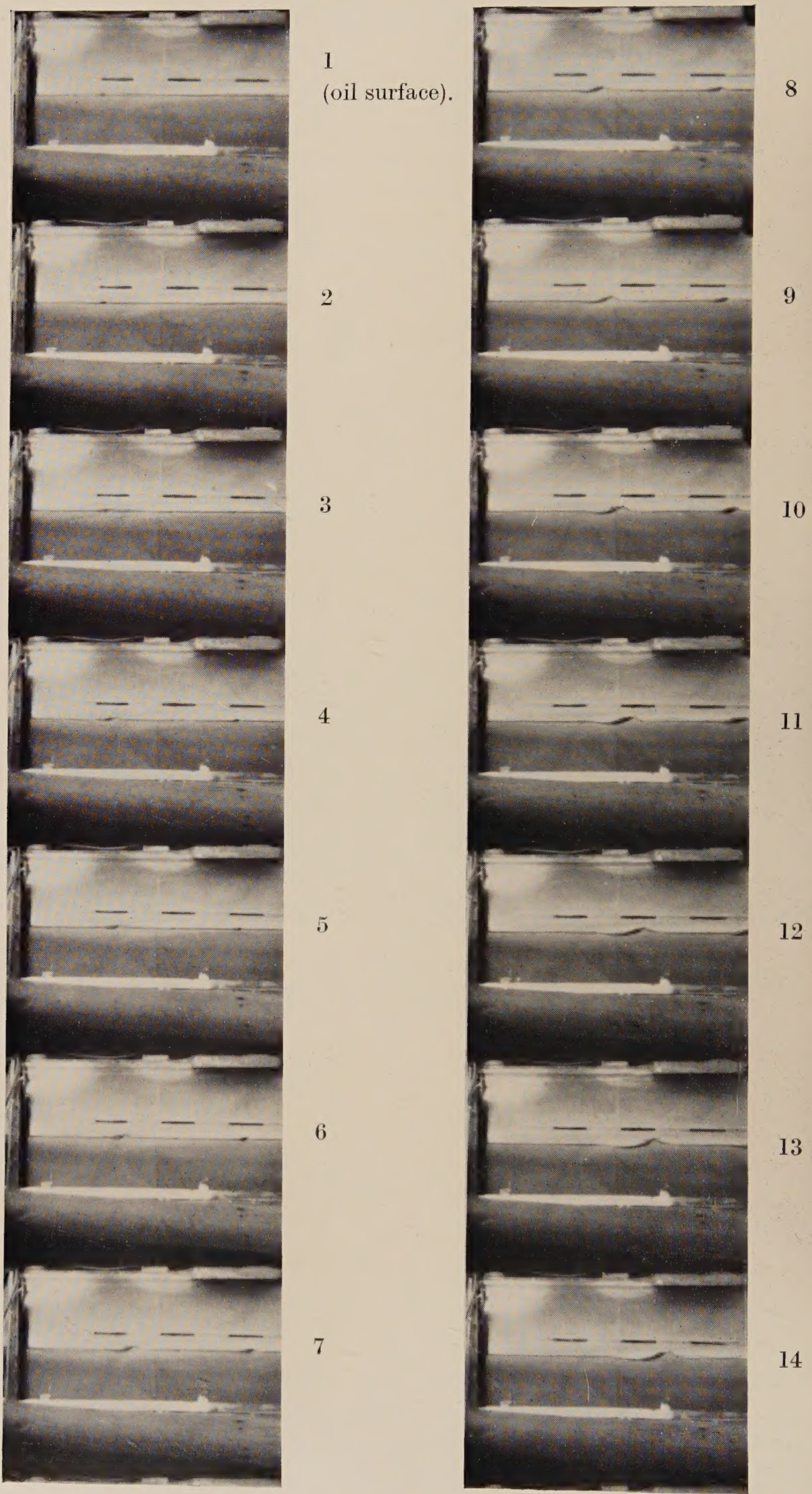

Cine photographs of unstable wave growing on oil surface. Wind from left to right. Camera speed 24 frames sec^{-1}. Scale of black and white 10 cm strips. A secondary wave started on this occasion downwind of the first unstable wave.

Fig. 3

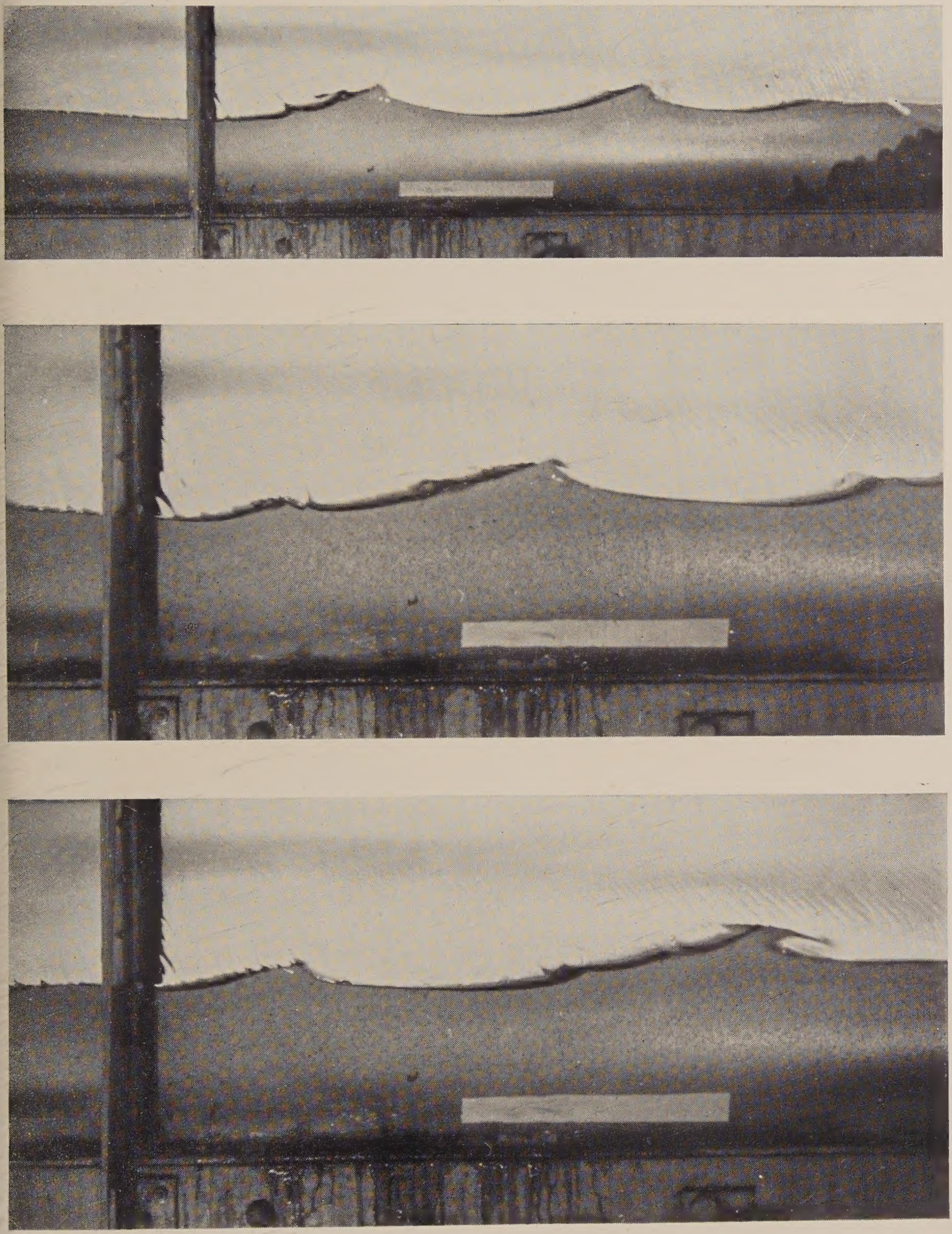

Examples of oil waves in wind tunnel at a windspeed of 13 m sec^{-1}, e.g. a higher wind than the critical. Wind left to right ; the white horizontal strip is 25 cm long. The streaks on the glass above the wave are due to an oil film which has been corrugated by the wind. Exposure time 1/80 sec.

Fig. 7

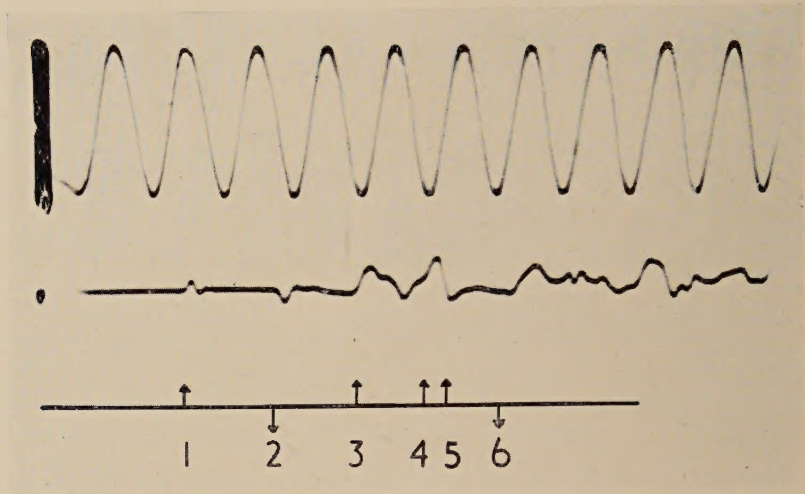

Oscillograph record from condenser microphone at centre of one face of steel cylinder 10·4 cm long and 7·6 cm in radius when 0·1 g of lead azide is detonated at the centre of opposite face. (Period of timing wave 10 μsec.)

Fig. 8

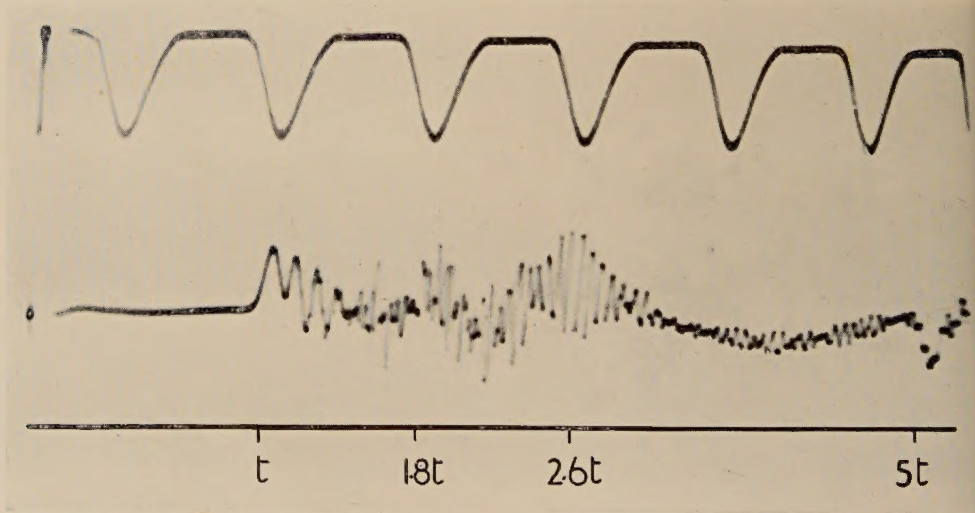

Oscillograph record from cylindrical condenser microphone on 2·5 cm diameter steel bar 60 cm from end at which 0·1 g charge has been detonated. (Period of timing wave 100 μsec.)